Train-induced Dynamic Response of Railway Track and Embankments on Soft Peaty Foundations.

A Thesis Submitted to the College of Graduate Studies and Research in Partial Fulfillment of the Degree of Master of Science in the Department of Civil Engineering,
University of Saskatchewan, Saskatoon, Canada

By
Michael Thomson Hendry

Permission to Use

In presenting this thesis in partial fulfillment of the requirements for a Postgraduate degree from the University of Saskatchewan, I agree that the Libraries of this University may make it freely available for inspection. I further agree that permission for copying of this thesis in any manner, in whole or in part, for scholarly purposes may be granted by the professor or professors who supervised my thesis work or, in their absence, by the Head of the Department or the Dean of the College in which my thesis work was done. It is understood that any copying or publication or use of this thesis or parts thereof for financial gain shall not be allowed without my written permission. It is also understood that due recognition shall be given to me and to the University of Saskatchewan in any scholarly use which may be made of any material in my thesis.

Requests for permission to copy or to make other uses of materials in this thesis in whole or part should be addressed to:

Head of the Department of Civil and Geological Engineering
University of Saskatchewan
Saskatoon, Saskatchewan S7N 0W0
Canada

OR

Dean
College of Graduate Studies and Research
University of Saskatchewan
107 Administration Place
Saskatoon, Saskatchewan S7N 5A2
Canada

Disclaimer

Reference in this thesis to any specific commercial products, process, or service by trade name, trademark, manufacturer, or otherwise, does not constitute or imply its endorsement, recommendation, or favouring by the University of Saskatchewan. The views and opinions of the author expressed herein do not state or reflect those of the University of Saskatchewan, and shall not be used for advertising or product endorsement purposes.

Abstract

The mainline railway track between Dublin and Belfast in Northern Ireland was constructed during the 1850's. Substantial lengths of railway embankment were constructed over poor-quality peaty soils. This was accomplished using tree trunk fascines placed directly on the natural ground surface; with poor-quality local peaty soils used as light weight fill.

In recent years, Northern Ireland Railways have noticed that these sections of railway track have been deteriorating more rapidly than sections of the track where the foundations are more competent. The magnitudes of displacement of the track under train loading appear to be increasing gradually over time and train speeds have had to be reduced.

This thesis is based on the research done to monitor the response of these railway track and embankment structures to dynamic train loading. The displacements were monitored for two different embankments under a variety of loading conditions and for various seasonal conditions. These displacements were recorded using a sensor created for this task. The sensor consisted of a photo-sensitive array mounted on the sleepers and a laser, which was placed outside the area of influence of train loading, and shone on the photo-sensitive array.

Analytical (Winkler) modelling was conducted to determine the effects of train speed and the cause of the large train-induced displacements. Analytical and finite element modelling were used to determine the effectiveness of alternative methods of embankment stabilization.

The results from the analytical modelling suggest that the deformation of the embankment under train loading was not due to dynamic excitation, but static deformation of the poor-quality fill and soft foundation materials. From both the analytical and finite element modelling of possible remediation techniques, methods that stiffen the embankment and foundation material are shown to be the most effective at reducing the train induced deflection of the embankment.

Acknowledgements

The completion of this thesis would not have been made possible without the support and help of various organizations and people. Northern Ireland Railways provided financial support for the research program of which this thesis is the first component of a larger appraisal of and research into the geotechnical structures which form the basis for the Northern Ireland Railways infrastructure.

I am grateful to both of my supervisors. I would like to thank Dr. Lee Barbour who provided me with the opportunity to pursue a Master's degree, to live and work in Belfast, Northern Ireland for a year, and for the many counselling sessions on MSN. Also, many thanks to Dr. David Hughes, who provided both the project and the funding; also for opening his home to Nadine and I on Christmas, it was a tough time to be away from our families and we thank you for sharing yours. I consider both of these men both mentors and friends.

I owe special thanks Kenny McDonald, for his technical support both on the railway line and in the shop. His patience with the uncertain scheduling and willingness to wade knee deep in bog with me, were greatly appreciated. Without Kenny it is quite possible this project may not have gotten off the ground.

Last but definitely not least, my wife Nadine, whose strength and support always held me up whenever I was in doubt of myself. Her sense of adventure and willingness to travel half way across the world to both struggle and explore, pleasantly surprised me, and brought us so much closer together.

Dedicated
to my wife Nadine for
her sacrifice, strength and love.

Table of Contents

List of Tables

List of Figures

Nomenclature

β	Damping ratio used in analytical modelling
$\delta(x,t)$	Dirac-delta function notation
θ	Velocity ratio used in analytical modelling
λ	Coefficient defining the static wave length
ρ	Density of beam element used in analytical modelling
ν	Poisson's ratio
ν_E	Poisson's ratio of the embankment fill material used in FE modelling
ν_F	Poisson's ratio of the soft foundation material used in FE modelling
ρ_b	Density of ballast used in analytical modelling
A	Cross-sectional area of beam element used in analytical modelling.
B	Width of base of beam elements used in analytical modelling
c	Damping coefficient used in analytical modelling.
c_{cr}	Critical damping coefficient in analytical modelling.
d	Depth of ballast used in analytical modelling.
d_B	Depth of ballast used in FE modelling
d_F	Depth of soft foundation material used in FE modelling
E	Young's modulus of beam element used in analytical modelling.
E_S	Elastic (Resilient) modulus of soil calculated from analytical modelling
E_E	Young's modulus of the embankment fill material used in FE modelling
E_F	Young's modulus of the soft foundation material used in FE modelling.
F(y)	Fourier transform notation
G	Shear modulus
I	Second moment of inertia
k	Elastic (spring) constant for visco-elastic foundation used in analytical modelling.
L	Power lost to damping, used in analytical modelling.
M	Moment generated in beam element due to loading
P	Magnitude of applied axle load.
t	Time
W	Work done to overcome damping, used in analytical modelling.
V	Velocity of train
V_{cr}	Critical velocity of train.
V_p	Velocity of compression waves in soil.
V_s	Velocity of shear waves in soil.
V_R	Velocity of Rayleigh waves in soil.
V_L	Velocity of Love waves in soil.
$\vec{v}$	Fraction of the peak particle velocity transmitted by the waves

Chapter One: Introduction

As in many countries around the world, the railway network in the United Kingdom has experienced declining use, leading to reduced investment over the last century. The decline in use is largely due to the greater dependency on road freight transport and the phenomenal growth in the number of private cars for personal transport.

This trend of decline, however, has begun to reverse in recent years. Railways are becoming increasingly important for meeting transportation requirements throughout Europe. Public rail transport is being supported as a solution to the problems of traffic congestion in large cities, the ever increasing cost of fuel, and environmental concerns such as smog and greenhouse gases.

There has been a recent initiative to increase the use of public transportation in Northern Ireland, and consequently a renewed interest and investment in the Northern Ireland Railways (NIR) network. This investment is evident in a plan instituted in 2005 by the Department of Regional Development Northern Ireland (DRDNI 2005). The £1.57 billion plan contains proposals to enhance public transport infrastructure, including improved rail and bus service in order to reduce the public's reliance on private cars for transportation.

As part of this reinvestment in public transport, the upgrading of existing rail infrastructure and the remediation of existing 'problem' sites has become a funding priority for NIR. NIR is conducting an appraisal of its existing earthworks infrastructure through Queen's University, Belfast. The focus of this appraisal is on several cuttings and embankment structures that are maintenance or safety concerns. The purpose of

this appraisal is to determine the magnitude of the problems and also to suggest possible remedial solutions.

The two embankment sites included in this study, Adavoyle bog and Brackagh bog, are of particular concern as they are sections of the main (highest traffic) Belfast to Dublin line. Thus, any reduction in serviceability of these embankments will have a large impact on the rail traffic in Northern Ireland.

Due to increased maintenance requirements and train-induced dynamic motion, these embankments have both a reduced train speed and a reduced capacity. These, and similar restrictions on other sections of the line, have resulted in what should be a two hour trip from Belfast to Dublin taking upwards of three hours.

1.1 Description of the Sites

The embankments being studied are located at Adavoyle bog, south of Newry, just north of the border with the Republic of Ireland, and Brackagh bog which is located just south of Portadown (Figure 1.1). At both sites the railway line runs on an embankment which is 2 to 4.2 m high. The embankments were constructed over areas of low-lying, poorly-drained peaty soil located in the Bann floodplain. These low lying peaty areas are flooded in the winter months with up to 0.4m of standing water (Figure 1.2).

These embankments were originally constructed in the mid 1850s, at the beginning of the railway era in Ireland. Information provided by the infrastructure department of NIR show that this type of embankment was typically constructed using tree trunk fascines placed directly on the natural ground surface, with poor-quality local peaty soils used as light weight fill, all of which was capped with ballast.

These sections of the main Dublin-Belfast line were raised with ballast in 1997, as part of a rehabilitation program. Little information could be found as to the specifications of this contract; however, a report (Ferguson McIlveen 2002) listed a lift of up to 1m of ballast had been placed on the embankments throughout this section of the line.

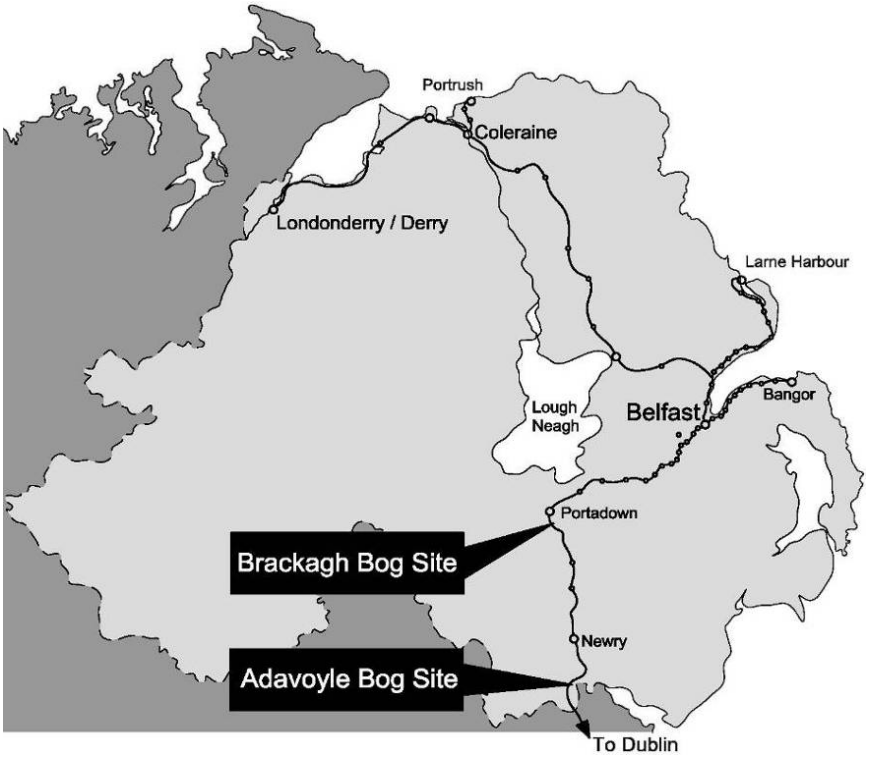

Figure 1.1: Current extent of Northern Ireland Railways and the location of embankment sites. (original map courtesy of NIR)

Figure 1.2: Embankment at Brackagh bog with surrounding area flooded during winter months

1.2 Description of Problem

The problems at both the Adavoyle bog and Brackagh bog sites are similar. In the last ten years the amount of maintenance required on these embankments to maintain their serviceability has risen substantially. Reports of excessive movement in the track and the embankment during the passage of trains have been made by maintenance crews working on these embankments. Also, train engineers report the trains become 'bogged down' or more precisely requiring increased power to maintain speeds. These reports were of sufficient concern to require the maximum train speeds over these embankments to be reduced from 145 km/h (90 mph) down to 96 km/h (60 mph), in response to safety concerns.

The frequency of maintenance required on these embankments has also increased markedly in the last ten years. Regular inspections of the railway line have noted that the rail alignment of these sections is very poor, with uneven spacing and vertical bumps. It was also noted that the sleepers often become 'skewed' to the rail and unevenly spaced (Figure 1.3). The rails often need to be lifted and realigned and the sleepers re-squared, to maintain the serviceability of the line. The surface of the embankment also requires regular addition of ballast and regrading. This sustained increase in maintenance infers that the rail and embankment structure are undergoing increased and ongoing deterioration, thus causing NIR to use a disproportionate amount of its maintenance budget on these sections of the line.

These embankments have been in service for over 150 years, while the problems have become apparent within the last ten years. This coincides with the introduction of the faster and heavier Belfast-Dublin 201 which replaced the 111 series locomotives. The introduction of these new locomotives has increased the load on the track from 986 kN to 1095 kN, and the operating speed from 113 km/h (70 mph) to 145 km/h (90 mph). Also coinciding with the start of the problems was the raising of the embankments with up to 1 m of ballast on this section of the line.

Northern Ireland Railways has pursued this project in an attempt to find possible solutions, as the increased maintenance and the reduction of speed on its major traffic corridor is reducing the level of the service it can provide.

Figure 1.3: Skewed Sleeper at Adavoyle bog site, common problem at both bog sites.

1.3 Research Program

The focus of the earthworks appraisal being conducted by Queen's University Belfast is on several cuttings and embankment structures that have become maintenance or safety concerns. The purpose of this appraisal is to ensure the safe passage of the railway traffic, and to allow for the increase of passenger capacity and service through an increase in train speeds.

A detailed study of the effects of dynamic loading on soft sub-grades is required for the appraisal of the Adavoyle bog and Brackagh bog sites. There has been significant research into the effects of dynamic loading, and this body of knowledge is to be called upon and applied to this research program.

Determination of the magnitude of the problems requires that the performance of the embankment be measured and that the mechanisms causing this deformation be characterized. Field measurements of deformation were made and these were

interpreted with the aid of models in order to identify the mechanisms that are causing the reduction in embankment performance. These models can then be used to identify possible remediation techniques.

1.4 Study Objectives

The overall objectives of the Adavoyle bog and Brackagh bog research program are to define the mechanisms responsible for the increased deformation under train loading, and provide direction and recommendations as to what remediation possibilities should be further explored for these sites.

The specific objectives of this thesis are to:

1. Design a methodology for the measurement of the dynamic displacement of the embankments under train loading.

2. Collect a series of displacement measurements of the track under loading. These measurements are to account for the various loading scenarios and differing seasonal variations in the ground water table experienced by the embankment.

3. Develop a preliminary analysis of the mechanisms responsible for the rail displacement using analytical modelling.

4. With the aid of analytical and finite element modelling, illustrate how the potential effectiveness of different remediation techniques on these embankments could be evaluated. Also, provide direction for further research into the remediation of these embankments.

1.5 Overview of Thesis

A brief overview of each chapter in this thesis is provided below:

Chapter Two contains the necessary literature review for this study.

Chapter Three describes the methodology employed in the measurement of the dynamic deflection of the rail-embankment structure.

Chapter Four presents the data obtained during the study, and the verification of its accuracy. This data includes the results of a site history search, the site survey, and the measurement of the dynamic displacement of the rail-embankment structure.

Chapter Five presents the analysis of the data acquired during this study. This analysis includes the use of an analytical model to study the existing behaviour of the embankments. Both the analytical model and FE models are used to determine the effectiveness of possible remediation techniques.

Chapter Six presents the conclusions and recommendations developed from this study.

Chapter Two: Literature Review

This chapter provides background information and a review of the literature published on topics related to this project. There are four sections of this literature review: first, the basic theory of dynamic motion is presented; second, methods of measuring dynamic motion used in contemporary studies are listed with their strengths and weaknesses; third, the use of analytical and finite element modelling of dynamic motion and the stress-strain relationship within soil structures is presented as it has been developed and used in previous studies; and finally, case studies which have been conducted on similar projects and the methods of remediation used are detailed.

2.1 Dynamic Motion (Vibration Theory)

To discuss train-induced dynamic motion, it is necessary to provide a background on vibration (wave) theory as it pertains to moving loads. This is because all dynamic loading generates waves, and the strain, deflection and stress at any point on or within the earthwork structure is due to the waves generated by this dynamic loading.

2.1.1 Source of Vibration

There are many modes of train-induced ground vibrations, which vary in both amplitude and frequency. All vibrations are induced in the same way, a change in loading is applied to a material in the form of an increase or decrease in load, an impulse or a moving load. This change in load induces strain and shear strain gradients within the material which are propagated as a wave outward from the source. (Hall 2000; Krylov et al. 2000; Hall 2003)

The response of the rail structure to the wheel axle loads is the source of the largest amplitude of induced vibration (Figure 2.1). The magnitude of these induced waves is influenced by the magnitude of the applied axle load and the rate of application of the load. These waves usually exist in a low frequency band (0-10 Hz), and can propagate well beyond the limits of the rail support structure. In the case of train-induced loading, or simply moving loads, these waves exist in a quasi-static state, which is static with respect to the load as long as a constant velocity is maintained. (Hall 2000; Krylov et al. 2000; Hall 2003).

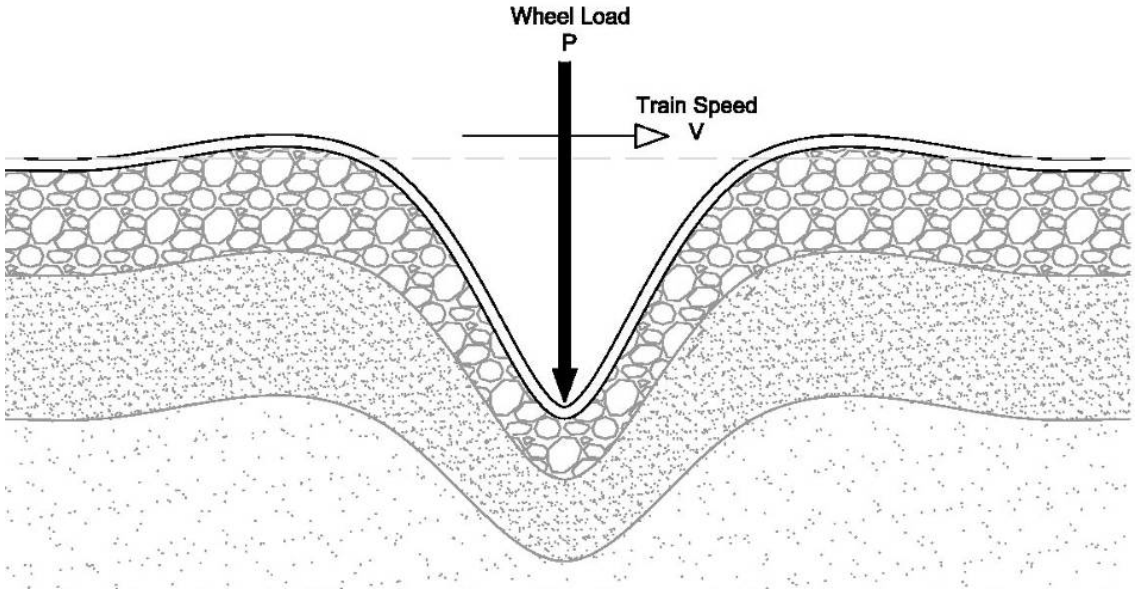

Figure 2.1: Generation of ground vibrations (after Hall (2000))

Other modes of train–induced ground vibrations can be caused by many other factors, including common imperfections in the rail and rail joints, and wheels either becoming unbalanced or having flat spots. For a more complete list of modes of train-induced ground vibrations refer to Table 2.1. These vibration sources have much less influence on the deflection due to their small magnitude. The effect of these vibrations is usually filtered out by the rail structure and embankment, as they occur at high frequencies. (Hall 2000; Brandl 2001)

Table 2.1: Factors influencing train-induced ground vibrations (after Hall (2000))

Stress waves induced by the track structure response
• Axle weight
• Spacing of wheel axles
• Speed of train
Vibration source at the wheel-rail interface
• Unsteady riding of the vehicle (bouncing, rolling, pitching)
• Dynamic properties of the vehicle bogies
• Wheels defects (eccentricity, imbalance, flats)
• Misalignments of motors
• Acceleration and deceleration of train
Discontinuity on the track
• Rail defects (unevenness, waviness)
• Spacing and interval of rail joints
• Switches
• Curves and tilting track (centrifugal forces)
Variable Support
• Geometry, stiffness and spacing of sleepers
• Geometry, stiffness and heterogeneity of the ballast
• Stiffness and geometry of the ground

2.1.2 Propagation

Once a strain gradient is introduced in the structure, the vibration will propagate through the material away from the source. The speed of the wave is dependant on the properties of the material(s) through which it is moving. Waves occur in different forms: body waves (compression-dilation and shear waves) which exist within the material; and surface waves (Rayleigh and Love waves) that are a result of the interactions of the body waves and the surface (Figure 2.2) (Woods 1978; Athanasopoulos et al. 2000; Hall 2000).

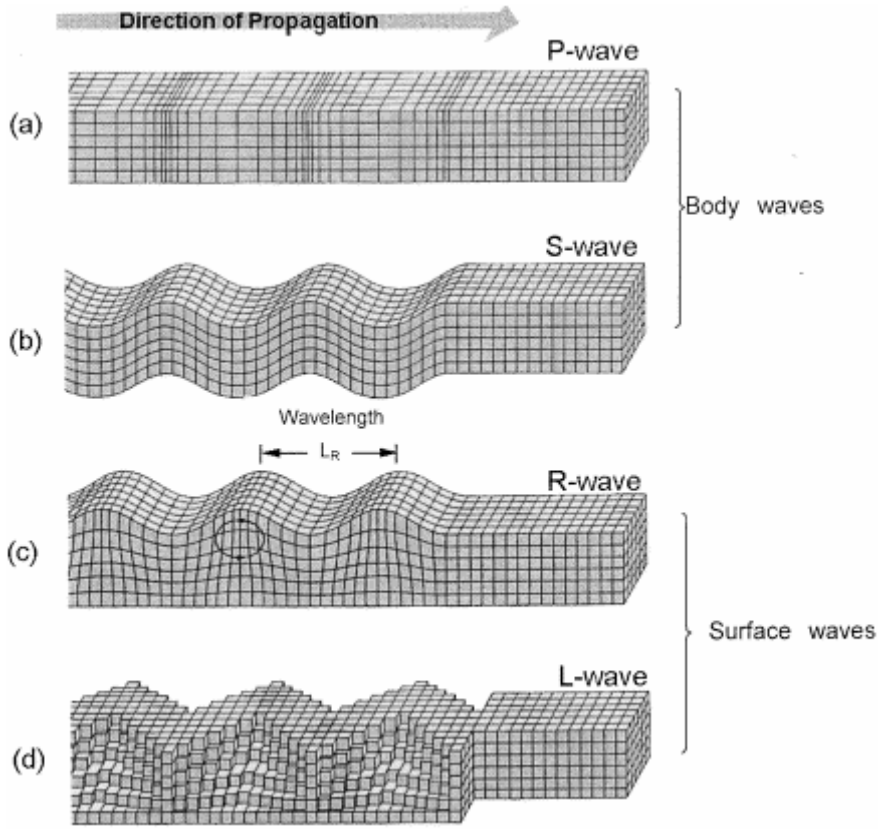

Figure 2.2: Types of seismic wave propagating in the ground (a) compression-dilation waves (b) shear waves (c) Rayleigh waves and (d) Love waves (Athanasopoulos et al. 2000)

The first type of body wave (Figure 2.2a) is the compression wave (also known as a P-wave). These waves consist of successive waves of compressive and tensile stresses. The motion the particles undergo with this wave form is one of movement back and forth parallel to the direction of propagation. Compression waves can travel through both liquids (water) and solids, and the speed of transmission is strongly dependant on the water content of the soil. For saturated soils the transmission through water becomes dominant (speed of transmission through water is 1525 m/s). The velocity of a compression wave can be calculated by Equation 2.1. (Woods 1978; Athanasopoulos et al. 2000; Hall 2000)

$$V_P = \sqrt{\frac{G(2-2\nu)}{\rho(1-2\nu)}} \qquad (2.1)$$

where, V_P is the velocity of a compression wave within a material with a shear modulus G, a density of ρ and a Poisson's ratio of v.

The second type of body wave (Figure 2.2b) is the distortional wave (also known as the S-wave or shear wave). This is so named due to the shear strains produced in the transmission of this type of wave. Unlike the compression wave, this waveform has particles that move within a plane perpendicular to the direction of propagation. The direction of particle movement and the amplitude of movement within that plane can be divided into two component directions in the vertical and the horizontal directions. As liquids (water) are unable to transmit shear strains, the transmissions are propagated solely through the solid materials and not pore-water. The velocity of a shear wave can be calculated using Equation 2.2. (Woods 1978; Athanasopoulos et al. 2000; Hall 2000)

$$V_S = \sqrt{\frac{G}{\rho}} \tag{2.2}$$

where, V_S is the velocity of the shear wave within a material, with a shear modulus of G and a density of ρ.

The first type of surface wave (Figure 2.2c) is the Rayleigh wave (also known as the R-wave). This is produced by the interaction of the vertical component of the shear wave and the compression wave at the surface of the material. The Rayleigh wave moves vertically up and down while alternating between compression and dilation. The velocity of a Rayleigh wave can be approximated using Equation 2.3. (Woods 1978; Athanasopoulos et al. 2000; Hall 2000)

$$V_R \approx \frac{0.87 + 1.12\nu}{1 + \nu} V_S \tag{2.3}$$

where, V_R is the velocity of the Rayleigh wave within material, V_S is the shear wave velocity in the same material and v is the Poisson's ratio of the material in which the wave is travelling.

The Love wave (also known as the L-wave) is a much more complex wave (Figure 2.2d). It consists of the horizontal component of the shear wave at the surface moving in a horizontal side to side motion within the plane of the surface. A Love wave can be generated near the surface where a material with a higher shear wave velocity overlies a material with a lower shear wave velocity. The Love wave is commonly described as a wave trapped by multiple reflections within the upper layer. The Love wave also occurs in homogeneous soils with shear wave velocities which increase with depth. The transmission velocity of the Love wave can be calculated with Equation 2.4. (Woods 1978; Athanasopoulos et al. 2000; Hall 2000)

$$TAN\left(2\pi f\sqrt{\frac{1}{V_{S1}^2}-\frac{1}{V_L^2}}\right)=\frac{V_{S2}^2\rho_2\sqrt{\frac{1}{V_L^2}-\frac{1}{V_{S2}^2}}}{V_{S1}^2\rho_1\sqrt{\frac{1}{V_{S1}^2}-\frac{1}{V_L^2}}} \tag{2.4}$$

where, V_L is the velocity of the Love wave within upper material with a higher shear wave velocity of V_{S1}, and a density of ρ_1. This higher shear wave material overlies a material with a lower shear wave velocity of V_{S2}, and a density of ρ_2.

In cases of multiple sources of vibration, such as a train with multiple axles, the motion of the ground at any point will be the sum of all of the waves at that point from all sources.

2.1.3 Attenuation (Damping)

Vibrations travel in the direction of propagation away from the source. The magnitude of the wave decreases the further the wave travels from the source. This decrease in magnitude is caused by both material damping and geometric damping.

Material damping is the loss of mechanical energy through friction within the material as the particles move with the waves. The mechanical energy is transferred into heat energy. This damping is a material property, which varies with the wave velocity (another material property) and the frequency of the wave (due to the loading scenario). The greater the velocity or the frequency of the wave the greater the material damping

(Hall 2000). From Woods (1978) material damping is a particularly strong for soft peaty organic soils.

Geometric damping is the diffusion of the energy of the wave over a greater volume of soil as it moves away from the source. This reduces the intensity of the wave at any one location, but increases the volume of soil through which the wave propagates. Two cases are presented in Figure 2.3 to demonstrate geometric damping of a point impulse on the surface of a soil medium. The effect of geometric damping on body waves and surface waves varies greatly. This can be seen in the reduction of particle velocity transmitted by the waves in equation 2.5.

$$\vec{v} = r^{-m} \tag{2.5}$$

where $\vec{v}$ is the fraction of the peak particle velocity transmitted by the waves, and r is the distance traveled away from the source. The m value is a factor dependant on the type of wave transmitted. For body waves m is equal to 2, while it is 0.5 for surface waves. This demonstrates the much greater decrease in body wave peak particle velocity compared to the decrease in surface wave peak particle velocity due to geometric damping as the waves move away from the source (Hall 2000).

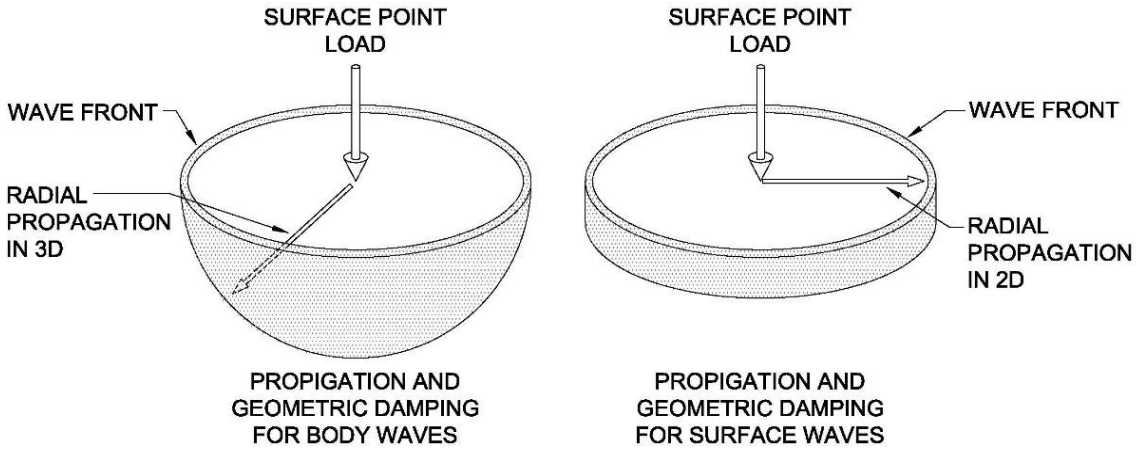

Figure 2.3: Geometric damping for different wave types for surface point load. (after Hall 2000)

2.1.4 Reflection and Refraction

When a wave of any type encounters an interface between two materials of differing properties, a component of the wave will be reflected back into the source material with a differing wave length and amplitude. The remaining component will cross over the boundary and can be refracted into waves of different types with differing wave lengths and amplitudes. (Hall 2000)

2.2 Measurement of Dynamic Motion

In order to quantify and characterize the dynamic motion of the embankment under the loading of a train, it is necessary to measure this motion. The most common instruments used for measuring the displacement of an embankment under loading are accelerometers, geophones and extensometers. These instruments are often installed in the embankment to directly measure displacements. (Hall 2000; Heelis et al. 2000; Kaynia et al. 2000; Madshus and Kaynia 2000)

2.2.1 Geophones / Accelerometers

Both geophones and accelerometers carry out the same function although they are constructed differently. Geophones (also called seismometers) consist of a coil of wire suspended in a magnetic field circuit (Figure 2.4). When the geophone moves as a result of vibration, the coil moves through the magnetic field, this produces a voltage which can be measured and interpreted as acceleration. Geophones are very rugged and reliable, but the use of geophones for measurement of low frequency movements (such as 1-2 Hz for the loading due to train axles) becomes very expensive. (Hall 2000)

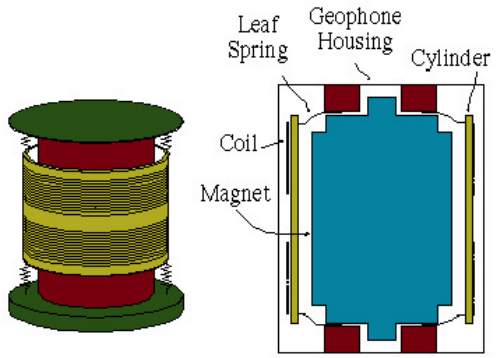

Figure 2.4: Construction and components of a Geophone (Hall 2000)

Accelerometers come in three configurations; piezoelectric, resistance strain gauge, and piezoresistive. The most widely used accelerometer is the piezoelectric accelerometer, which consists of a mass that, when accelerated, applies a force to a quartz crystal. This quartz crystal produces an electrical voltage proportional to the applied force (Figure 2.5). A resistance strain gauge accelerometer utilizes a very thin foil or fine wire which changes in electrical resistance when a strain is applied. The piezoresistive accelerometer acts in a very similar manner to the resistance strain gauge accelerometer but instead of foil or wire, a semiconductor with similar properties is used.

Both geophones and accelerometers are installed on the surface or embedded within the embankment. The displacement can be calculated from integrating the resulting acceleration versus time curve twice with respect to time. Geophones and accelerometers are very sensitive and require a large amount of additional equipment and computing time to condition the signals and filter 'noise' from the data sets.

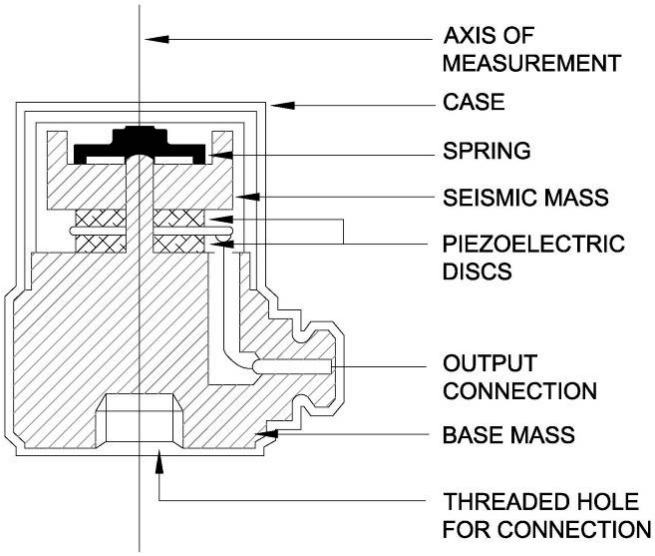

Figure 2.5: Construction and components of a piezoelectric accelerometer, in cross-section of sensor. (after MacMillan (1998))

2.2.2 Extensometers

Extensometers used for this purpose are installed in boreholes, and measure relative displacement between the 'reference head' at the surface and an anchor grouted in the

bottom of the borehole (Figure 2.6). In this application several extensometers are installed at a site, and with this data it is possible to determine where measured strains are occurring within the embankment structure and foundation soil. The measurements taken within the reference head can be measured with a variety of instruments, most commonly piezoelectric sensors.

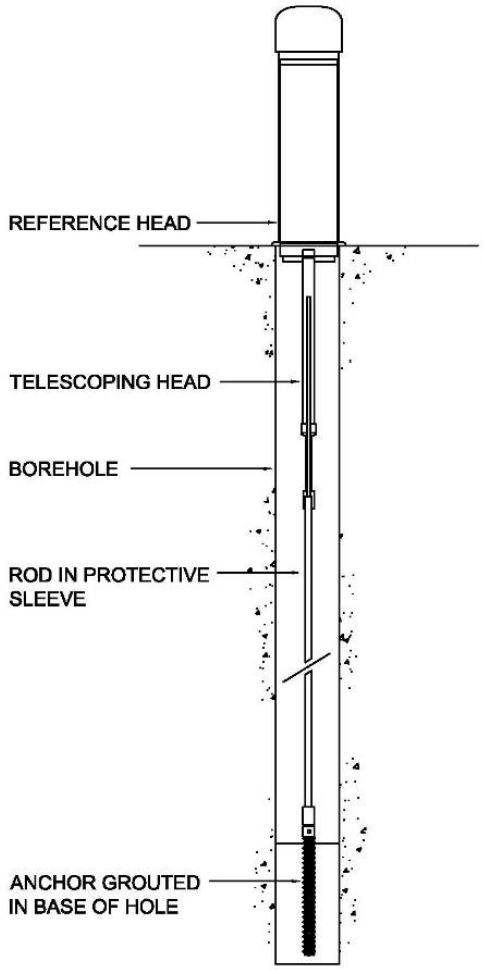

Figure 2.6: Extensometer installed in bore hole with anchor grouted in base of hole. (after Rod Extensometer (2004))

2.3 Spectrum Analysis

The data sets collected for the investigation of train-induced deflections are, by nature, time dependant. Most intuitive of the methods of analysis is the use of the displacement versus time domain with extractions from this data of velocity or acceleration versus time. All these presentations of the data are extremely useful in the interpretation of the reactions of the embankment structure and the foundation materials.

Spectrum analysis or frequency domain analysis was originally developed for use in seismology and earthquake engineering. The basis of this method is that any complex waveform can be broken down into a series of discrete sinusoidal curves. This deconstruction of a complex curve is best presented in Woods (1978). A simple example of this construction is provided in Figure 2.7, which demonstrates the construction of a complex curve (based on data measured during the course of this study) from three simple sinusoidal curves of differing period (frequency) and phase angles.

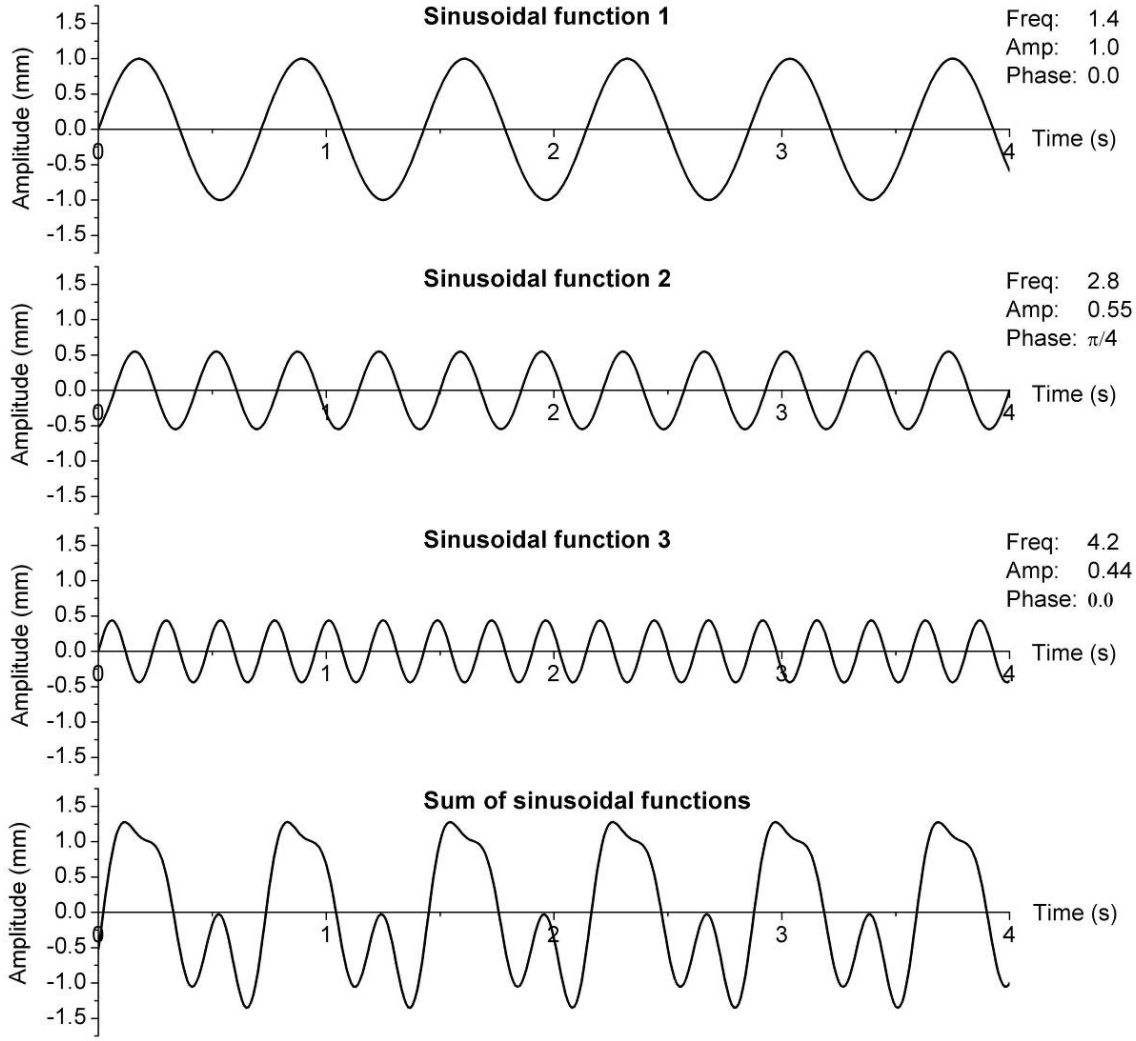

Figure 2.7: Creation of complex waveform (based on data measured during the course of this study) from three simple sinusoidal curves of differing period (frequency) and phase angles.

The frequency domain plot is the representation of the finite to infinite number of simple sinusoidal curves which combine to form the complex time domain curve. The complex curve from Figure 2.7 can be represented by the three vertical lines in the frequency domain plot in Figure 2.8, labelled as “Actual sinusoidal functions”.

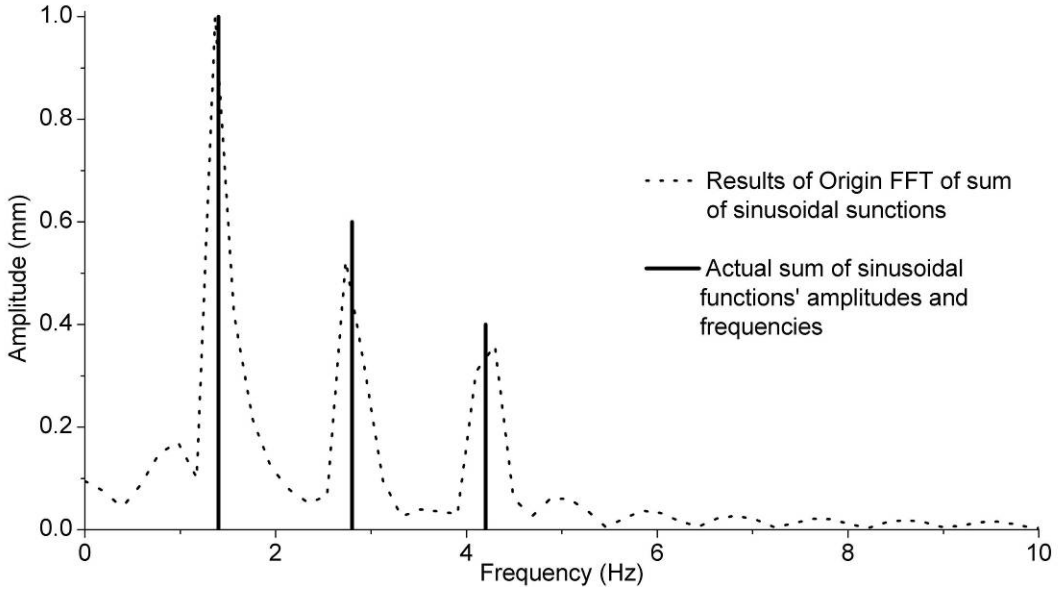

Figure 2.8: Resultant frequency domain plot from the sum of sinusoidal functions (Figure 2.7)

To translate a complex time domain curve into the frequency domain, it needs to be resolved with the classical Fourier Transform shown in equation 2.6. (Woods 1978)

$$F(y) = \int_{-\infty}^{\infty} f(x) \cdot e^{-2\pi xy} dx \qquad (2.6)$$

In the case of data as a series of points, and not as an equation, the data set can be resolved with a computer algorithm of the Fast Fourier Transform (FFT), based on the Discrete Fourier Transform (Cooley and Tukey 1965). The FFT provides a useful approximation for a complex time domain curve in the frequency domain. In Figure 2.8 the comparison can be made between the actual frequency domain plot of the complex curve from Figure 2.7, to the result of the FFT applied to the same complex curve with the program Origin (OLC 2002). The FFT correctly identifies the frequencies and amplitude of the major contributing sinusoidal functions; however, the FFT does

produce some extra ‘noise’ consisting of contributions of frequencies which are not represented in the complex curve.

The benefit of this spectrum analysis plot in this application is the ability to identify the relative magnitude of contribution of each cyclical component of loading to the deflection of the rail-embankment structure. These differing components of loading and response typically consist of: (a) whole train passing, which occurs at a very low frequency (<0.1Hz), (b) the passage of the pairs of bogies from the connection of cars, (c) the passing of the individual bogies and (d) the passing of individual wheel axles.

2.4 Modelling of Train-induced Displacement

A large quantity of research has been devoted to modelling the effects of dynamic loading, and specifically the modelling of train-induced dynamic loading. Original modelling was based on analytical models which simplified the dynamic loading and displacement as a mechanical vibration problem. (Timoshenko 1926; Biot 1937; Criner and McCann 1954; Kenny 1954; Vesic 1963; Frýba 1972; Heelis et al. 1999)

More modern modelling has moved into Finite Element (FE), Finite Difference (FD), and Boundary Element (BE) analyses. Finite Element has emerged as the most common approach and has advantages over analytical modelling. For instance, FE models are able to determine stress concentrations and to expand to a three-dimensional analysis. Despite these benefits the models are still limited to simplified soil models, and their construction and execution requires substantially more computing time. (Krylov 1995; Hall 2000; Krylov et al. 2000; Hall 2003; Paolucci and Spinelli 2006)

2.4.1 Analytical Modelling

Analytical methods of modelling train-induced dynamic motion have been around for the better part of a century. These models provide solutions with minimal computational requirements while still modelling and predicting complex relationships. The analytical models are based on very simplified physical representations and they often contain factors for which only approximate correlations can be made to fundamental material properties.

The Winkler model is a very prevalent and simple numerical model. In the Winkler model, the embankment/rail/foundation material structure is simplified as a beam on an elastic or visco-elastic foundation (see Figure 2.9). The visco-elastic foundation follows the basis of the original Winkler hypothesis presented in Winkler et al. (1867), that the foundation is represented by a series of 'discrete' springs and dashpots, that is, the soil reaction is limited to a one-dimensional elastic response with no shear interactions. This simplification is significant, but has been shown to predict static and dynamically induced deflections well (Vesic 1963; Hall 2000; Heelis et al. 2000). Further development of the Winkler model, specifically for the purpose of modelling railway support structures, was under taken in Timoshenko (1926) and later in Kenny (1954). The mathematics of this model were elaborated upon and simplified in Frýba (1972) providing a good reference for the programming of this model.

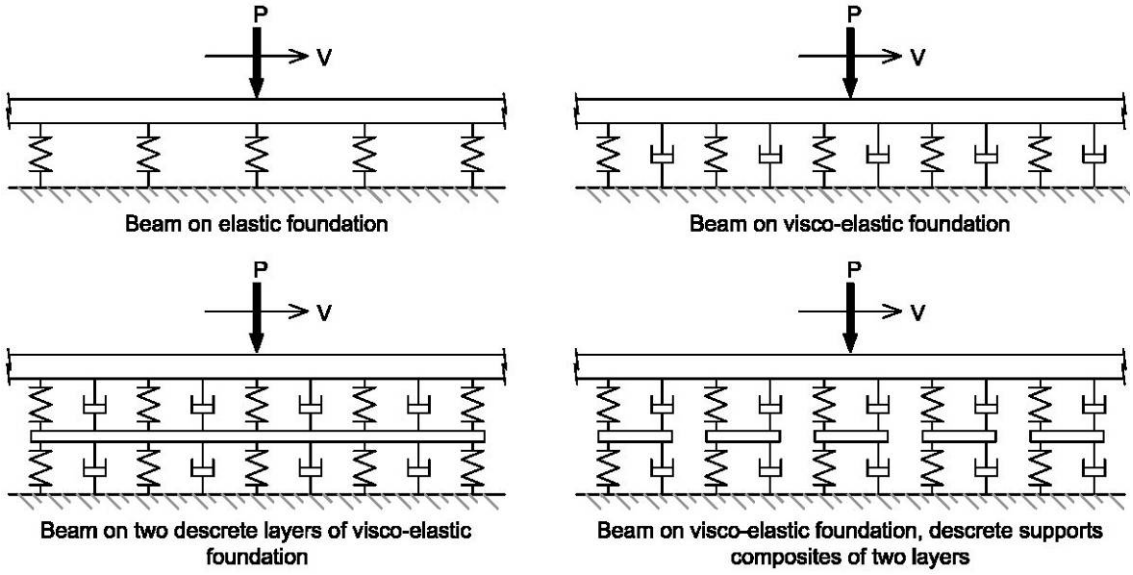

Figure 2.9: Different variations on the Winkler model foundation (after Hall (2000))

The governing equation (2.7) for this model was derived in Timoshenko (1926) and Kenny (1954) based on the loading per unit length of a beam, and constitutes a force balance in the vertical (y) direction.

$$EI\frac{\partial^4 y}{\partial x^4}+\rho A\frac{\partial^2 y}{\partial t^2}+c\frac{\partial y}{\partial t}+ky=P\delta(x,t) \tag{2.7}$$

The components of this governing equation are as follows. The flexural rigidity of the beam (EI) and is used to calculate the force, per unit length of the beam, resulting from the bending moment. The stiffness coefficient for the foundation (k) is used to calculate the force response of the elastic foundation to the applied load. The mass per unit length of the beam (ρA) is used to calculate the inertial force resulting from the acceleration of the beam element. The coefficient c is the damping coefficient of the foundation and represents the resistive damping force of the foundation material. The term Pδ(x,t) represents the applied point load with the dirac-delta function limiting the load of magnitude P to a single point on the beam.

The solution provided in Kenny (1957) is an exact solution; however, it is cumbersome to use and difficult to program. Frýba (1972) provides a good approximate solution for cases with light damping and is easily programmed. This is the solution used within the analysis section of this thesis, and is presented in Equations 2.8 through to 2.19.

For the case of x < 0:

$$y(x) = \frac{P\lambda}{2k} \frac{2}{a_1\left(D_1^2 + D_2^2\right)} e^{-b\lambda x}\left(D_1 \cos a_1\lambda x + D_2 \sin a_1\lambda x\right) \tag{2.8}$$

For the case of x > 0:

$$y(x) = \frac{P\lambda}{2k} \frac{2}{a_2\left(D_3^2 + D_4^2\right)} e^{b\lambda x}\left(D_3 \cos a_2\lambda x - D_4 \sin a_2\lambda x\right) \tag{2.9}$$

Where P is the magnitude of the applied point load, k is the stiffness coefficient for the foundation and x is the horizontal distance from the point load (positive values of x denote distance in front of the point load, and negative values denote the distance behind the point load). The variable λ is defined in Kenny (1954) as the coefficient defining the static wave length and is calculated as per Equation 2.10. The remaining variables ($a_{1,2}$, $b_{1,2}$, $D_{1,2,3,4}$) are used to simplify the calculations and are calculated as per Equations 2.11 through to 2.19.

$$\lambda = \left(\frac{k}{2EI}\right)^{\frac{1}{4}} \tag{2.10}$$

$$D_1 = a_1 b \tag{2.11}$$

$$D_2 = a_2 b \tag{2.12}$$

$$D_{3,4} = b^2 \mp \frac{1}{4}\left(a_1^2 - a_2^2\right) \tag{2.13}$$

For the case of α < 1; β << 1:

$$a_{1,2} \approx \left[1 + \theta^2 \pm \frac{2\theta\beta}{\sqrt{1-\theta^2}}\right]^{\frac{1}{2}} \tag{2.14}$$

$$b \approx \sqrt{1-\theta^2} \tag{2.15}$$

For the case of α = 1; β << 1:

$$a \approx a_1 \approx a_2 \approx \sqrt{2}\left(1 + 2^{-\frac{3}{4}}\sqrt{\beta}\right) \tag{2.16}$$

$$b \approx 2^{-\frac{1}{4}}\sqrt{\beta} \tag{2.17}$$

For the case of α > 1; β << 1:

$$a_{1,2} \approx \sqrt{\theta^2 + 1} \pm \sqrt{\theta^2 - 1} \tag{2.18}$$

$$b \approx \frac{\theta\beta}{\sqrt{\theta^4 - 1}} \tag{2.19}$$

The solution of the differential equation can also be used to calculate the critical velocity (V_{cr}) (Equation 2.20) (Kenny 1957). This is the velocity at which the model predicts a maximum response, or resonance (Figure 2.10). Following this is the velocity ratio (θ) which is the ratio of a velocity to the critical velocity (Equation 2.21).

$$V_{cr} = \sqrt[4]{\frac{4kEI}{(\rho A)^2}} \tag{2.20}$$

$$\theta = \frac{V}{V_{cr}} \tag{2.21}$$

The critical velocity acts as a threshold value. The increase of displacement due to the increase of train speed is caused by the inertia becoming a strong driving force. This inertia-driven displacement is not only in the downwards direction but also upwards as well, increasing to a maximum at the critical velocity where it is nearly as large in magnitude as the downwards deflection. The inertial forces begin to act to limit the vertical dynamic displacement after the critical velocity; this is illustrated in Figure 2.10. For a value of θ equal to 2, the maximum displacement is delayed until after the passage of the axle load.

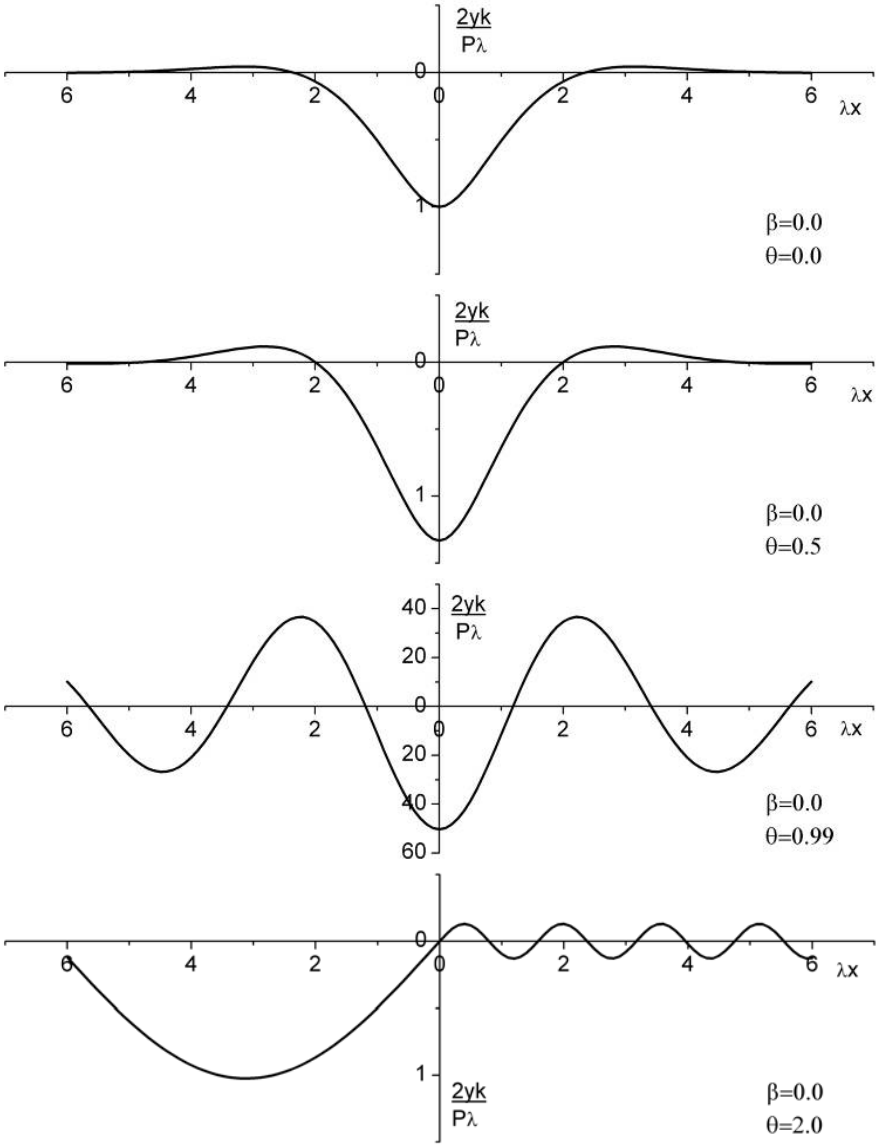

Figure 2.10: The effects of velocity on the Winkler model for displacement of a beam on an elastic foundation (after Kenny (1957))

At velocities less than the critical velocity vibrations and waves are unable to propagate out from the point of loading. For example, in the case of θ equal to 0 and 0.5 in Figure 2.10 the undamped response is limited to the area local to the applied axle load. As the velocity of the load approaches the critical velocity, the area affected grows substantially. For velocities equal to or greater than the critical velocity, waves freely propagate beyond the local area of the load as for the case of θ equal to 2 (Figure 2.10).

As with the critical velocity and velocity ratio Kenny (1957) also defines a critical damping value (c_{cr}) (Equation 2.22), and a damping ratio (β) (Equation 2.23).

$$c_{cr} = 2\sqrt{k\rho A} \tag{2.22}$$

$$\beta = \frac{c}{c_{cr}} \tag{2.23}$$

The solution of the governing equation models the deflection of an infinite beam on an elastic foundation for a single moving load. For the purposes of modelling a complete train it is necessary to model a series of moving loads from all wheel axles along the length of the train. The train is modelled as a quasi-static loading of a beam as the coordinate system moves with the train. The deflection at any point along the length of the rail is the sum of the deflections from all the wheel axles at that point (Equation 2.24):

$$y(x)_{Total} = P_1 y(x_o - x_1) + P_2 y(x_o - x_2) + ... + P_n y(x_o - x_n) \tag{2.24}$$

There are limitations to the Winkler model. It is limited to two-dimensional applications, with linear visco-elastic soil models. No shear stresses or strains can be modelled and stress concentrations must be found through other methods.

2.4.2 Estimation of the Elastic (Resilient) Foundation Modulus

The stiffness coefficient of the foundation (k) has been extensively correlated with the elastic modulus (E_S) of the sub-grade material with reasonable success. The most

commonly used correlations are from Biot (1937) (Equation 2.25) and Vesic (1963) (equation 2.26). Vesic (1963) provides an upper limit and Biot (1937) provides a lower limit.

$$k = \frac{0.65 E_S}{\left(1-\nu^2\right)} \sqrt[12]{\frac{E_S B^4}{EI}} \tag{2.25}$$

$$k = \frac{0.95 E_S}{\left(1-\nu^2\right)} \left(\frac{E_S B^4}{\left(1-\nu^2\right) EI} \right)^{0.108} \tag{2.26}$$

The parameter B in Equations 2.25 and 2.26 is the width of the beam element that transfers the load to the discrete visco-elastic foundation and is illustrated in Figure 2.11 as it was originally defined in Biot (1937) and Vesic (1963). For the application of these equations to railway structures, the beam element width (b) has been extended to the width of the ties as per Hall (2000), or the width or the embankment or part of embankment included in the beam element as per Heelis et al. (1999).

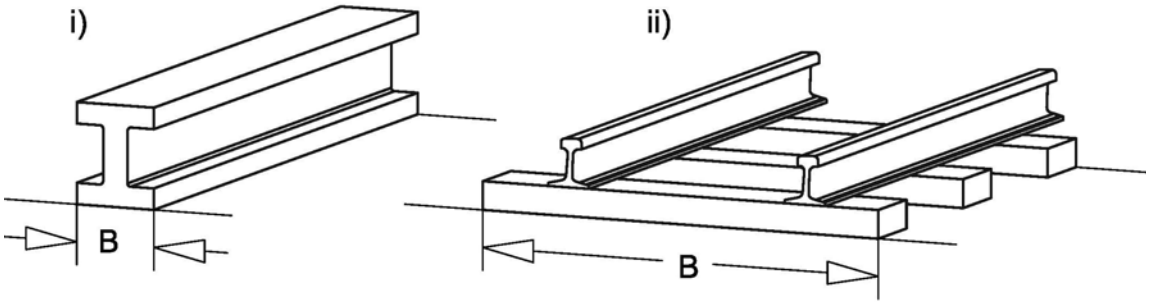

Figure 2.11: Definition of 'B' variable i) as used for the calculation of the modulus of the foundation as per Biot (1937), and ii) as used for the calculation of the modulus of foundation in this thesis.

The correlations from Biot (1937) and Vesic (1963) provide very similar results, as Vesic (1963) is an extension of Biot (1937). Both correlations are derived from an assumption of an infinite beam on a semi-infinite continuum (infinite depth) of material supporting the beam. Vesic (1963) also goes beyond Biot (1937) and provides solutions for finite beam lengths with laboratory testing to prove the validity of the solutions for these cases.

2.4.3 Finite Element Modelling

The purpose of finite element analysis within this thesis is to take advantage of the ability of this type of model to show the stress-strain relationship spatially within the soil. This will provide insight in to the locations of concentrations of strain, allowing for a determination of the weaknesses within the structure. The complexity of the definition of the soil properties, geometry and the ability to add structures such as beams allow for a detailed exploration of embankment stiffening techniques. This can be used to conduct a preliminary evaluation of two embankment stabilization techniques being explored for Brackagh bog and Adavoyle bog sites.

The software package used for the finite element analysis within this thesis is Geostudio's SIGMA/W (GEO-SLOPE 2004). SIGMA/W is a well tested and widely used stress-strain finite element modelling software. SIGMA/W was specifically designed with geotechnical finite element modelling in mind, allowing for very complicated analyses when used in conjunction with Geostudio's other modelling software.

Since SIGMA/W is a well documented, commercial software, this literature review only contains the very basics, and further explanations on the use of this program for this modelling exercise are provided within chapters three and four. For a much more in-depth discussion into the theory and application of the FE model, the book "Stress and Deformation Modelling with SIGMA/W" (Krahn 2004) is a very good resource.

Basic Theory of Finite Element Analysis

Finite element analysis divides a material into elements. Strain is allowed to vary with respect to a selected soil model (linear-elastic, nonlinear-elastic, elastic-plastic models) within each element. Loads or deformations are applied to the elements through boundary conditions and the response of the elements to these boundary conditions is reflected in displacements of the nodes. The nodal displacements are calculated through shape functions based on the geometry of the elements. Simple shapes (triangles and trapezoids in 2D) are used in the discretization of the materials into elements. These simple shapes have well-defined shape functions. From the sum of these elemental nodal displacements a modelled response of the material to the applied stresses can be calculated (Hall 2000).

Linear Elastic Soil Model

A linear elastic soil model was used in this initial investigation of the behaviour of the train-induced behaviour of the embankment/foundation structure. This simple model was used due to the apparent reversibility of the displacements and the proportionality of the displacement load response. A complex soil model requires much more computing power, knowledge of soil properties and time to properly construct and calibrate a model.

The linear elastic model assumes a simple linear relationship between the stress applied and the strain-induced (Figure 2.12). The resulting stress-strain relationship for the material within the element is given in Equation 2.27 for a two-dimensional analysis (Krahn 2004), where E is the elastic (Young's) modulus and ν is the Poisson's ratio of the material being modelled.

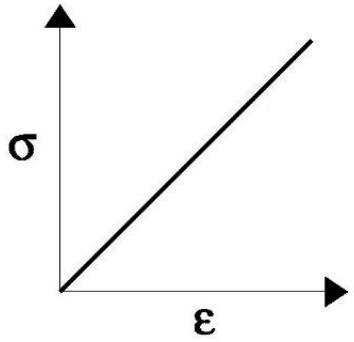

Figure 2.12: Linear-elastic soil model (Krahn 2004)

$$\begin{Bmatrix} \sigma_x \\ \sigma_y \\ \sigma_z \\ \tau_{xy} \end{Bmatrix} = \frac{E}{(1+\nu)(1-2\nu)} \begin{bmatrix} 1-\nu & \nu & \nu & 0 \\ \nu & 1-\nu & \nu & 0 \\ \nu & \nu & 1-\nu & 0 \\ 0 & 0 & 0 & \frac{1-2\nu}{2} \end{bmatrix} \begin{Bmatrix} \varepsilon_x \\ \varepsilon_y \\ \varepsilon_z \\ \gamma_{xy} \end{Bmatrix} \quad (2.27)$$

where: σ_x, σ_y and σ_z are the stresses in the x, y and z directions; τ_{xy} is the shear stress in the xy plane; ε_x, ε_y and ε_z are the strains in the x, y and z directions; and, γ_{xy} is the shear strain in the xy plane. Equation 2.27 can be further simplified, as a plane-strain condition is imposed due to the two-dimensional nature of the model, the values of σ_Z and ε_z are 0, this reduces the matrix to a three by three matrix. A limitation imposed by this formulation is that the Poisson's ratio cannot be equal to 0.5 (as is the case for a

saturated soil) as this produces numerical problems. Thus, Poisson's ratios are limited to a maximum of 0.49.

Two-dimensional Analyses

SIGMA/W is limited to two-dimensional and axisymmetric analyses. This requires a simplification in the loading scenarios applied to the structures. These simplifications cause shortcomings and distortions; this requires interpretation when evaluating the results.

A two-dimensional analysis will force a plane-strain condition on the model. The model will therefore act as though what is defined in the two dimensions is projected into and out of the page infinitely. This includes loading; thus, a point load becomes a linear load. This tends to cause inaccuracies within the model as it can overestimate the confining stresses within the soil and the magnitude of loading when trying to model the effects of a point load.(Hall 2000)

An axisymmetric analysis approximates a three-dimensional response from a two-dimensional model. The axisymmetric model does this by assuming symmetry around an axis in 360º. The object(s) being modelled must lend itself to this assumption of symmetry.

2.5 Case studies

The following contains a summary of case studies which directly correspond to the research conducted and presented within this thesis. Three of the case studies pertain directly to measurements of the dynamic displacements under train loading and numerical and analytical modelling carried out on the resulting data. The two remaining case studies are a presentation of two promising methods for the stabilisation of the embankment.

2.5.1 Dynamic Motion of Railway Embankments, Measurement and Modelling

Dynamic motion study #1

This first study was conducted by Hall (2000) and continued in Hall (2003). The study consisted of the measurement of vibrations (with accelerometers, geophones, and

extensometers) induced by railway traffic on embankments. It focused on the response of high-speed trains at Lesgård, Sweden, for the Swedish National Rail Administration. This study conducted an analysis of the measured vibrations with an investigation into the dynamic soil properties of the site, analytical modelling and two-dimensional Finite Element (FE) and three-dimensional FE modelling of the train-induced ground vibrations.

The focus of this project was to determine the effectiveness of the analytical and two-dimensional FE modelling with respect to the much more complex three-dimensional modelling. The conclusions were; first, that analytical (Winkler) modelling could provide a good prediction of the track and embankment response, although only through a direct correlation to measured data sets. Secondly, that three-dimensional modelling could simulate the vibrations of approximately the same magnitude and shape as in actual measurements with a proper determination of soil properties; two-dimensional modelling and axisymmetric modelling could be a useful alternative to three-dimensional FE modelling when three-dimensional modelling proved too time-consuming.

Dynamic motion study #2

The second study was presented in Madshus et al. (2000), using the data from Lesgård, Sweden. The focus of this paper was the use of numerical models in the determination of the track and embankment response under train loading. This numerical modelling was undertaken to validate a computer code (TrainVib). This modelling did not, however, use the Winkler foundation model. Rather, the sub grade material is modelled as a discrete Green's function, while the rail and embankment is modelled as a FE beam element. This Green's function is solved in the frequency domain and is transformed into the displacement time domain with a reverse discrete Fourier transform. The paper provided confirmation of the ability of the analytical model to achieve a very good correlation with the measured data; and of the model's ability to accurately predict the critical velocity and the magnitude of displacement.

Dynamic motion study #3

This third study was conducted by Heelis et al. (1999) and Heelis et al. (2000). These papers detail the use of analytical (Winkler) modelling to predict the critical velocity of

the train and embankment structure, as well as the displacements under train loading. This paper details the use of modelling the beam element from the Winkler model as including not only the rail and sleepers, but also all or part of the embankment. This paper concludes that this is a powerful analytical tool for the prediction of the critical velocity and displacements.

2.5.2 Mass Stabilization of Irish Soils

This case study, presented in Hebib et al. (2003) and Hebib et al. (2004), details a study undertaken to quantify the effects of mass stabilization techniques on Irish soils, particularly peaty and organic soils. Differing types and amounts of binder agents mixed into samples were tested. This study included both laboratory testing and large scale field testing.

The process of mass stabilization in the field consists of an excavator with a special mixing tool attached. This mixing tool stirs up soil to be stabilized up to a depth of 5 m, while mixing in the binding agent. Typically, an embankment or other structure is then built on top of the stabilized soil. The method appeared to be somewhat effective, with results from one site where peaty soil was stabilized achieving a reduction of final settlement under an embankment of 28% as compared to an embankment constructed on the same peat material without stabilization.

2.5.3 Geogrid Stabilization of a Railway Embankment

This case study presented in Fenwick (1992) details the efforts to stabilize an embankment constructed over Newham Bog in England near the Scottish border so that train speeds could be increased. The paper details the reconstruction of an embankment using geotextiles and a geogrid filled with chipped rock to provide a stiffer embankment for the trains to travel over the bog. Of note, the project conducted in 1989-1990 cost £640,000 for the stabilization of a 0.75 mile section of track. The conclusions drawn in this paper are that the method was both an economical and effective solution.

The geogrid used within this case study is further presented in the literature provided by Tensar International Limited, the company which produces the geotextiles. It is claimed

that the geogrid will reduce train-induced deflections by up to 40% while also the increasing integrity of the ballast in the embankment. This increases the bearing capacity of the embankment with minimal addition of fill and reduces the maintenance required for these embankments. (Tensar 2006b)

Chapter Three: Overview of Methodology

This chapter provides the methodology employed during the collection of background and site data, the measurement of the dynamic data and the analysis of the data to determine the mechanisms involved in the deformations.

3.1 Site Background Study

In order to determine the construction of the embankments at the Adavoyle and Brackagh bog sites, and to try to determine the nature of the required maintenance, a search of NIR maintenance records and construction records was conducted. Also, interviews were held with the head infrastructure engineer and maintenance crews.

3.2 Site Survey

The survey was conducted by members of the Geography department of Queen's University Belfast, using a dGPS surveying system (Figure 3.1 and Figure 3.2 at Brackagh bog site, also, Figure 3.3 and Figure 3.4 at Adavoyle bog site). Initial surveying was conducted on September 1, 2005 at the Brackagh Bog site, and September 2, 2005 at the Adavoyle bog site. Present for both days were Conor Graham and John Meenley (both of Gridpoint and Queen's University Belfast, Geography Department), Kenny McDonald (Technician, Queen's University Belfast, Civil Engineering), and Michael Hendry (University of Saskatchewan, Civil Engineering Department).

During the course of the dGPS survey the accuracy of the data collected was monitored to ensure that the error in the measurements did not exceed ± 4 cm.

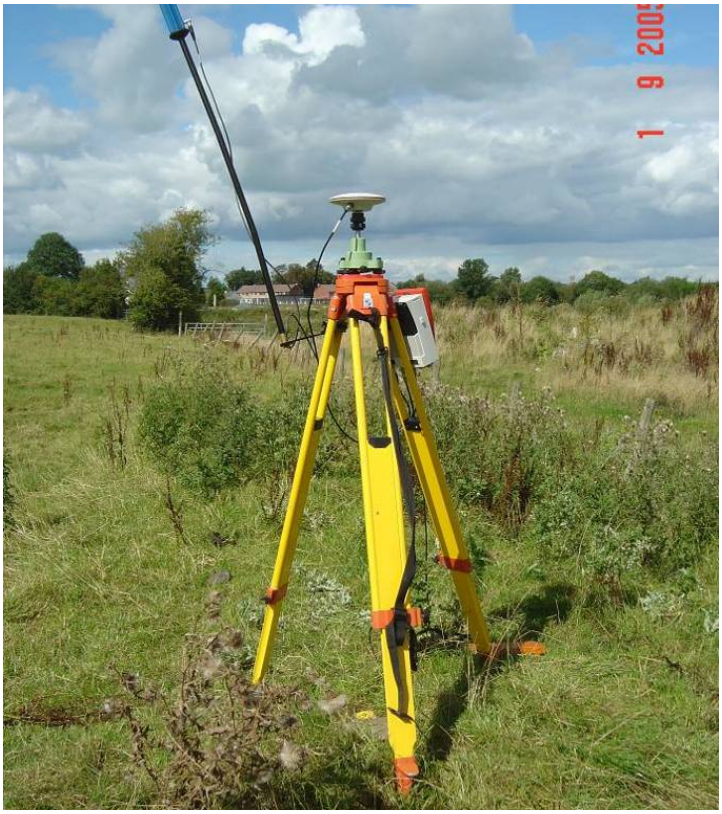

Figure 3.1: dGPS base station set up in field adjacent to Brackagh bog site.

Figure 3.2: dGPS roamer unit in use at Brackagh bog site, cross sections of embankments being taken.

Figure 3.3: dGPS base station set up in private yard adjacent to Adavoyle bog site.

Figure 3.4: dGPS roamer unit in use at Adavoyle bog site, cross sections of embankments being taken.

3.2.1 Brackagh Bog site

Three cross sections of the embankment at Brackagh bog site were detailed extending well into the surrounding terrain. Six smaller cross sections were taken of the

embankment from toe to toe at intermediate points between the larger sections. Points for the survey on the embankments were selected to define abrupt changes in elevation and to locate positions at which there was a change in material including the interface between the ballast and fill. The locations of the sleepers and the rail were also marked. While conducting the survey the passage of several trains was observed and movement of the embankment, rail and sleepers was quite noticeable.

3.2.2 Adavoyle Bog site

The same methodology as was used for the survey at Brackagh bog site was applied for the survey at the Adavoyle bog site. However, only three cross sections of the embankment were detailed due to time limitations.

The passage of several trains was also observed at the Adavoyle bog site and the movement of the embankment, rail and sleepers was not as pronounced as the movements observed at the Brackagh Bog site.

3.3 Measurement of Dynamic Displacement

It was necessary to directly measure the dynamic displacement of the rail and embankment structure under train loading. This section details the methodology employed in taking these measurements.

3.3.1 Development of Technique

An alternative method for the measurement of the displacements of the rail embankment structure was required as the commonly used measurement devices (accelerometers, geophones and extensometers) were initially too time consuming to install and NIR required measurements to be taken as soon as possible. It was later decided that these more common methods were not required due of the success of the developed measurement method and the complications and sensitivity of the data obtained with accelerometers and geophones (refer to Section 2.2).

The method developed for the measurement of the dynamic displacement involved the use of a laser and target. The laser (Figure 3.5) was set-up at a distance of 20m from the embankment in order to provide a stable reference point from which to measure the

change in elevation. The laser dot on the target provided a fixed reference point to monitor change in location of the target that was clamped to a sleeper. The target initially consisted of a grid and the relative motion of the laser beam was video taped and later transcribed frame by frame to a spread sheet (Figure 3.6).

Figure 3.5: Laser set-up on tripod in field at Brackagh bog site

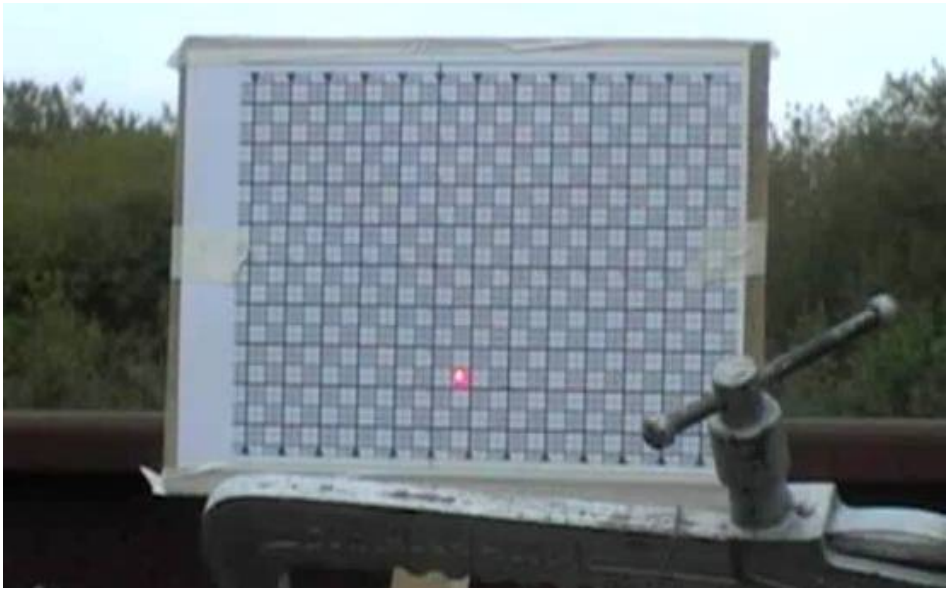

Figure 3.6: Frame from video, laser dot shown on the target in the bottom center

3.3.2 Further Development

To increase the accuracy of the measurements and the number of usable data sets, the final measurement technique consisted of an array of photo-sensors (Figure 3.7 and Figure 3.8). Each photo-sensor in the array provided a voltage output directly proportional to the amount of light energy which shone on its surface. When the laser dot or part of the laser dot was located over a photo-sensor, the voltage output of that sensor increased 10% to 100%, depending on the background light. These voltage outputs for each cell were recorded along with a time of occurrence by a data collector attached to the photo-sensor array.

An algorithm was developed in a spreadsheet to convert the voltage outputs from the photo-sensors to a displacement value. The algorithm was simple. The center of each photo cell was assigned a y-coordinate, with the y-coordinate of the center of the bottom cell as zero. During measurements the laser dot was focused so that it was smaller than the width of three photo cells, and larger than one photo cell. For all time values the photo cell most affected by the laser dot was identified from the magnitude of the voltage output. The effects of the background light were removed from the output voltage of this cell along with the photo cell above and below. The remaining output from these three cells was then used as weighting values for averaging the location assigned to the center of each cell. From the average location of the laser dot before the passage of the train, the location on photo sensor array vs. time data could be 'zeroed'.

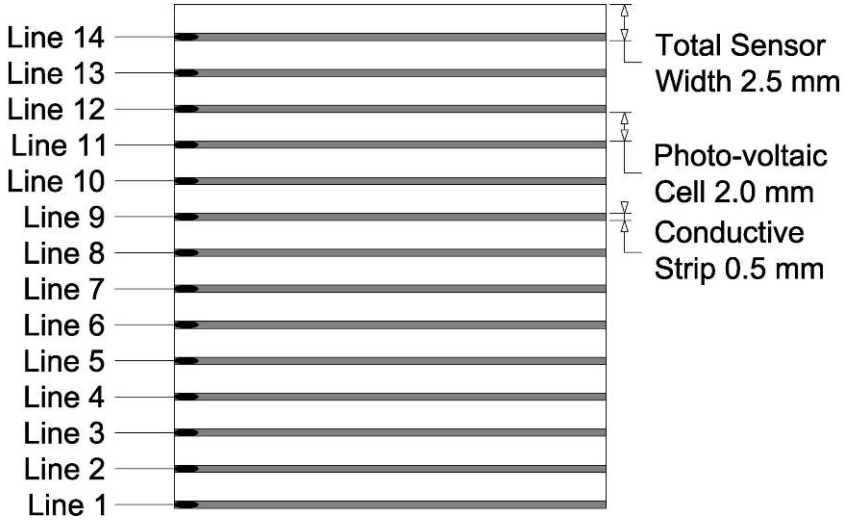

Figure 3.7: Diagram of photo-sensor array showing output lines and dimensions.

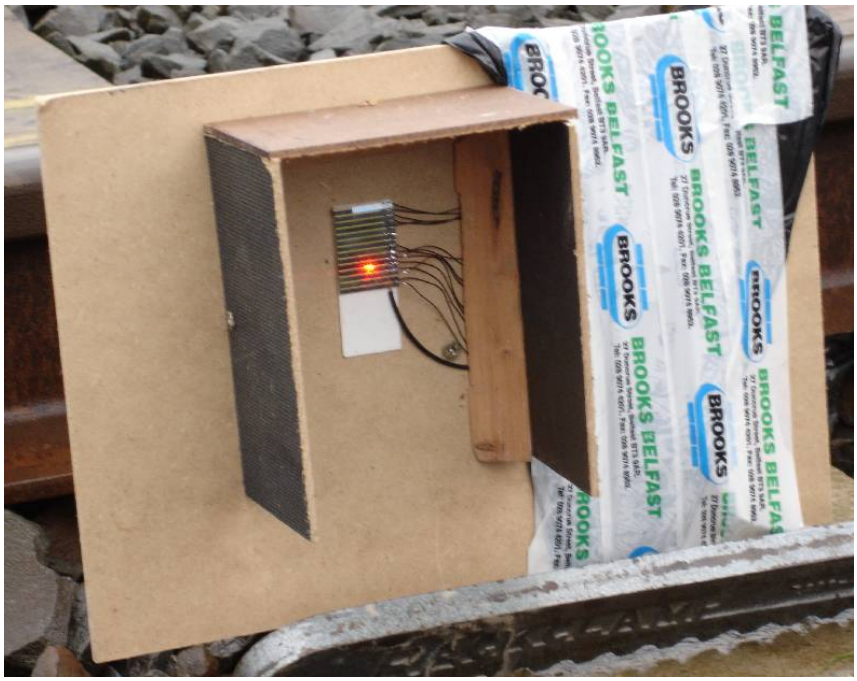

Figure 3.8: Photo-cell array clamped to sleeper at Brackagh bog site. Laser dot is visible on the photo cell array.

3.3.3 Development of Measurement Regime

Initial measurements of the dynamic movement of the embankment were conducted to determine the magnitude of displacement of the embankment under the train loading. Several other factors were identified which may affect the magnitude of deflection, including the speed at which the train was traveling, the presence and variation in depth of ponded water, and the variation and configuration of the loading.

The effect of the train speed on the magnitude of loading was of particular concern as the speed on the line had been restricted due to the dynamic displacements at both of the embankment sites. To determine the effect of the train speed numerous measurements of train deflections were taken at both sites and a train was made available for one day to run at lower speeds across the Brackagh Bog site embankment.

The presence of ponded water and the variation of the local water table were identified as possible factors, due to its effect on the saturation of the soils and the effective stresses within the embankment and the foundation material. In order to determine if

the water table was affecting the magnitude of displacement, measurements were scheduled for various times during the course of the seasons. As these dynamic measurements were taken before the instrumentation of the site, the elevation of the water table can only be described qualitatively and not with measured data. The measurements were taken in early September, October, December, and February. Further analysis of the data sets provided no apparent variation in magnitude due to the presence of the ponded water.

The variation of the configuration of the loading was difficult to observe as the Enterprise cross-border service was, for the most part, the only train to run across these sections of track. Only occasionally smaller passenger trains are used for local service in the case of special events in Belfast. These smaller passenger trains did not cross over the embankments during the course of measurements. The effects of variation of the magnitude and configuration of loading were explored through the comparison of the resulting deflections from passenger cars and locomotives.

3.4 Analysis (Modelling) of Dynamic Displacement Data

The purpose of this modelling was to establish the effects of the train speed on the magnitude of the displacement of the embankment, to quantify the strength of the embankment and sub-grade material in terms of an elastic or resilient modulus, and to explore the effects of various remediation techniques considered for these sites.

3.4.1 Analytical Modelling

The method of numerical modelling was selected for its conceptual simplicity and ability to provide a reasonable match to the measured data. This model is commonly referred to as the Winkler model. This model has been presented within the literature review (refer to Section 2.4.1) of this thesis, along with all relevant equations and derivations.

The model was first used to determine the current ability of the embankment and foundation material to support the train loading. Due to the lack of a ground investigation, the model properties of flexural rigidity and inertia were calculated from reasonably assumed values, consistent with the site history and visual inspection (depth and weight of rail, sleepers, and ballast). From these calculated values the

model was ‘fit’ to the measured data sets in order to determine a value for the spring constant. A sensitivity analysis was conducted on the model and the calculated parameters. The Winkler model was then used to evaluate the stiffness of the current embankment and the effectiveness of methods of embankment stabilization. The calculations of the model properties are provided in detail in Section 2.4.2.

3.4.2 Finite Element Modelling

The purpose of the finite element modelling was to gain some understanding of the effects of the variation of material properties used in the construction of the embankments and the foundation material, and to determine the effectiveness of the stabilization techniques on these embankments. Finite element modelling was selected for this task, because of its ability to determine stress-strain relationships and concentrations within a material continuum, and allow for the application of structural elements to the earthworks structure.

To gain this understanding, two two-dimensional models were constructed in SIGMA/W; the first a cross section of the embankment, the second a lengthwise section of the embankment. As the ground investigation is still pending there is a lack of information as to the material properties and the depth of material layers. These two finite element models were constructed, and material properties selected so as to fit the deflections of the measured data. Two different methods of stabilization were simulated to evaluate if these methods might be effective in reducing the deflection, and consequently if these options should be studied further.

Chapter Four: Data Presentation and Verification

This chapter presents all of the data collected during the course of this study. This data includes the results from the site background study; the site survey; the train configuration and loading; and the dynamic displacement measurements.

4.1 Site Background Findings

After reviewing the NIR maintenance and construction records, it became apparent that little data exists on these sites. These embankments date back to the original construction of the railway in Ireland in the mid-1800s. The construction of these embankments is assumed to be the same as contemporary embankments built over poor-quality foundation material. Historically, this type of embankment was constructed using tree trunk fascines or bundled brush placed directly on the natural ground surface, with poor-quality local peaty soils used as light weight fill, and then capped with ballast.

From the review of the maintenance and construction records, a report was found detailing the results of an embankment renewal project carried out by NIR starting in 1997 (Ferguson McIlveen 2002). This project called for the raising of the embankments with ballast by up to 1m.

This timing coincides with the introduction of the Belfast-Dublin 201 series locomotives operating on this line in 1995-1997, replacing the 111 series locomotives which had been operating since 1980. This resulting in an increase in loading from 986 kN to 1095 kN per locomotive. The 111 series locomotive was limited to a speed of 112.7 km/h (70 mph), where as the newer 201 series was limited to a speed of 144.8 km/h (90 mph).

4.2 Site Survey Data

The results of the site survey are presented as an overlay on the dGPS data on the local topography from the Northern Ireland Ordinance Survey. The dGPS data consist of cross-sections taken of both embankment sites, these sections are presented in elevation.

4.2.1 Description and Topography of Site

The purpose of the overlay of the dGPS data on the Northern Ireland Ordinance Survey maps is to locate both the embankment sites in relation to their surrounding topography, and the cross-section data to its location along the embankments.

For the Adavoyle Bog site, the local terrain has been heavily drained to utilize the land for agriculture. From observations and the Ordinance Survey map (Figure 4.1) it can be seen that the land has been segmented into agricultural plots. Deep ditches and a drainage culvert under the embankment (at mile post 65 ½) provide drainage for the site year round.

From the provided map (Figure 4.2) and from visual inspection during the site survey, the land at the Brackagh bog site is not as developed. The section of land to the west of the embankment, between the embankment and the drainage ditch is unused land, and is very soft to walk on in the summer months and flooded with up to approximately 0.4 m of water during the winter months. To the east of the embankment there are fields for grazing cattle in the summer months, and the land is flooded during the winter months with up to 0.1 m of standing water.

4.2.2 Embankment Cross-sections

The site-survey and the dGPS cross-sections provide valuable information as to the composition of the embankments due to the location of the surface interface between the ballast and the fill material. These cross-sections were used in the finite element modelling of the embankment.

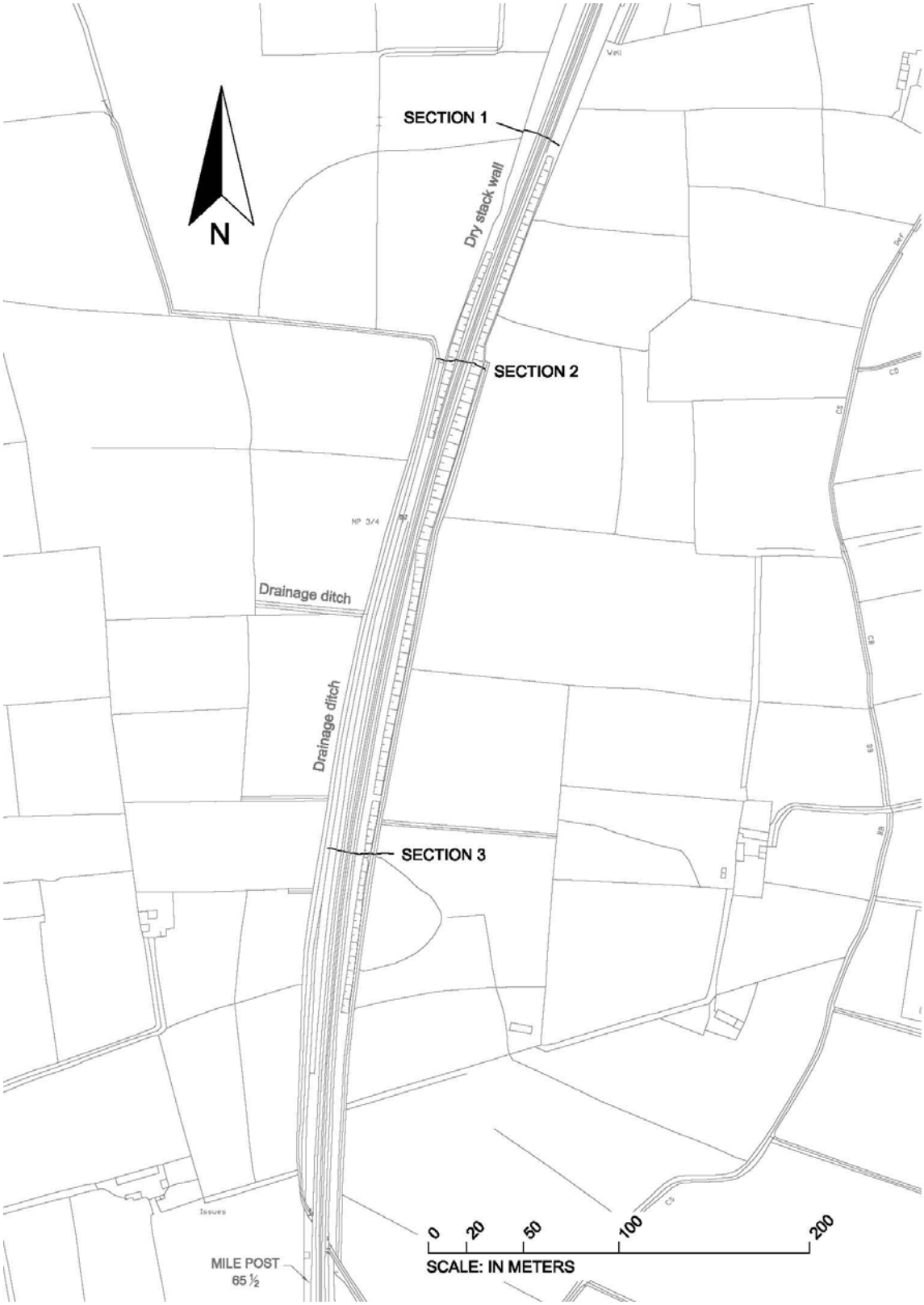

Figure 4.1: Survey sections overlaid on an Ordinance survey map of Adavoyle bog site study area.

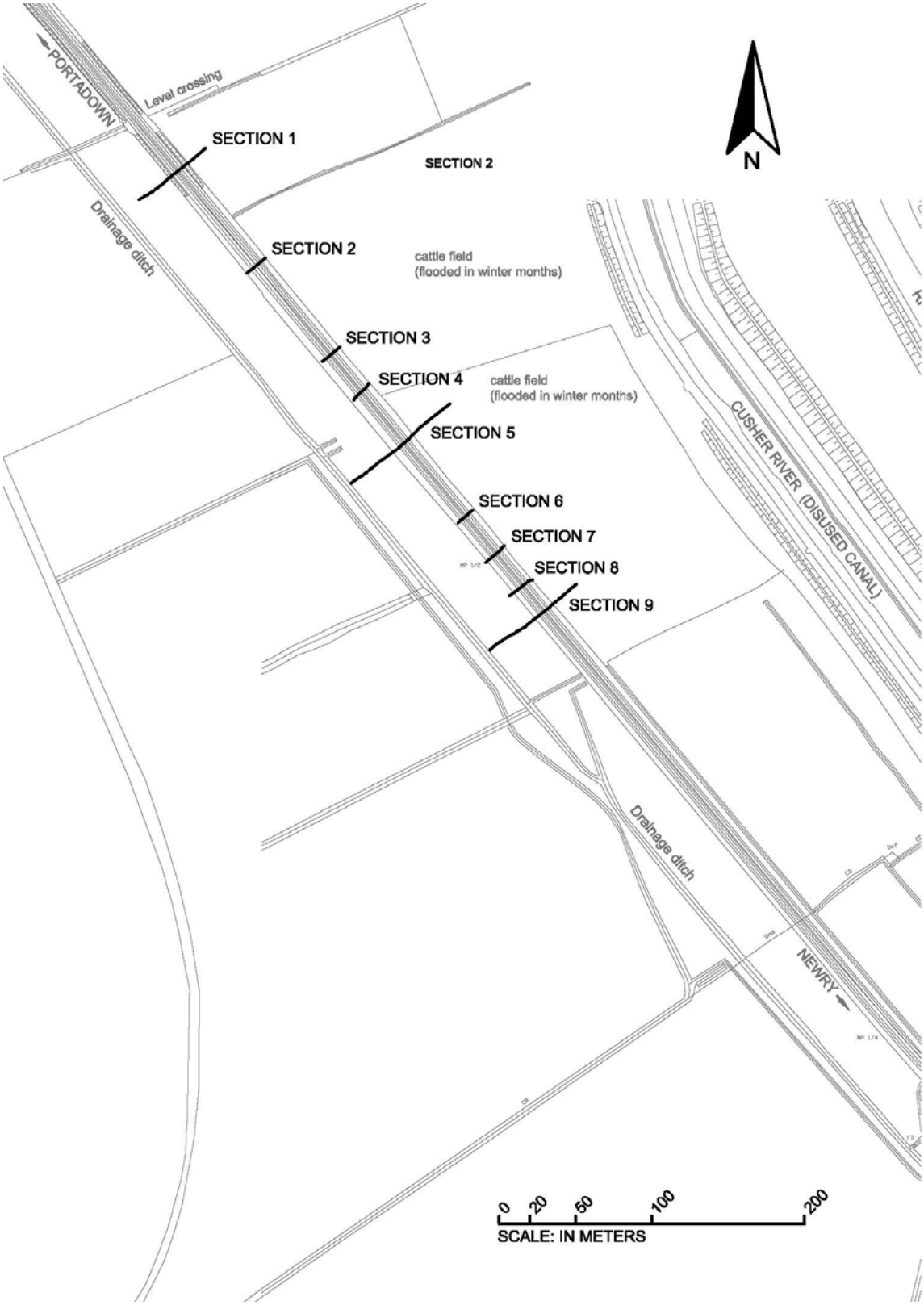

Figure 4.2: Survey sections overlaid on an Ordinance survey map of Brackagh bog site study area.

From the Adavoyle bog site cross-sections (Figure 4.3) the height of the embankment at the point where dynamic measurements were taken (Section 2, Figure 4.3) is approximately 3.4 to 4.2 m. From the location of the surface interface between the ballast and fill material, the depth of ballast can be estimated to be between 1 m and 1.4 m. From the cross-sections, both the embankment and the local terrain dip significantly in the southerly direction. The embankment center line drops approximately 3.8 m in 420 m and the local terrain approximately 4.1 m over the same distance. There is a developing camber in the embankment as it leads south into a curve in the line.

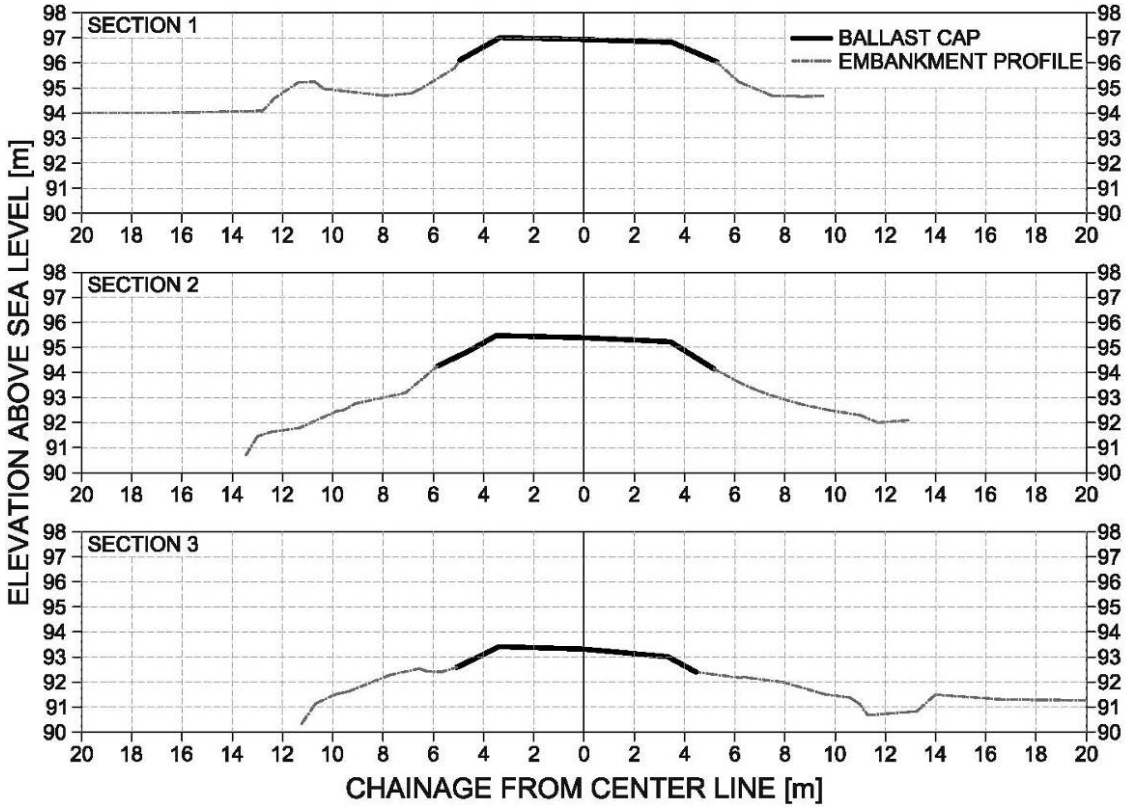

Figure 4.3: Cross-sections from Adavoyle bog site survey

From the Brackagh Bog site cross-sections (Figure 4.4) the height of the embankment at the point dynamic measurements were taken (Section 5, Figure 4.4) is approximately 2 m. From the location of the surface interface between the ballast and fill material, the depth of ballast can be estimated to be between 0.8 m and 1.1 m. From the cross-sections, both the embankment and the local terrain stay relatively constant over the section surveyed.

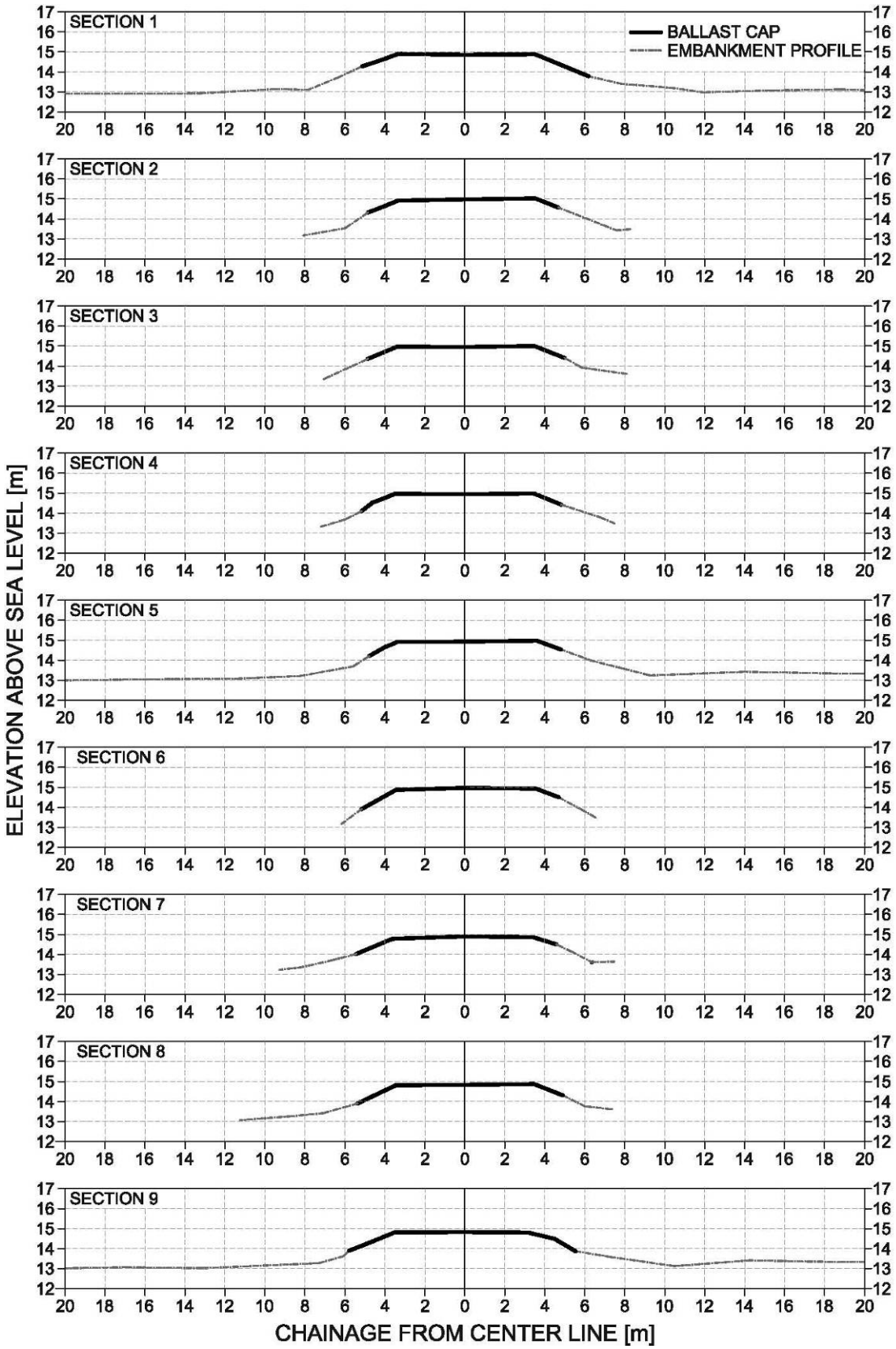

Figure 4.4: Cross-sections from Brackagh bog site survey

4.3 Train Configuration and Loading

The following data on the train configuration and loading was provided by NIR in the form of original schematic drawings from the manufacturers of the locomotives and passenger cars (GM 1993; De Deitrich 1994; De Deitrich 1995). The data is critical for the analysis of the passage of trains over the embankment site as it provides both the frequency and magnitude of loading.

Northern Ireland Railways owns two locomotives for the Enterprise service. These locomotives are General Motors 201 class, and are constructed to both push and pull passenger cars. The first of these locomotives were introduced by 1994. Iarnród Éireann (Irish Rail) also owns two 201 class locomotives used for this service. The passenger cars and control cars were both manufactured by De Dietrich Ferroviaire, with Northern Ireland Railways and Iarnród Éireann both sharing ownership. A typical train consists of a locomotive pushing or pulling six or seven passenger cars and one control car. Typically the locomotives push the cars to Dublin and pull the cars to Belfast. The spacing of the axles for all components of the Enterprise train is provided in Figure 4.5. The axle loads are provided in Figure 4.6. These axle loads are for empty passenger cars and locomotives. Passengers and fuel represent a maximum increase in loading of 13 % (5500 kg) for the passenger cars and 3.5 % (4500 L of diesel) for the locomotives.

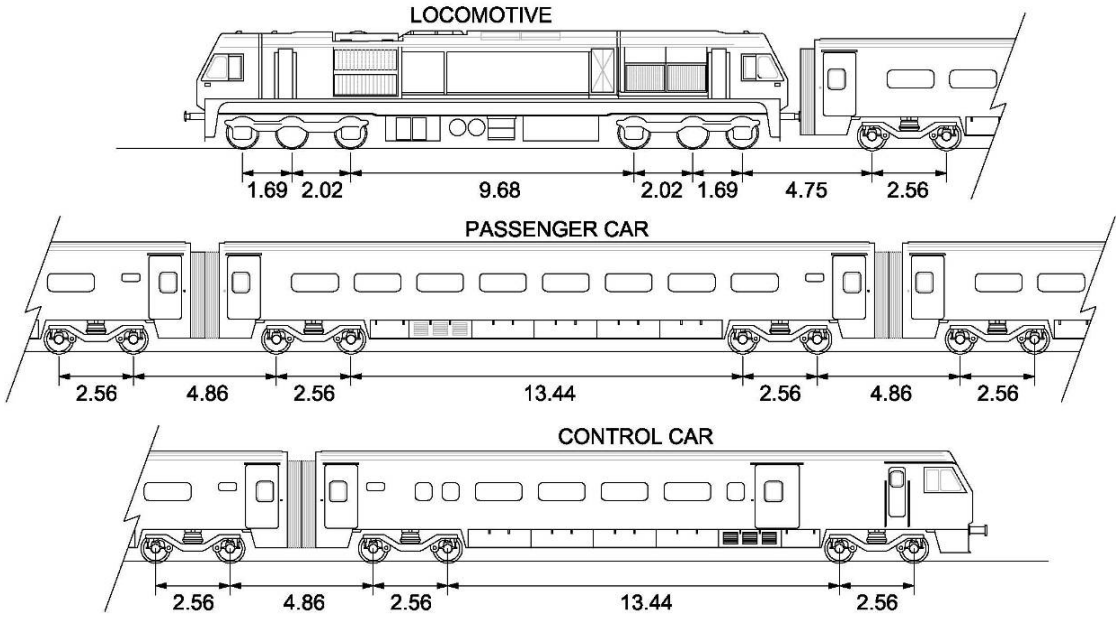

Figure 4.5: Spacing between axles for all components of Enterprise trains (all dimensions in meters) (after GM (1993), De Deitrich (1994) and De Deitrich (1995))

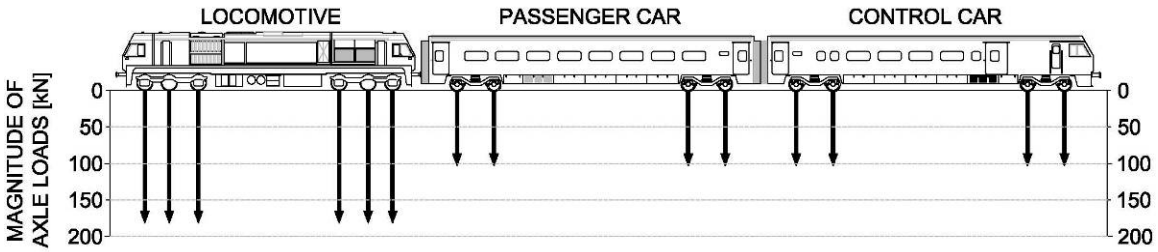

Figure 4.6: Axle loads for all components of Enterprise trains. (after GM (1993), De Deitrich (1994) and De Deitrich (1995))

4.4 Dynamic Data Sets

The data sets collected from the Adavoyle bog and Brackagh bog sites with the photo-sensor targets provided high resolution (measurements taken at 15 Hz for the video data to 20 Hz for the photo-sensor array) measurements of displacement versus time. All data sets are summarized and presented in their displacement versus time form in Appendix A. Figure 4.7 is an example of a typical data set taken in the course of the study. Two large displacements occur under each of the locomotive bogies, followed or preceded by smaller displacements from the passage of the passenger car bogies, are typical of all data sets.

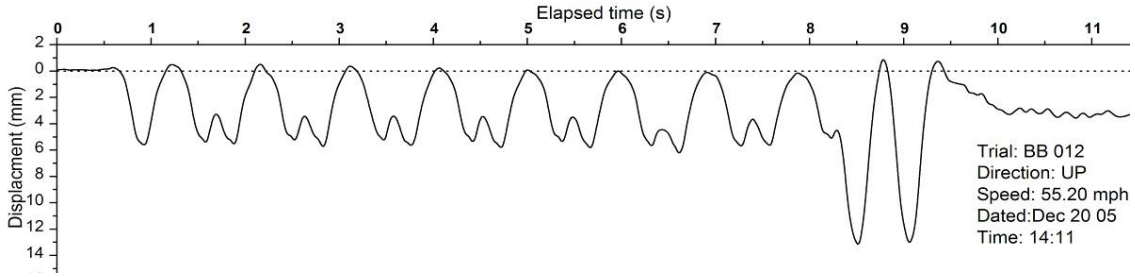

Figure 4.7: Typical Brackagh bog data set after conversion from voltage outputs to displacements. Plotted in displacement (mm) vs. time (s)

In the process of gathering these data sets, after the train has passed, the laser was immediately shut off and the target removed before the data collector was shut off, this was done in order to move to the other line on the embankment, where another train was due within minutes. This quick take down of the measurement equipment was necessary to maximize the number of readings but often left inconsistencies at the end of the data sets as shown in Figure 4.7.

The quality of these data-sets is apparent when compared to the applied loading as shown in Figure 4.8. The data set presented in Figure 4.8 was recorded at the Brackagh bog site for a train travelling at 88.8 km/h (55.2 mph). It was then converted using the train speed to a displacement (mm) versus distance along train from the leading bogie (m). From this comparison the direct response of the embankment to the axle loads of the train becomes visible.

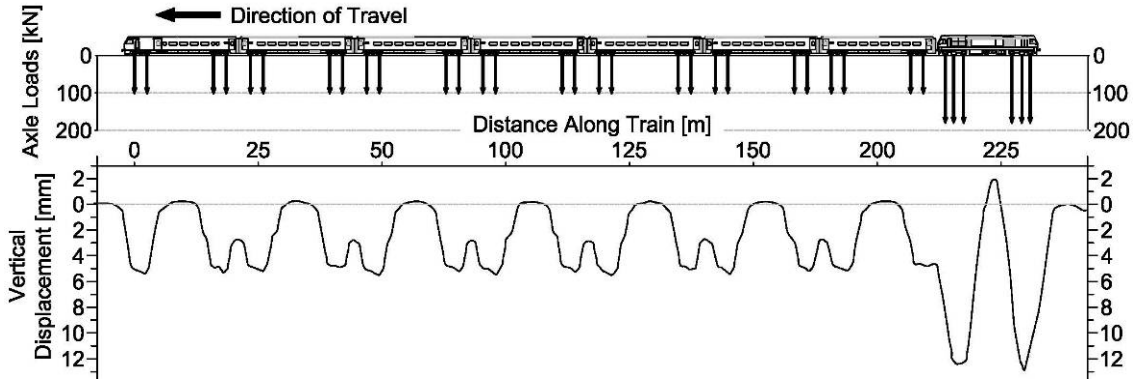

Figure 4.8: Comparison of applied axle loads from train to dynamic displacement data taken at Brackagh bog site.

The data sets taken from these embankment sites are comparable, qualitatively, to data sets from contemporary studies. Figure 4.9 and Figure 4.10 show data sets from the case studies presented in section 2.5 (Kaynia et al. 2000; Hall 2003). The common traits of the data sets are the well defined response of the loading from individual bogies and the variation in response to different loading (locomotive vs. passenger car displacements).

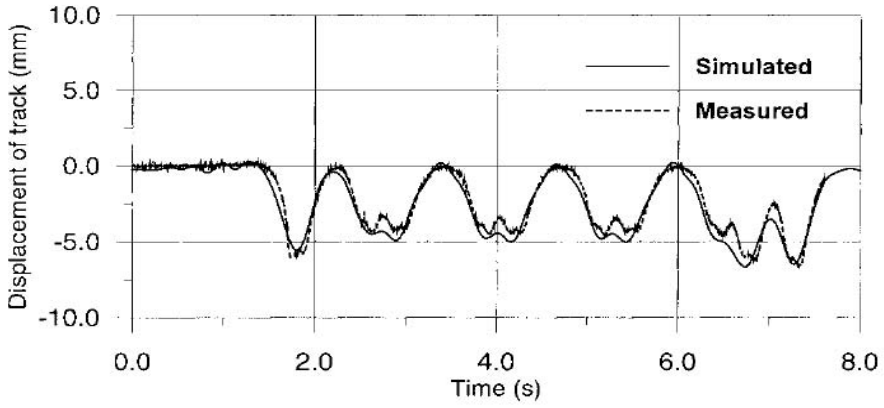

Figure 4.9: Displacement of rail structure measured under train loading (Kaynia et al. 2000)

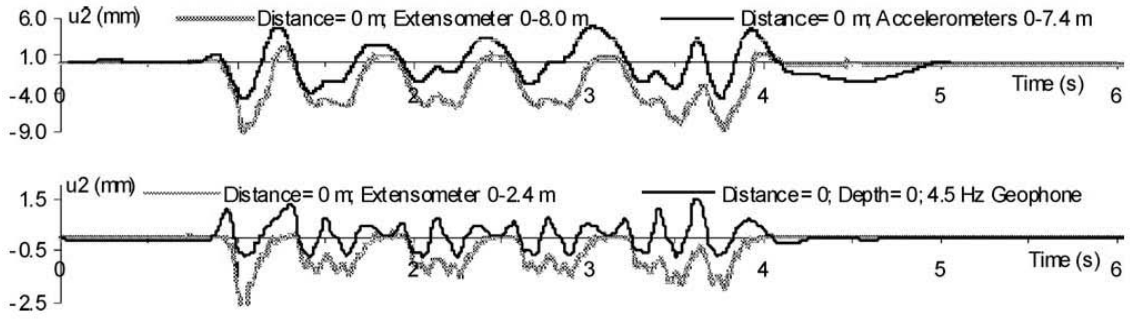

Figure 4.10: Displacement of rail structure measured under train loading, measured with extensometers, accelerometers and geophones (Hall 2003)

Figure 4.10 from Hall (2003) presents data sets from two extensometers with anchors at depths of 8 m and 2.4 m, an accelerometer buried at a depth of 7.4 m, and a 4.5 Hz geophone on the surface of the embankment. The measured deflections measured by the extensometers bear a strong resemblance to the data sets measured during the course of this study, specifically with only small upwards deflections between bogies; both the extensometers and the photo-sensor array directly measure the displacement. The data from the accelerometers and the geophones show large upwards deflections in the same order of magnitude of the downwards deflections. The accelerometers and geophones are much more prone to error, during the conditioning and baseline correction of the analog output; these errors are magnified during the integration of the acceleration curve to a displacement curve (Hall 2000).

Displacements of up to 19mm underneath the locomotives were measured at the Brackagh bog site. Similar measurements taken at Adavoyle bog site yielded maximum displacements of 10 mm.

Mean values for the displacement which occurs under a locomotive bogie and under a passenger car bogie were determined from each data set. This data is plotted below in Figure 4.11 versus train speed.

Figure 4.11 shows a trend of increasing displacement with increasing train speed. This is illustrated by linear trend lines applied for each data set. As noted previously the displacements at Adavoyle bog site are significantly smaller than those found at the

Brackagh bog site. Also apparent, is that the trend of increasing displacement with train speed is stronger at the Brackagh bog site than at the Adavoyle bog site.

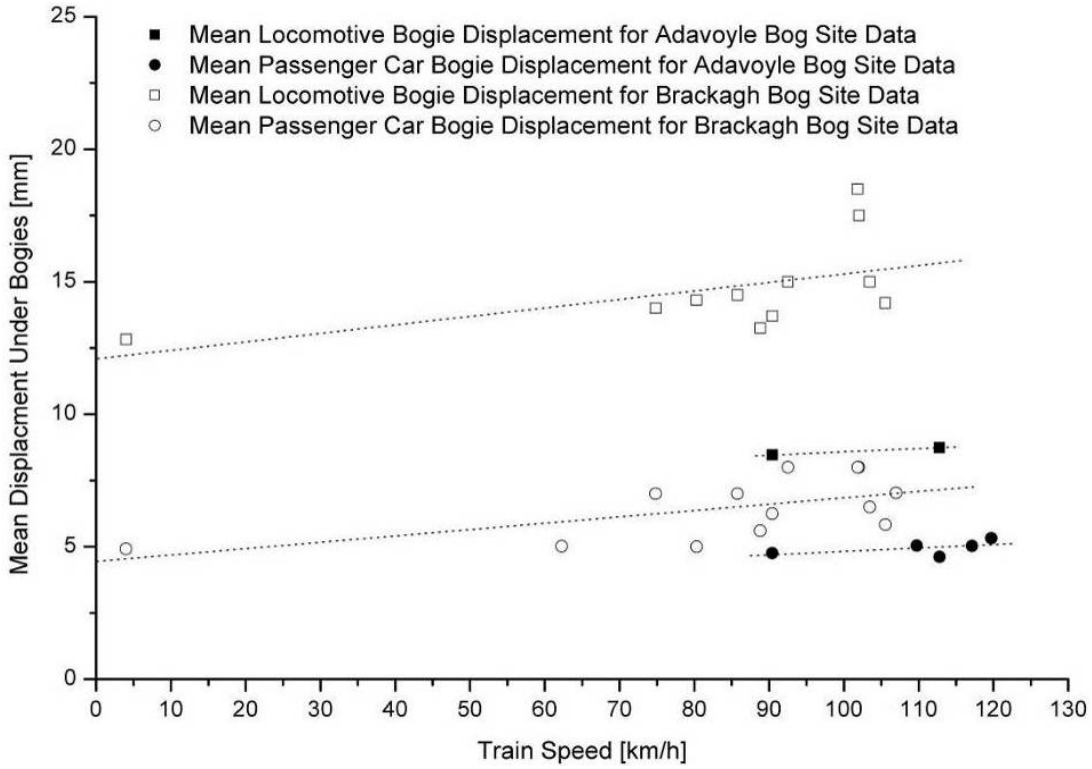

Figure 4.11: Plot of mean measured displacements under bogies vs. train speed with linear trend lines. (contains data sets measured with both video/target and photo-sensor array methods)

The trend from Adavoyle bog and Brackagh bog sites shown in Figure 4.11 is similar to the trend shown in Figure 4.12 taken from Kaynia et al. (2000). Both data set show in increasing downward deflection from train loading for increasing train speed. Figure 4.12 also shows a trend of increasing upward displacement from increasing train speed; however, this is not evident in the data sets from Adavoyle bog and Brackagh bog sites. From Section 2.4.1 the Winkler model predicts an inertia driven upwards displacement increasing from zero, in the static case, to a maximum at the critical velocity. As this is not evident in the data it is an indicator that the train speeds at which the measurements are taken are not near the critical velocity of the embankment structures.

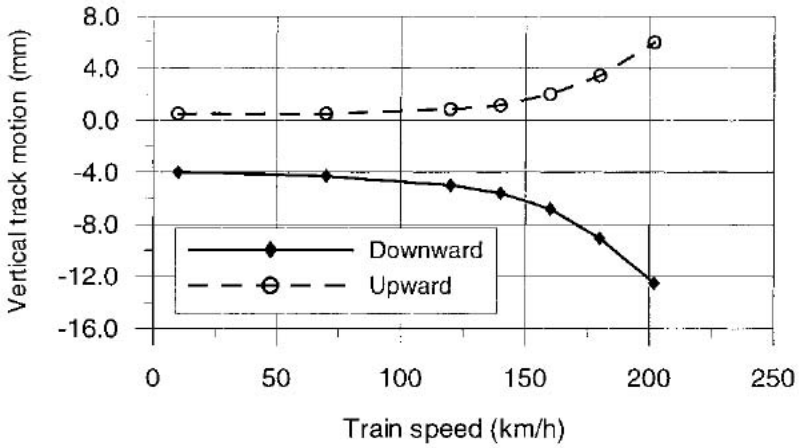

Figure 4.12: Average measured vertical displacement of track for different train speeds (Kaynia et al. 2000)

4.4.1 Measurement Error

As with any measurement technique there is inherent error. As these measurements were taken with an instrument developed in the course of this study with no history of use, the error itself was investigated in this study. Points of error were determined for both the video-based measurements and the photo-sensor array measurements.

Video Data sets

For the video base measurements, the actual recording of the laser dot moving with respect to the target is considered to be accurate. The sampling rate of 15 Hz provides a low resolution which may not record the peak deflections underneath the axle loads used later in the modelling of this data. The source of error of greatest concern is the reading and interpretation of the video footage. A large quantity of the data sets recorded were simply unreadable due to the lighting conditions. Frames recorded during large vertical velocities of the target appear blurry and require interpretation. This high velocity occurs between maximum and minimum displacement values and not at the peaks themselves. The accuracy of reading the frames under the best circumstance is limited. The smallest interval in the gridlines on the target is 5 mm, and the location of the laser dot is estimated, but it is reasonably accurate to determine whether the center of the dot is in the top half or bottoms half of this interval.

All of these sources of error reduce the confidence in these data sets; however, the trends and characteristics of the data sets are true, and the repetitive nature of the loading provide a number of bogie displacements under similar loading for comparison within each data set. The only quantifiable error is the reading error and this is estimated to be ±2.5 mm or half the smallest grid line interval.

Photo-sensor array data sets

For the measurements taken with the photo-sensor array, the errors were much simpler to quantify. Three major sources of error where identified: (1) the movement of the laser mounted tripod with the passage of the train, (2) the ability of the sensors to accurately pick up the effects of the laser dot, and (3) the conversion of the output of the sensors to a displacement vs. time data set.

To determine the influence of the movement of the laser, a tripod with the photo-sensor array mounted atop was placed at the location of the laser set up during the normal measurements. The laser was moved a further 20 m from the embankment and measurements were made during the passage of a train. The measured displacements were minimal, in the order of a tenth of a millimeter, and it was not possible to determine if this movement was in fact from the train or simply other effects such as wind on the tripod.

The ability of the sensors to accurately record the position of the laser dot and the ability of the algorithm to accurately convert the output of the sensors to a displacement vs. time data sets were both indiscernible from one another. The net effect of these two sources of error was however measurable.

The photo-sensor array was placed into a frame in the laboratory which allowed it to be moved vertically with a micrometer at 1 mm intervals. This movement was recorded manually from the micrometer and by the photo-sensor array. From the resulting data it was possible to calibrate the photo-sensor array and computer algorithm output and measure the error from these measurements. The resulting data sets for the photo-sensor data and micrometer data are plotted together in Figure 4.13.

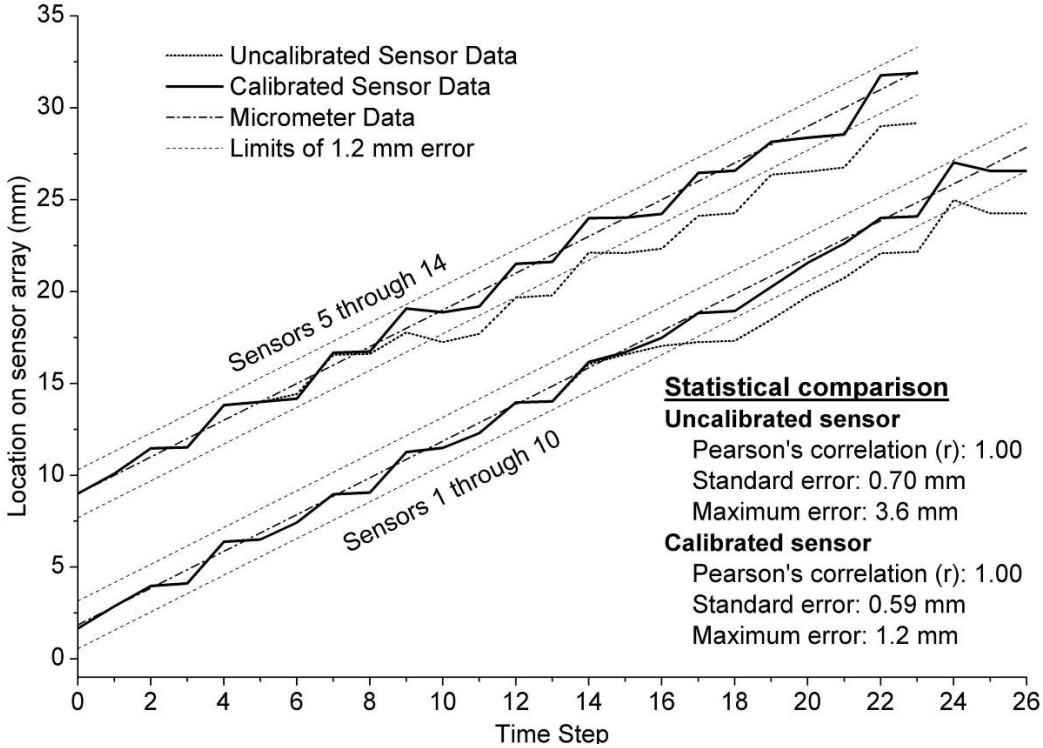

Figure 4.13: Results of Calibration of photo-sensor array and computer algorithm with micrometer.

The sensor array exceeds the length which the micrometer could measure. The measurements were thus conducted in two parts, measurements over photo-sensors 1 through 10 and for photo-sensors 5 through 14. Both sets of measurements show discontinuities in the measured data at sensor 8, with photo-sensor array data from above and below sensor 8 data running parallel to the micrometer measurements. As this error is consistent for both sets of measurements it is not considered to be errors from the operation of the calibration equipment, and is assumed to be the result of inaccuracies in the geometry in the production of the individual cells, and their assembly by hand into an array. A calibration factor was added to the algorithm to correct for the error at sensor 8; the results of this correction are shown in Figure 4.13.

The net error in the ability of the sensors to accurately pick up the effects of the laser dot and the ability of the algorithm to accurately convert the output of the sensors to a displacement versus time data after calibration is ± 1.2 mm, with a standard error of ± 0.59 mm and a Pearson's correlation (r) of 1.00.

The resolution of the photo-sensor array data still allows for the possibility that the peak deflections may occur in an interval between measurements, and thus not be recorded. This is much less likely as the frequency of measurement is 20 Hz. From the examination of the data sets this is likely to be approximately ± 0.2 mm for locomotive loading and extremely small for passenger car loading.

The photo-sensor array data sets provide more accurate measurements than the video data sets, and the error is more quantifiable. A range of confidence for the photo-array data is estimated to be ±1.5 mm.

4.5 Spectrum Analysis Plots

Spectrum analysis plots provide another plane in which to compare the measured displacement data to the applied loading.

The Fast Fourier Transform is very sensitive to the amount of extra data on either side of the displacements due to the train loading. The transform adds an infinite amount of sinusoidal curves with differing phase angle, magnitude and frequency that sum to zero for times when the train is still approaching or after it has passed. This has the effect of making the characteristic frequency domain pattern of the data indiscernible. To limit this result, the data set is cropped on either side of the train passage in order to maximize the features visible in the spectrum analysis plot.

Figure 4.14 and Figure 4.15 are examples of typical data sets taken in the course of the study plotted in the frequency domain. Both data sets show similar characteristics; however, they are occurring at different frequencies. This is due to the differing train speeds of the data sets, with higher train speeds increasing the frequency at which the characteristics occur. Plotted along with the data sets in Figure 4.14 and Figure 4.15 are the frequency domain plots of the train loading applied to the embankment (as transmitted by the rails and sleepers). This loading was calculated using the Winkler model, as presented in Section 2.4.1, and calculated with the parameters used in the analytical modelling which can be found later in this thesis (Section 5.1.2). This match of the data sets to the applied loading further confirms the quality of these data sets.

Typical of all frequency data sets is the very close match to the train loading when plotted in the frequency domain. The sources of the characteristic peaks are presented in Figure 4.16. A noticeable difference between the train loading and the data set plotted in the frequency domain is that there is reduction in the effect of the loading on the measured sleeper/embankment displacement with increasing frequency. The probable causes of this frequency dependency are presented in Sections 2.1.1 and 2.1.3; these include: the material damping of the earthen structure which dampens higher frequency loading, and the stiffness of the structure spreading out the load, and thereby diminishing the effect of the higher frequency loading from individual axles.

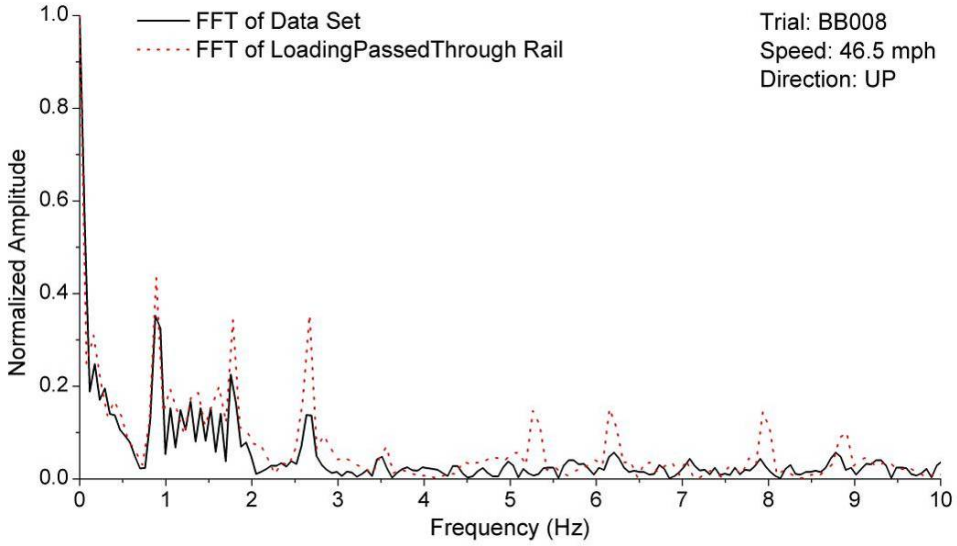

Figure 4.14: Frequency domain plot of Brackagh bog data set BB008

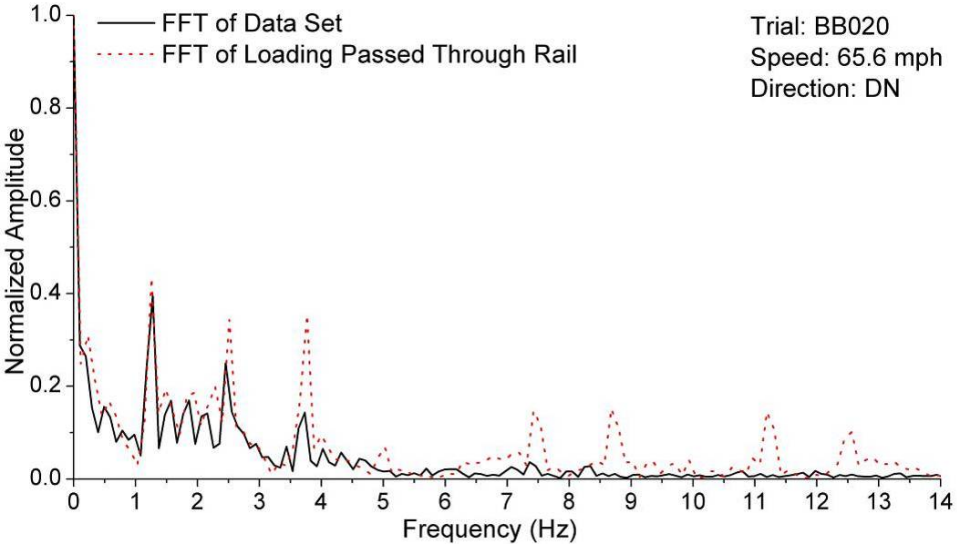

Figure 4.15: Frequency domain plot of Brackagh bog data set BB020.

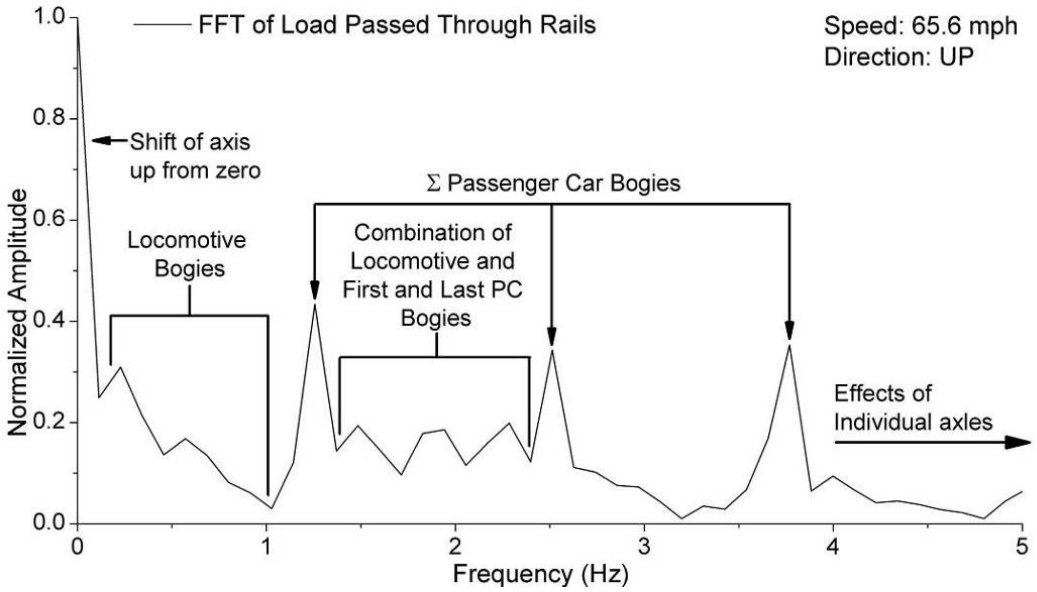

Figure 4.16: Causes of characteristic peaks in train loading frequency domain plot.

Chapter Five: Analysis and Interpretation

This chapter presents the analyses conducted on the data collected during the course of this study. This includes both the analytical modelling conducted to determine the effects of train speed and cause of the large train-induced displacements and the analytical and finite element modelling of the effectiveness of possible embankment stabilization methods.

5.1 Analytical modelling

The purpose of this modelling was two-fold; to establish the effects of the train speed on the magnitude of the displacement of the embankment, and to quantify the stiffness of the embankment and sub-grade material in terms of an elastic (resilient) modulus.

5.1.1 Winkler Model

The method of numerical modelling was selected for its conceptual simplicity and ability to provide a reasonable match to the measured data. The train is simplified to a series of point loads moving at constant velocity along an infinite beam supported on a discrete visco-elastic foundation (Kenny 1954; Frýba 1972). This model has been extensively presented within the literature review (Chapter Two) of this thesis, along with all pertinent equations and derivations.

5.1.2 Selection of Material Properties

There are a number of different methods used to determine the values for the model variables. The system can be modelled in two different ways: with the beam element comprised solely the railway tracks, and with the embankment and sub-grade as the visco-elastic foundation (Hall 2000); or with part or the entire embankment included in

the beam element, with the remaining embankment and sub-grade as the visco-elastic foundation (Heelis et al. 1999).

In the first method the beam element comprises solely the railway tracks, and the visco-elastic foundation consists of the embankment and sub-grade. The following values were calculated for this case: $EI=3.92MNm^2$, $\rho A=612.98kg/m$ (this includes sleepers along with the tracks). From these values, the passage of a train can be modelled for both sites, as the type of rails and sleepers used are the same. A foundation stiffness (k) can be calculated for each site, from the correlation of the magnitude of the displacements to the data sets. These were found to be 8.99 MPa for the Adavoyle bog site and 5.88 MPa for the Brackagh bog site.

The resulting modelled displacement versus time curves are overlaid on an actual data set taken at Brackagh bog site in Figure 5.1. This model is shown to be a poor representation of the data set. From Figure 5.1 it is apparent that this method grossly underestimates the EI value for the system. Hall (2000) noted similar discrepancies when this approach was used and noted that a factor of three had to be applied to the EI value in order to produce a 'satisfactory' match to the measured data sets. An increase of the EI value by a factor of 3 had limited impact on the results from this study and a much higher increase in the beam stiffness is required to produce satisfactory results.

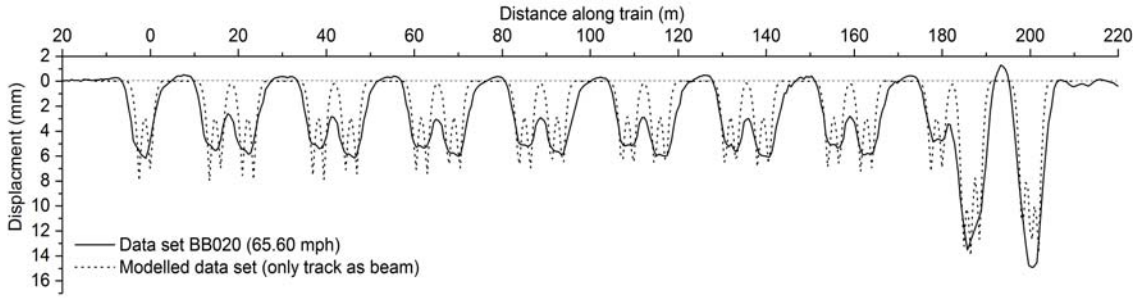

Figure 5.1: Modelled train displacements with parameters taken from model of beam as railway track and sleepers only, overlaid on actual data set taken at Brackagh bog site.

This large underestimation of the beam stiffness is due to the assumption made in the conceptualization of the model that the rails are the sole mechanism of spreading the load over the length of the embankment. This is not the case, as the embankment, and to a smaller degree, the foundation will act to further spread out the loading.

The second method was used to obtain results which provide a closer match to the measured values. As the embankment contains poor-quality fill, and is capped with ballast, the model was modified to include the ballast cap as part of the beam element. The poor-quality fill material remains as part of the visco-elastic foundation. This is similar to the methodology employed in Heelis et al. (1999). From the visual inspection of the railway embankments and the sections taken during the site survey (Section 4.2), the depth of the ballast is approximately 1.2 m at the Adavoyle bog site and 1m at the Brackagh bog site. The Winkler conceptual model using this method is illustrated in Figure 5.2.

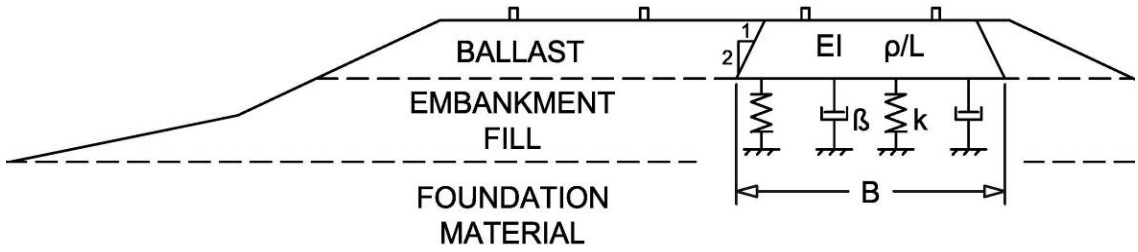

Figure 5.2: Beam element including ballast cap, poor-quality fill and sub-grade to be modelled as visco-elastic foundation

The properties calculated, using this conceptual model, were: EI=121.71 MNm^2, ρA=8269.0 kg/m (including sleepers, track and ballast) for the Adavoyle bog site and EI=71.21 MNm^2, ρA=6793.0 kg/m (including sleepers, track and ballast) for the Brackagh bog site. From the correlation of the magnitude of the measured displacements, the value for the foundation stiffness (k) can be estimated to be 5.56 MPa for the Adavoyle bog site and 4.07 MPa for the Brackagh bog site. This provided a very close 'fit' to the individual data sets as can be seen in Figure 5.3 through to Figure 5.6 for Adavoyle bog site and Figure 5.7 through to Figure 5.11 for Brackagh bog site.

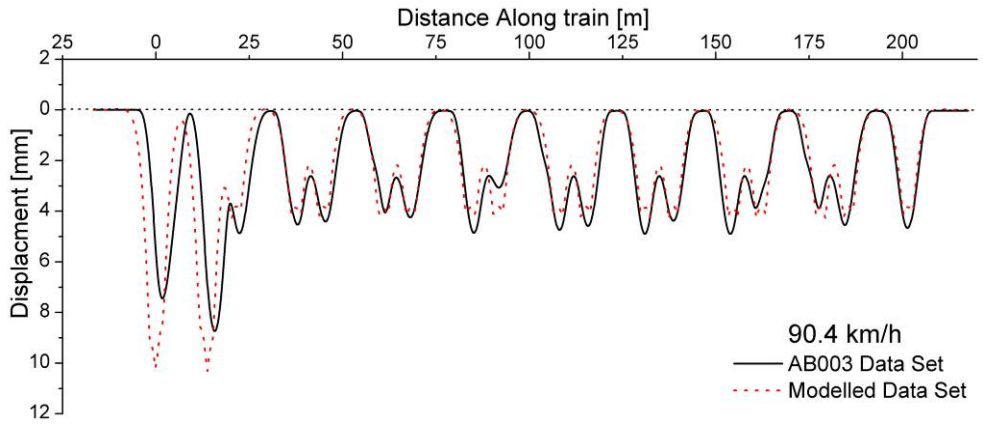

Figure 5.3: Comparison of measured displacements recorded at Adavoyle bog site for a train traveling 90.4 km/h overlaid with same event modelled.

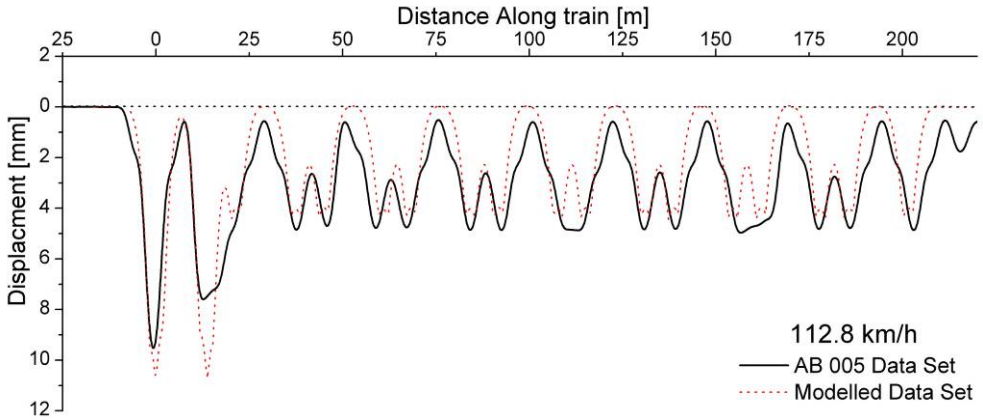

Figure 5.4: Comparison of measured displacements recorded at Adavoyle bog site for a train traveling 112.8 km/h overlaid with same event modelled.

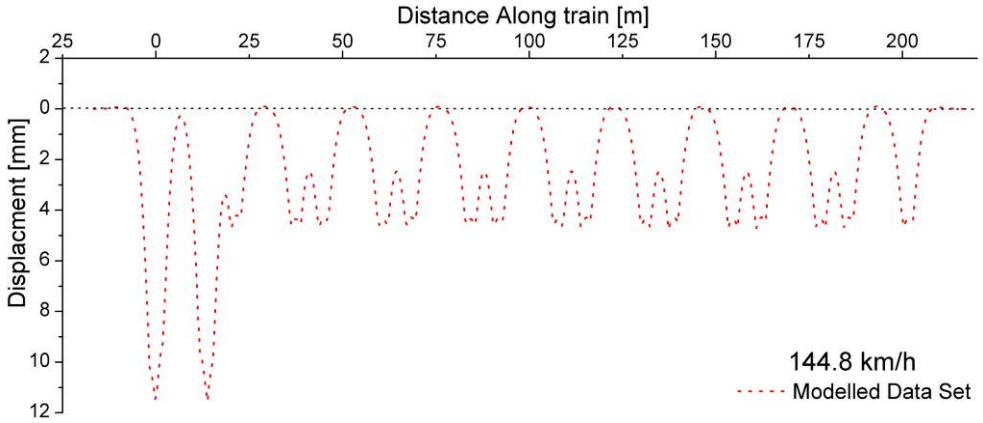

Figure 5.5: Modelled displacements of a train traveling 145 km/h (90 mph) at Adavoyle bog site. (maximum train speed on NIR lines)

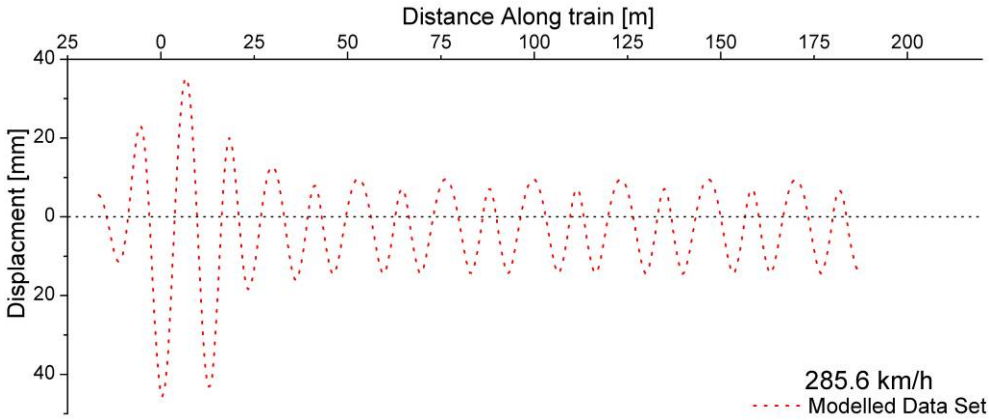

Figure 5.6: Modelled displacements of a train traveling at 285.6 km/h (modelled critical velocity of rail/embankment structure) at Adavoyle Bog site.

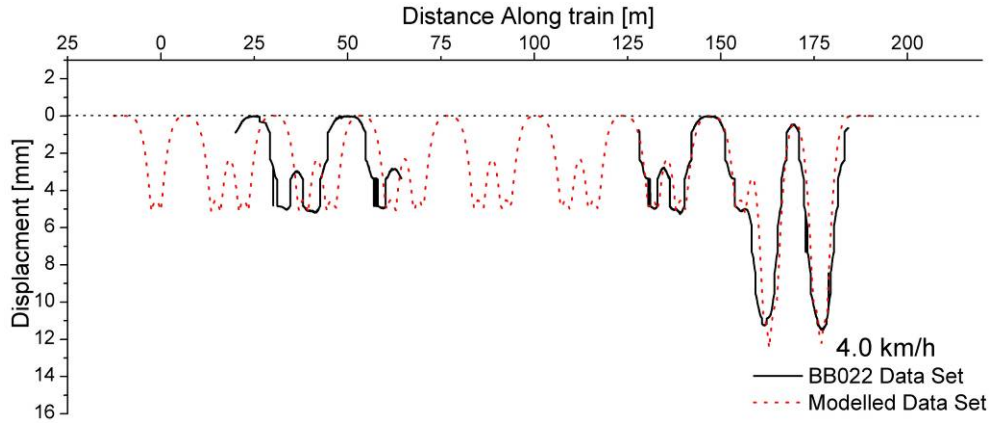

Figure 5.7: Comparison of measured displacements recorded at Brackagh bog site for a train traveling 4 km/h overlaid with same event modelled.

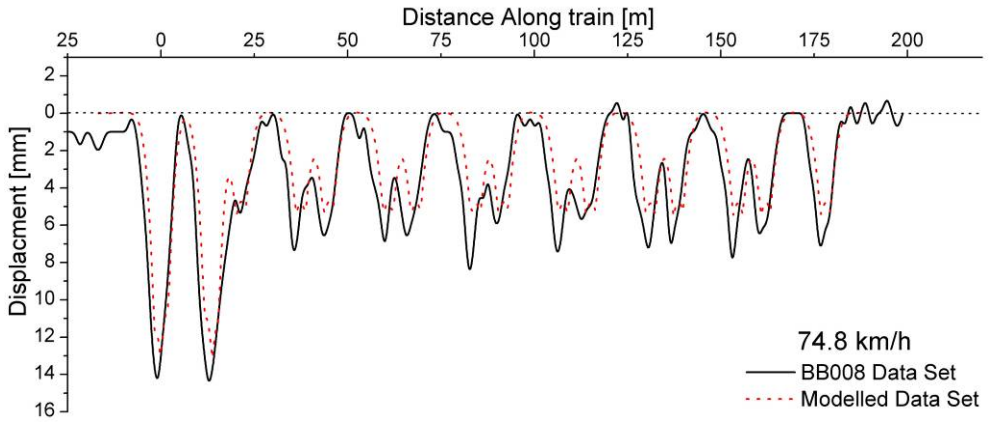

Figure 5.8: Comparison of measured displacements recorded at Brackagh bog site for a train traveling 74.8 km/h overlaid with same event modelled.

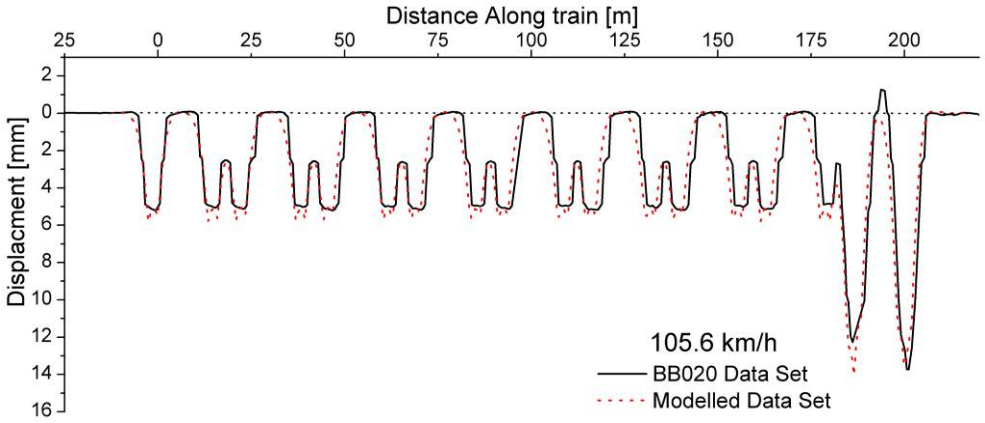

Figure 5.9: Comparison of measured displacements recorded at Brackagh bog site for a train traveling 105.6 km/h overlaid with same event modelled.

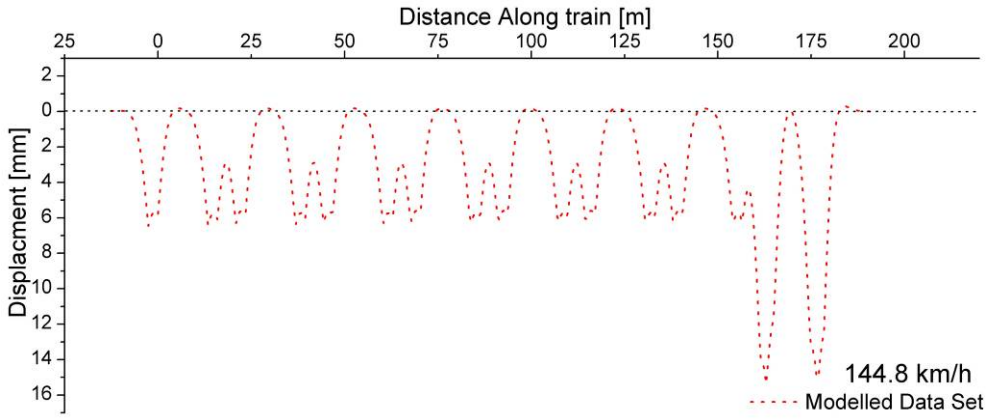

Figure 5.10: Modelled displacements of a train traveling 145 km/h (90 mph) at Brackagh bog site. (maximum train speed on NIR lines)

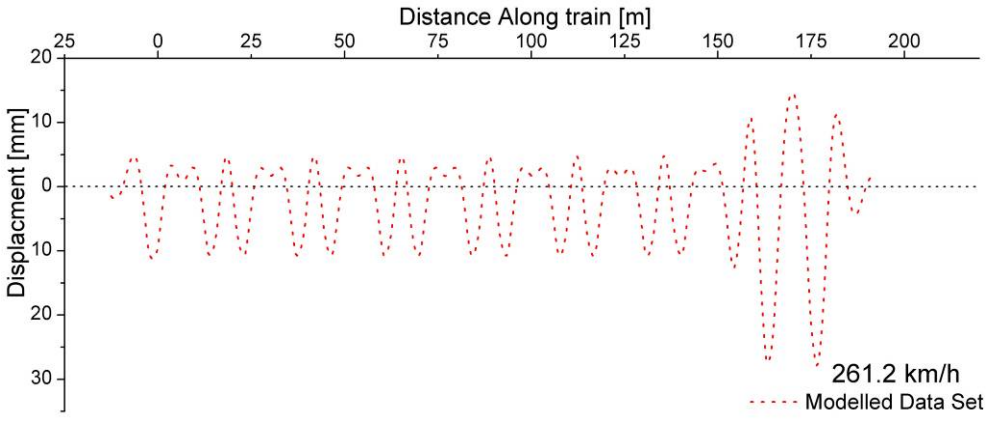

Figure 5.11: Modelled displacements of a train traveling at 261.2 km/h (modelled critical velocity of rail/embankment structure) at Brackagh Bog site.

The results from this model, using the parameters given above, are plotted for all of the data sets for Adavoyle bog site (Figure 5.12) and for Brackagh bog site (Figure 5.13). The modelled data is plotted for damping ratios (β) of 5%, 10% and 20%. Notable from this is that the value of the critical velocity is calculated to be 285.6 km/h (177.5 mph) for Adavoyle bog site and 261.2 km/h (162.35 mph) for Brackagh bog site. These values are much higher than the train speeds for the measured data sets and the maximum operating speed of NIR trains (145 km/h or 90 mph). The model also shows that the damping ratio has little effect on the modelled displacements within NIR operating speeds.

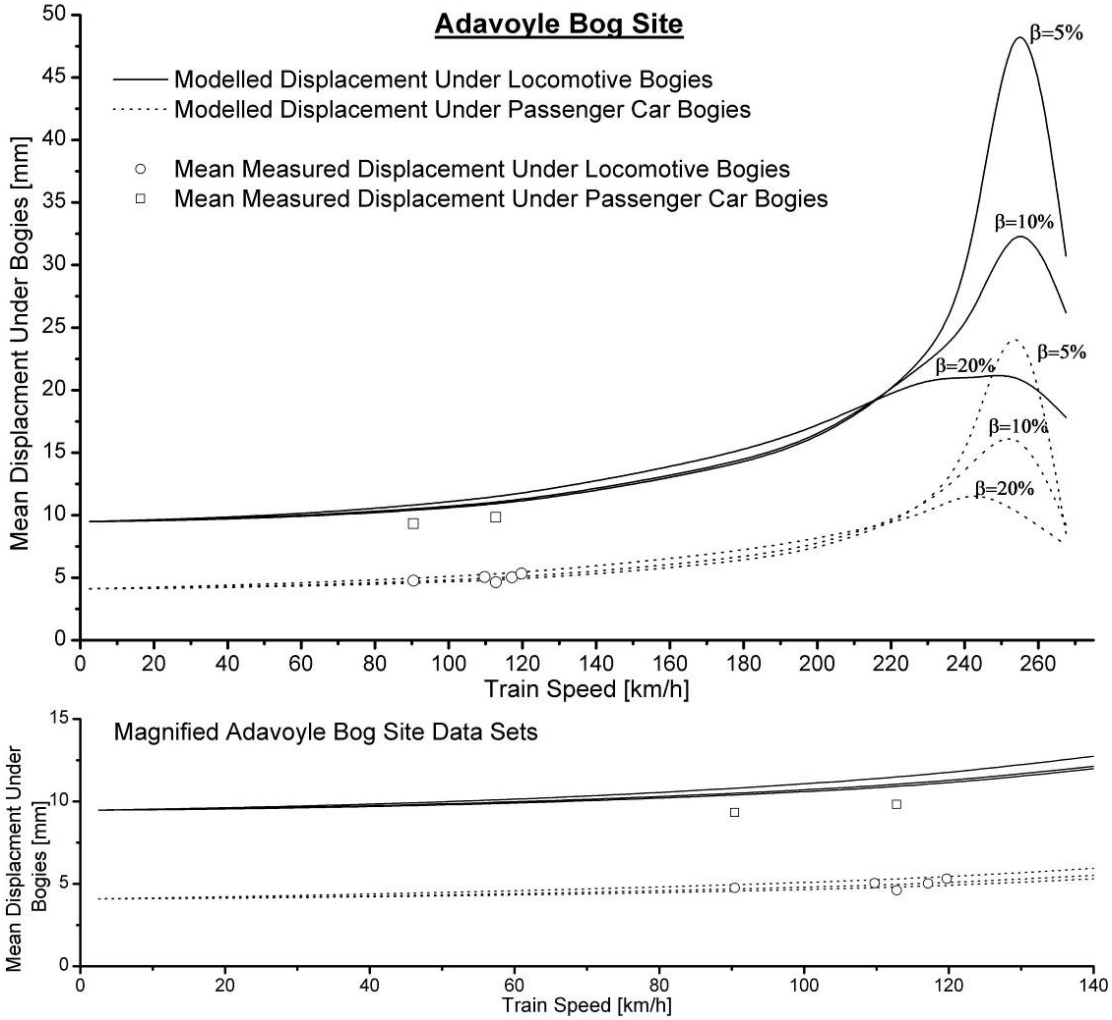

Figure 5.12: Results from modelling in Train speed vs. displacement domain at the Adavoyle bog site.

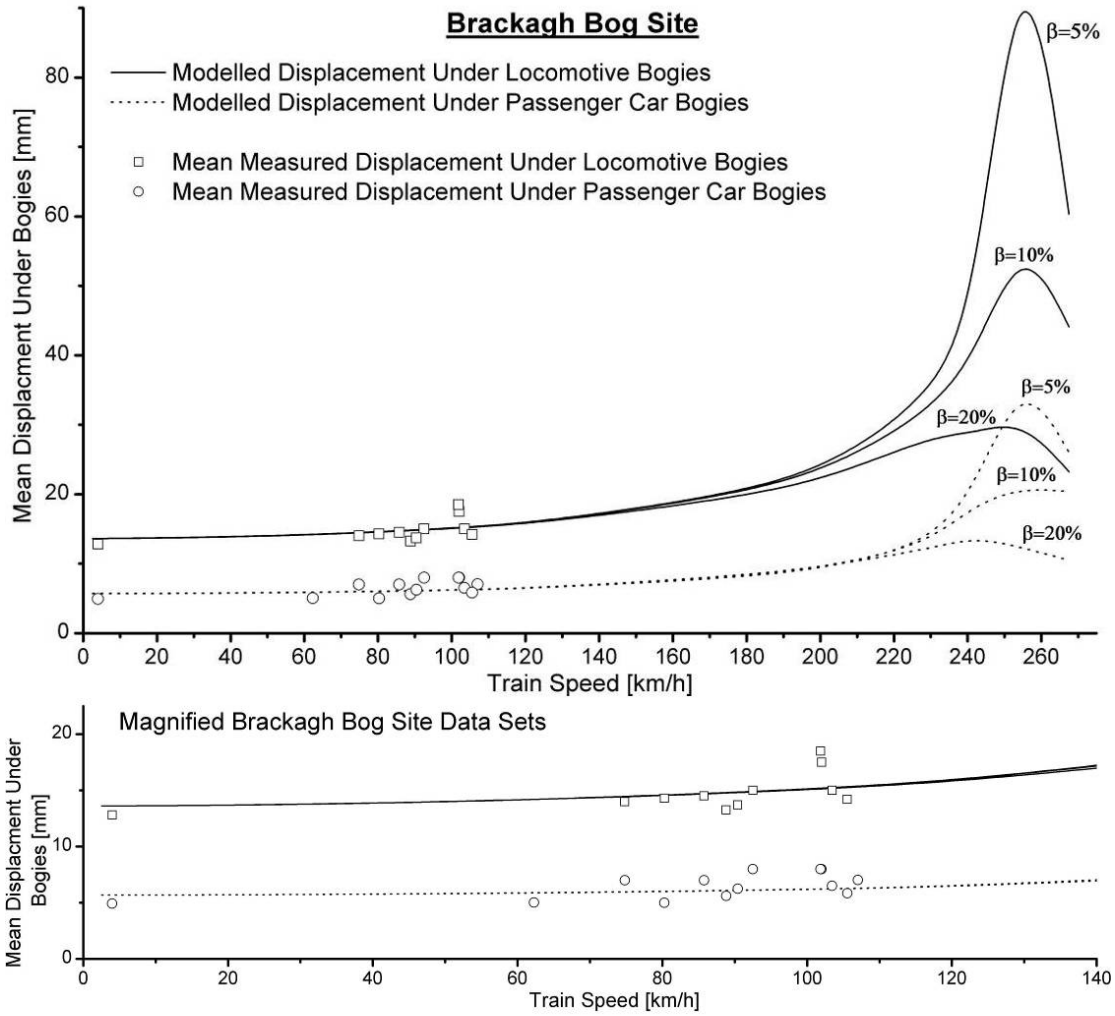

Figure 5.13: Results from modelling in Train speed vs. displacement domain at the Brackagh bog site.

The modelled displacements appear to be divided into two components; a static and a dynamic component. The static component is the displacement of the embankment directly due to the axle loads and is what would be measured under a stationary (static) train (Figure 5.14). The static component is influenced strictly by the applied load, the flexural rigidity (EI) of the beam element and the stiffness coefficient (k) for the visco-elastic foundation. The dynamic component of displacement is the increase in displacement over and above the static component, due to train traveling at a velocity greater than zero (Figure 5.14). This increase in displacement is driven by the inertial forces from the moving mass of the beam element (ρA term in the constitutive equation). The damping force (c term in the constitutive equation) acts to resist the dynamic displacements. The flexural rigidity (EI) of the beam element and the stiffness

coefficient (k) for the foundation determines the amount of dynamic deflection that results from these forces. This dynamic component of the displacement makes up a 16.2 % at the Adavoyle bog site and 20.5 % at the Brackagh bog site at the NIR maximum speed of 145 km/h (90 mph). Conversely the static component of displacement composes at least 83.8 % and 79.5 %, or a large majority of the displacements at the two sites at this speed.

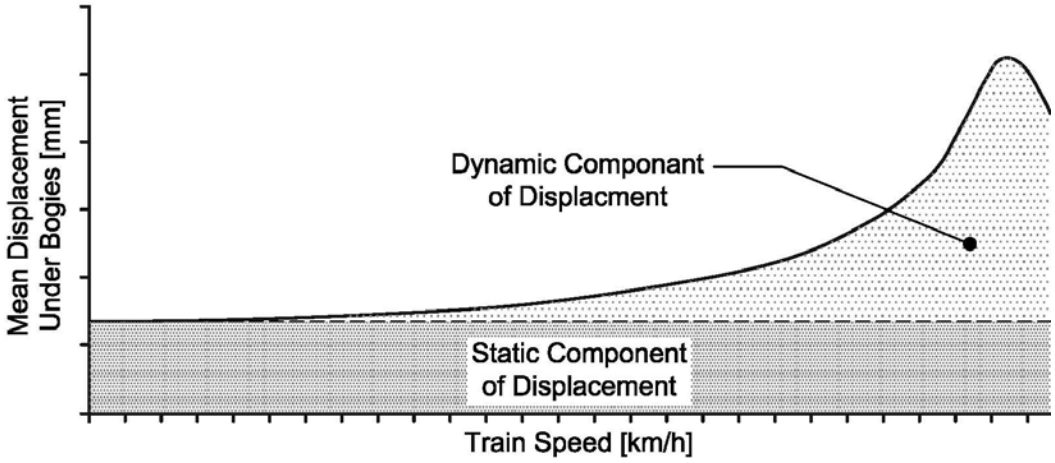

Figure 5.14: Definition of Static and Dynamic components of displacement.

5.1.3 Estimation of Elastic (Resilient) Modulus of the Foundation

The stiffness coefficient of the foundation (k) has been extensively correlated with the elastic modulus of the sub-grade with reasonable success. The most commonly used correlations are from Biot (1937) (Equation 2.25) and Vesic (1963) (Equation 2.26), discussed previously in Section 2.4.2. These correlations provide an E_S for the visco-elastic foundation material based on an infinite depth of the material, although this is not expected to be the case for these sites. Hence the E_S calculated here is not the elastic modulus of the material but a modulus for the embankment/foundation structure. Estimates of the material properties of the foundation and embankment fill materials are more aptly determined using finite element modelling in Section 5.2. The E_S values calculated are presented in Table 5.1. Vesic (1963) provides an upper limit and Biot (1937) provides a lower limit. The E_S determined in this section provides a measure of stiffness of the embankment/foundation structure, and provides a useful method of comparison between the two embankment sites.

Table 5.1: Estimated elastic modulus for a range of Poisson's ratios

	Poisson's Ratio	Biot E_s [Mpa]	Vesic E_s [Mpa]
Adavoyle Bog	0.30	4.26	6.39
	0.40	3.93	5.93
	0.49	3.56	5.41
Brackagh Bog	0.30	3.11	4.67
	0.40	2.87	4.33
	0.49	2.60	3.95

5.1.4 Sensitivity Analysis

With all models there is a range of uncertainty in the conceptualisation of the problem, and the selection of the material parameters and the boundary conditions. In this case this is more of a concern as the ground investigation is still pending. The following is an analysis of the sensitivity of the model to changes in the estimated values. Due to the uncertainty of the thickness of the ballast (d) this variable was varied by ±50%. The flexural rigidity (EI) of a beam that includes a granular material is difficult to calculate, as well there is a possible variation of the ballast's elastic modulus. With this in mind, the EI was varied by a factor of 10 (x10 and x0.1). The density of the ballast falls within a fairly well defined range. The assumed value was 2000 kg/m^3 with the ballast being between ±10% of this value.

The sensitivity analysis for the flexural rigidity of the beam (EI) showed that large variations in critical velocity results as EI is varied by a factor of ten. The model predicts very low critical velocities of 176.7 km/h for the Adavoyle bog sites and 153.6 km/h for the Brackagh bog site from the lower EI values. These are very close to the maximum NIR train speed of 145 km/h, and predict maximum displacements of 15 mm for the Adavoyle bog site and a 30 mm for the Brackagh bog site at train speeds of 145 km/h. These low values for the EI parameter are not feasible and are approximately in the same order of magnitude for values calculated using only the rails and sleepers as the beam element. These values can be rejected on the same basis, as they underestimate the EI value and provide a very poor fit to the individual data sets. This poor fit is illustrated in Figure 5.15. The upper limits of EI also provide a very poor fit to the data sets (Figure 5.16). Limiting the variance of the EI value to values which provide a

reasonable fit to the data sets results in the EI being varied by a factor of 2 (x 2 and x 0.5). The results of this sensitivity analysis are presented in Table 5.2 and Table 5.3.

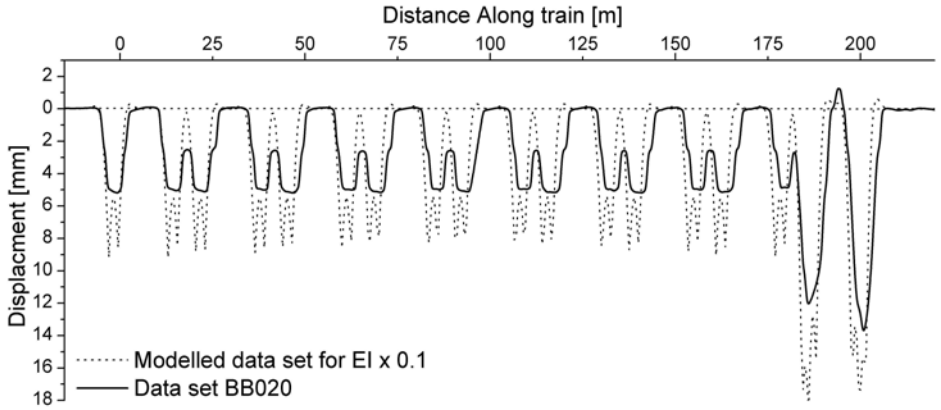

Figure 5.15: Modelled results for sensitivity analysis of flexural rigidity of beam (EI), reduced by a factor of 10 overlaid on actual data set taken at Brackagh bog site.

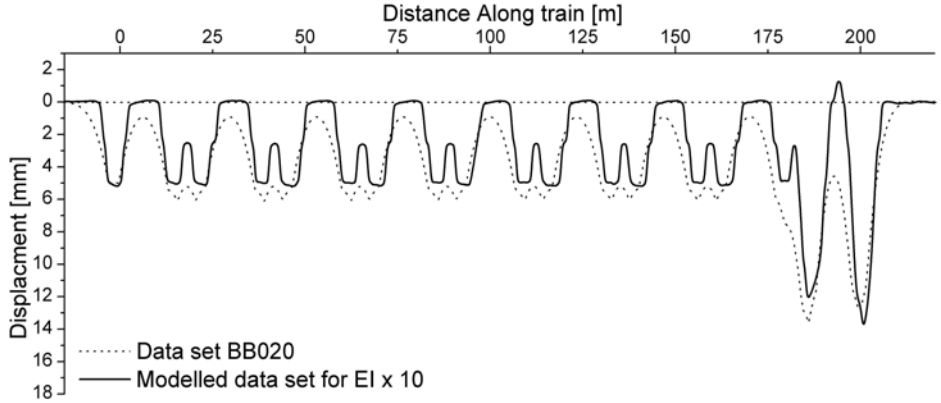

Figure 5.16: Modelled results for sensitivity analysis of flexural rigidity of beam (EI), increased by a factor of 10 overlaid on actual data set taken at Brackagh bog site.

Table 5.2: Results of the sensitivity analysis for the Adavoyle bog site modelling.

Parameter		Variation	Value	V_{cr}	E_S (BIOT)			E_S (VESIC)		
					v = 0.3	v = 0.4	v= 0.49	v = 0.3	v = 0.4	v= 0.49
				[km/h]	[Mpa]	[Mpa]	[Mpa]	[Mpa]	[Mpa]	[Mpa]
Depth of Ballast	d	+ 50%	1.8 m	289.6	3.7	3.4	3.1	5.4	5.0	4.6
		- 50%	0.6 m	264.4	4.5	4.1	3.7	6.9	6.4	5.8
Rigidity of beam	EI	x 2.0	243.4 MNm^2	325.7	3.9	3.6	3.3	5.8	5.4	4.9
		x 0.5	60.9 MNm^2	244.6	4.3	3.9	3.6	6.5	6.0	5.5
Density of Ballast	ρ_B	+ 10%	2200 kg/m^3	217.2	nc	nc	nc	nc	nc	nc
		- 10%	1800 kg/m^3	299.8	nc	nc	nc	nc	nc	nc

nc-no change

Table 5.3: Results of the sensitivity analysis for the Brackagh bog site modelling.

Parameter		Variation	Value	V_{cr}	E_S (BIOT)			E_S (VESIC)		
					v = 0.3	v = 0.4	v= 0.49	v = 0.3	v = 0.4	v= 0.49
				[km/h]	[Mpa]	[Mpa]	[Mpa]	[Mpa]	[Mpa]	[Mpa]
Depth of Ballast	d	+ 50%	1.5 m	267.2	3.0	2.8	2.5	4.5	4.1	3.8
		- 50%	0.5 m	243.8	3.4	3.1	2.8	5.3	4.9	4.4
Rigidity of beam	EI	x 2.0	160.3 MNm^2	294.7	3.0	2.8	2.5	4.4	4.1	3.8
		x 0.5	40.1 MNm^2	222.2	3.3	3.1	2.8	5.1	4.7	4.3
Density of Ballast	ρ_B	+ 10%	2200 kg/m^3	243.9	nc	nc	nc	nc	nc	nc
		- 10%	1800 kg/m^3	267.2	nc	nc	nc	nc	nc	nc

nc-no change

The Adavoyle bog model parameters which result in a critical velocity of 325.7 km/h also produce a displacement of 11.7 mm under the locomotive bogies of a train travelling 145 km/h (90 mph). The model parameters which result in a critical velocity of 244.6 km/h (lowest critical velocity calculated in the sensitivity analysis) also resulted in a modelled maximum displacement of 12.7 mm. This is a small increase (8.3 %) in the total displacement, but represents a significant increase (48.5 %) in the dynamic component of displacement, which is very sensitive to changes in the critical velocity.

The Brackagh bog model which results in a critical velocity of 294.7 km/h, also produces a displacement of 16.2 mm under the locomotive bogies of a train travelling 145 km/h (90 mph). The model parameters which result in a critical velocity of 222.2 km/h (lowest critical velocity calculated in the sensitivity analysis) also resulted in a modelled maximum displacement of 17.74 mm. This is a small increase (9.6%) in the total displacement, but represents a significant increase (60.1 %) in the dynamic component of displacement, which is very sensitive to changes in the critical velocity.

From this analysis, it is apparent that the elastic modulus of the visco-elastic foundation calculated as per both Biot (1937) and Vesic (1963) is fairly robust. This follows the above analysis which shows that the static displacement calculations are not sensitive to changes of the varied parameters. This lack of sensitivity is due to the elastic modulus being calculated from parameters which determine the static component of displacement, and not from those which are used solely to calculate the dynamic component. Variations in the estimated parameters led to small changes in the E_S

calculated as per Biot (1937) of +0.2 and -0.6 MPa (+0.9 % and -8.5 %) from the original calculated value for the Adavoyle bog site; and +0.3 and -0.1 MPa (+6.1 % and -3.4 %) for the Brackagh bog site. Similarly, the values of E_S calculated as per Vesic (1963) were +0.5 and -1.0 MPa (+1.7 % and -9.2 %) from the original calculated value for the Adavoyle bog site; and +0.6 and -0.3 MPa (+9.2 % and –5.8 %) for the Brackagh bog site. The largest changes in elastic modulus occur due to the variation of the EI parameter by a factor of 2.

5.1.5 Analytical Modelling Conclusions

In the first method described previously for the Winkler model the beam element is an actual beam (i.e. rail and sleepers), and the discrete visco-elastic foundation includes the entire earth structure. The conceptual change to the second method is that the beam element is no longer an actual beam, but is made up primarily of the ballast layer. Thus the EI value calculated in this method, although calculated the same way as a beam, should be correlated to the stiffness of the track structure (including the ballast layer) and possibly the embankment fill material as it is the stiffness of the soils which acts to spread the train loading foundation, not an actual beam.

From the sensitivity analysis, the EI value is required only to remain in the same order of magnitude to provide an adequate match between the analytical model and the measured data, and therefore should not be used to confirm the assumptions of the depth of ballast on the embankments.

This analysis of measured embankment displacements suggests that the current embankment and foundation are allowing significant movements of the ballast and track and provide poor support. The calculation of the modulus for the embankment/foundation structure, from the model parameters, supports this conclusion, as it is calculated to be between 3.6 and 6.4 MPa for Adavoyle bog site and 2.6 and 4.7 MPa for Brackagh bog site.

For all cases in the Winkler sensitivity analysis the calculated critical velocity is much higher than the maximum NIR train speed of 145 km/h (90 mph), thus large increases in the modelled displacement fall well outside of the normal operating speed of NIR.

From the model, the dynamic component of the track displacement approaches only 16.2 % and 20.5 % of the total displacement at 145 km/h at the Adavoyle and Brackagh bog sites. The remaining 83.8 % and 79.5 % is due to the static component. It follows from this modelled response that as there is not a large increase in displacement with train speed (within NIR operating speeds). That a significant portion of the displacements are not dynamically induced and therefore the solution to reduce the magnitude of displacement lies in the static analysis of the problem. Further confirmation of this conclusion comes from the lack of noticeable upwards deflection visible in the measured data sets (see Section 4.4), as well as the small increase in of the magnitude of displacement with train speed in the measured data sets (see Figure 4.11).

5.1.6 Effectiveness of Reduced Train Speed Order

A reduced train speed order has been issued for both of the bog sites due to the magnitude of the train-induced displacements. Further reduction of train speed is not a solution for NIR as it runs contrary to the stated goals of this project. It is, however, necessary to determine the effectiveness of this temporary solution. A reduction in the train speeds from 145 km/h (90 mph) to 97 km/h (60 mph) leads to a modelled reduction in displacement of 1.4 mm (12.1%) and 2.2 mm (12.9 %) for the Adavoyle and Brackagh bog sites respectively. This restriction of train speed is modelled to result in a small reduction of the magnitude of the total displacement of the embankment.

The reduction of train speed from 145 km/h (90 mph) to 97 km/h (60 mph) is perceived to be safe interim solution. The answer to why the reduced train speed is considered safer comes from the observation by the train engineers' of the train becoming 'bogged down' or experiencing a loss of power over sites of lower foundation strength. An analysis was conducted to determine if significant increases in power loss could be calculated from both increases in train speed and decreases in foundation stiffness.

The only irreversibility in the Winkler model's equation (Equation 2.7) is due to the foundation damping. It is from this irreversibility that the power loss from the system is calculated. Equation 5.1 was derived to calculate to power loss (L) due to the damping (see Appendix B for derivation).

$$EI\frac{\partial^4 y}{\partial x^4}+\rho A\frac{\partial^2 y}{\partial t^2}+c\frac{\partial y}{\partial t}+ky=P\delta(x,t) \tag{2.7}$$

$$L=2\beta\sqrt{k\rho A}\,\frac{\Delta y^2}{\Delta t^2} \tag{5.1}$$

Using Equation 5.1 the power loss was modelled for a train with seven passenger cars passing over the Brackagh bog embankment. The results of this modelling are presented in Figure 5.17, as plots of power loss for different damping ratios, and two different foundation moduli representing the current conditions at Brackagh bog site (E_S) and a remediated Brackagh bog site with a stiffer foundation (10 x E_S).

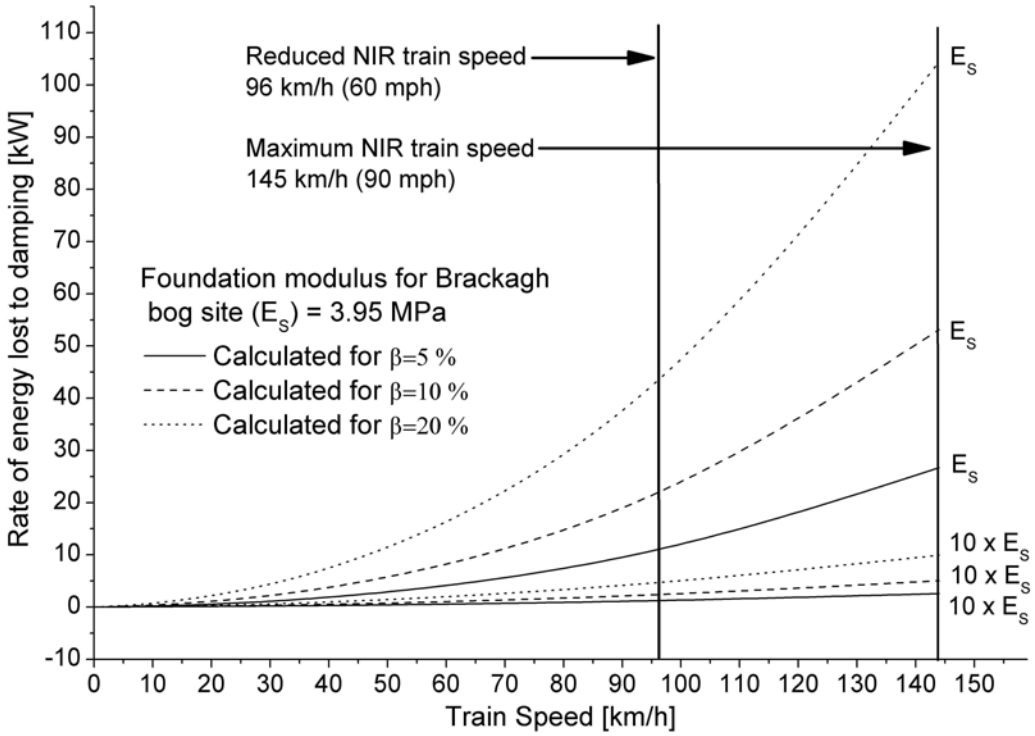

Figure 5.17: The modelled energy lost to damping for the Brackagh bog site, plotted for different damping ratios for a foundation modulus of E_S and 10xE_S.

The power loss at the Brackagh bog site has the potential to be large. In the case of high damping (β = 20%) this can reach 104 kW (139 Hp) at the NIR maximum speed of 145 km/h (90 mph); and drops significantly (by 65%) down to 37 kW (50 Hp) at the reduced speed limit of 96 km/h (60 mph). In the case of a higher foundation modulus the reduction of the power loss is still significant. In the case of high damping at 145

km/h (90 mph) the rate of energy loss is reduced from 104 kW (139 Hp) down to 10 kW (13 Hp) or a 90% reduction. This power loss is a function of the damping properties of the foundation, the foundation stiffness and the train speed.

From these results we can conclude that the train engineers' description of the train becoming 'bogged down' or experiencing a power loss over sites with lower foundation stiffness is possibly due to a loss of power to damping in the foundation.

It is possible that by reducing the train speed the train engineers were able to reduce the power lost to damping, and consequently reduce their sense of the train becoming 'bogged down'. Further determination whether this power fully accounts for the 'bogged down' feeling requires further study.

5.1.7 Effectiveness of Embankment Stabilization Methods

Pursuant of the goal of providing NIR with possible solutions for the stabilization of the embankment to reduce the displacements under train loading, several possible methods of stabilization have been researched. Two methods which could be implemented without significant reconstruction or lost use of the embankments were identified and were illustrated by the case studies in the literature review: the use of a geogrid in the ballast layer and the use of mass stabilization of the foundation material. The effectiveness of these methods is modelled using the same Winkler model as above.

Reduction in ballast thickness

Reductions in the thickness of the ballast layer would reduce the mass, and therefore the inertia (ρA term), of the beam element. A reduction in the inertial forces has a significant impact on the dynamic component of the displacement, but this also causes a reduction in EI and significantly increases the static component of displacement (Figure 5.18). As the dynamic component is small compared to the static component, there is a small net increase in modelled displacement.

Addition of ballast to embankment

A simple method of decreasing the train-induced displacements of the embankments is an increase of ballast thickness on top of the embankment. This serves to further spread out the load on the soft fill and foundation materials. This additional mass will not decrease the critical velocity so as to be close to NIR operating speeds; nor will increases in mass increase the dynamically induced component of the deflection. The modelled increase in beam stiffness from the increased ballast thickness will more than compensate for the increase in inertial mass.

The effectiveness of this method of stabilization is illustrated in Figure 5.18. Significant reductions of induced displacements require large increases in ballast for the Brackagh bog site. For the Adavoyle bog site this method only provides small reductions in peak deflections, even with large increases in ballast depth.

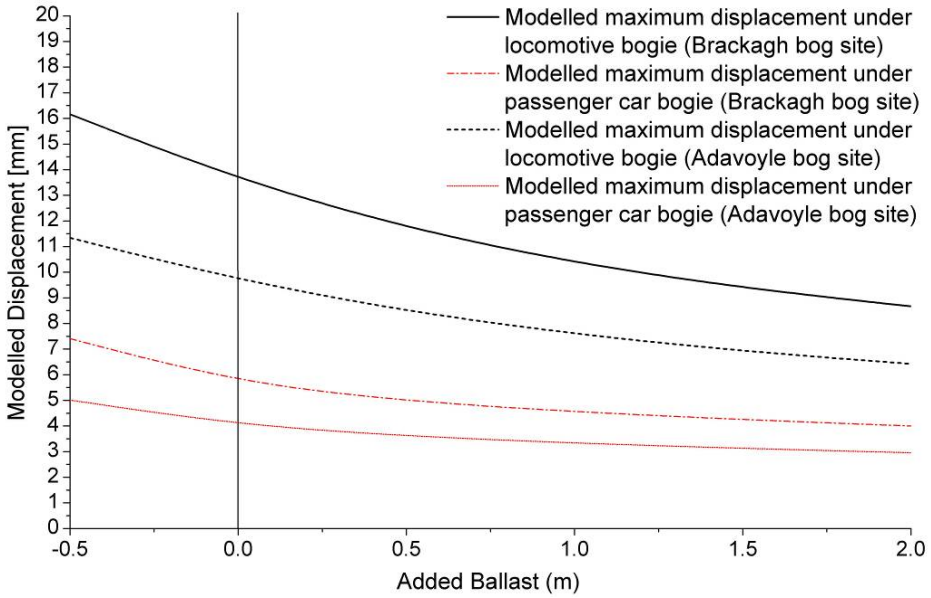

Figure 5.18: Modelled train-induced displacement with the reduction/addition of ballast to the embankment (for a static train).

Additional increases in ballast thickness will result in additional surcharges on the embankment fill and foundation material, and require the widening of the embankments. Before this method could be safely applied, a study is required to determine the effects of this additional surcharge on the embankment and foundation material.

Geogrid strengthening of ballast layer

The Winkler model's ability to model the installation of a geogrid is limited. The installation of a geogrid can be modelled as the increase of the beam rigidity, which would spread the load over a wider area. The calculation of the increase in rigidity is uncertain. From the literature (Tensar 2006a), German Railway trials of the performance of the Tensar geogrid resulted in a 400 mm thick ballast embankment reinforced with a geogrid providing the same support as a 600 mm ballast embankment un-reinforced on the same soft foundation material. Similarly a case study provided by Tensar from the Czech Republic (Tensar 2000) stated a reduction of required ballast thickness of 30%.

If the results from the case studies are scaleable then this would be analogous to a lift of 0.43 to 0.51 m of ballast at the Brackagh bog site, and 0.52 and 0.61 at the Adavoyle bog site. From Figure 5.18 this results in approximately 26 to 28% reduction in deflection at the Brackagh bog site and 13 to 15% reduction at the Adavoyle bog site. The modelling of the magnitude of the reduction of train-induced deflection of the embankments due to the installation of a geogrid would be more successful with a finite element model capable of modelling stress-strain relationships.

Mass stabilization of foundation material

From the analysis in this section, it appears that the cause of the magnitude of the displacement is due to the compressibility of the fill and foundation material simply. Solutions to reduce the dynamic displacement of the embankment under train loads should be focused on improving (stiffening) the foundation beneath the ballast. Figure 5.19 shows the effects of increasing the Young's modulus of the visco-elastic foundation on the modelled displacements. To achieve a 50% reduction in total displacement the elastic modulus of the foundation would have to be increased by a factor of two.

Grouting of the foundation soil in the mass stabilization process is usually done before the construction of the embankments. In the case of these embankments this is not possible and a different application of the grouting to stiffen the foundation is explored further using finite element modelling.

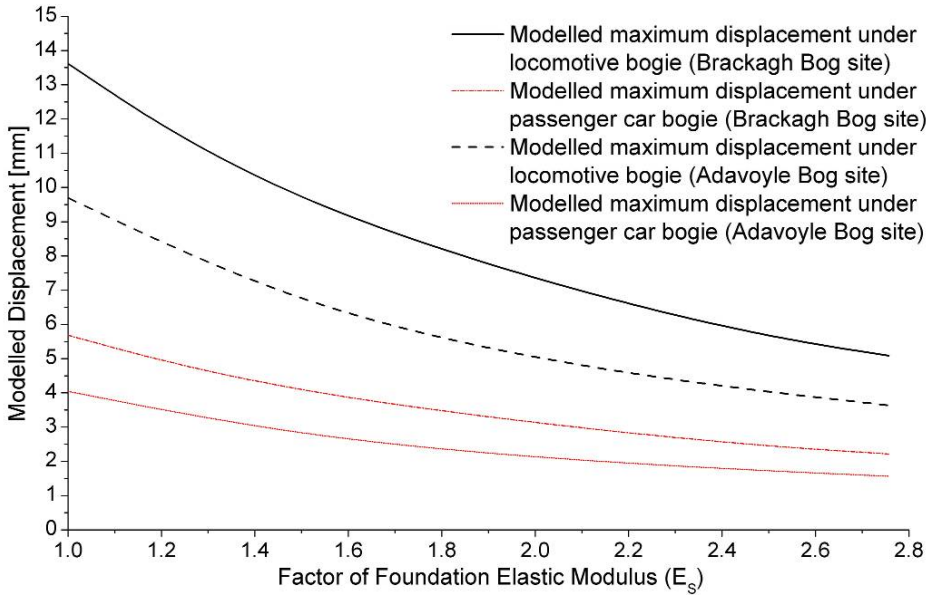

Figure 5.19: Modelled train-induced displacement with the increase of the elastic modulus of the foundation (for a static train).

5.2 Finite Element Modelling

The central conclusion from the analytical modelling was that the largest component of the displacements is not dynamically induced and therefore the solution lays in the static analysis of the problem. It follows that a static finite element (FE) modelling of the problem can provide some valuable insight into the solution.

The purpose of this FE modelling is to further relate the modulus of the foundation, as found through the analytical modelling, to the properties of the foundation material for limited depths of foundation material. The FE modelling is suited to simulating the more complicated stress/strain relationships associated with embankment/foundation stiffening methods, and will be used to explore the effectiveness of these methods. The use of finite element modelling has been limited to the analysis of the embankment at Brackagh bog site; however the resulting conclusions are applicable to both sites.

5.2.1 Construction of the Models

The finite element modelling was conducted using the program SIGMA/W. As SIGMA/W is limited to two-dimensional analyses, the three-dimensional embankment was represented by two two-dimensional models. The two-dimensional models consist

of a cross-section of the embankment and a section taken along the length of the embankment (length-wise).

The assumption of a plane strain condition is applicable to the cross-sectional analysis, as the structure can be reasonably modelled as infinitely long relative to its width in this plane. As well, the loading is spread along the embankment by the rails perpendicular to the plane of analysis. The plane strain condition is not applicable to the length-wise analysis as it does not meet the conditions listed for the cross-sectional model. This two-dimensional model along the length of the embankment can still provide insight into the distribution of the stresses and strains along the length of the embankment.

Cross-section FE Model

For the cross-sectional model, the cross-sections measured during the site survey were used to determine the geometry of the embankment. Due to the complexity of the cross-sections developed from the site survey, it was simplified to a symmetrical structure (Figure 5.20). The sleepers were modelled as extremely rigid beam elements, which will not deform under the applied loading.

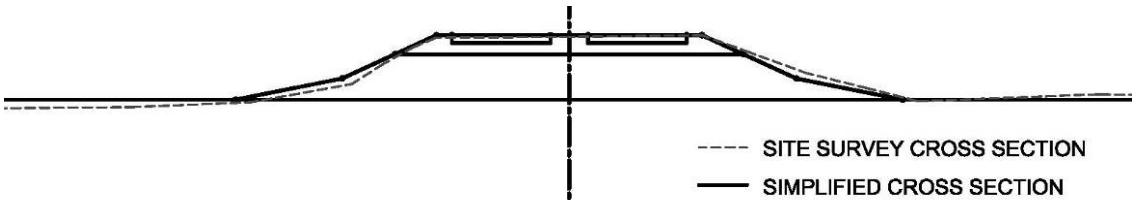

Figure 5.20: Comparison of simplified cross section to the cross section from the site survey.

The load was applied to the model as a distributed load along the upper boundary of the sleeper beam elements. The loads applied to the sleepers are not simply the result of a single axle load, but instead are the resulting distributed load transmitted by the rail to the sleepers. The Winkler numerical model was employed to calculate this load as per Hall (2000); specifically the first method from the analytical modelling. This calculated a maximum force under the locomotive bogies of 76.9 kN, and under the passenger car bogies of 36.7 kN. As the sleepers are 2.59 m in length the distributed loads applied to the element boundaries is 29.7 kN/m and 14.2 kN/m respectively. The finite element mesh generated is presented in Figure 5.21.

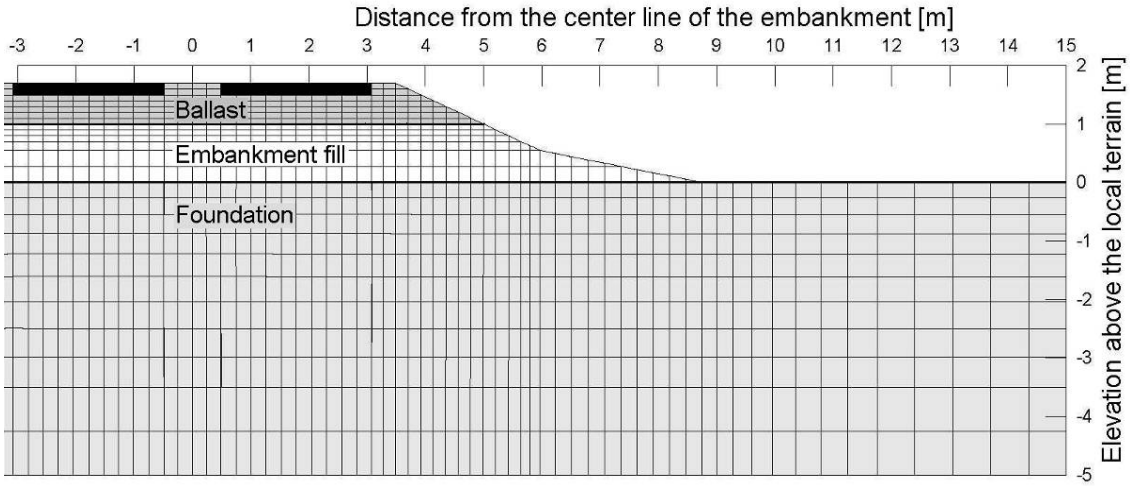

Figure 5.21: Section of the 2D FE Model constructed in SIGMA/W of the cross-section of the embankment at Brackagh bog site.

Length-wise FE Model

For the length-wise two-dimensional model, the embankment geometry is the same as the cross-sectional model. The rail was modelled as a beam element with the beam stiffness equivalent to the two rails which support the trains (Ex2I = 7.84 MNm^2 and 2xA = $1.2x10^{-2}$ m) divided by the length of the sleepers (2.59 m). The sleepers were added to the embankment, and were modelled as elements with a Poisson's ratio of zero and a Young's modulus of great enough magnitude to not undergo deformation ($1.0x10^7$ MPa). The finite element mesh generated is presented in Figure 5.22.

As the sleepers spread the loading over the surface of the embankment the axle loads are divided by the length of the sleepers (2.59 m) and the resulting loading for the locomotive axles are 70.46 kN/m and for the passenger car axles are 40.87 kN/m.

5.2.2 Determination of Model Parameters

Due to the lack of a site investigation, the material properties, stiffness with depth and the depth of soft material underneath of the embankment are unknown. This uncertainty provides a very large obstacle to the FE modelling of this embankment. To obtain some reasonable results for the stiffening techniques under consideration for these embankments it is necessary to produce an approximation for the embankment.

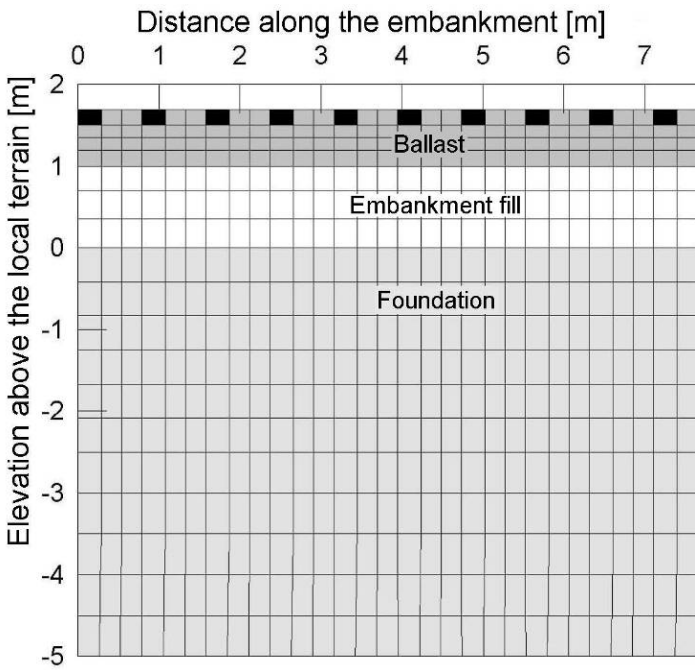

Figure 5.22: Section of 2D FE model constructed in SIGMA/W along the length of the embankment for Brackagh bog site.

In the construction of the model it was determined that there are six unknown parameters required for the definition of the composition of the embankment and foundation material. These six parameters are the depth of the ballast (d_B), the depth of the foundation material (d_F), the Young's modulus of the foundation material (E_F), the Young's modulus of the embankment material (E_E), the Poisson's ratio of the foundation material (ν_F) and the Poisson's ratio of the embankment fill material (ν_E). The Poisson's ratios are set equal to 0.5 as the materials are maintaining a constant volume (i.e. no consolidation) due to the elastic and quickly recoverable nature of the deflections measured.

There are two parameters specific to the model itself, and its ability to predict the response of the structure. These two parameters are the density of the mesh and the distance of the boundary conditions from the structure and/or loading.

Infinite combinations of material properties are possible that provide a good correlation between the modelled displacements and the measured response of the embankment. The Young's modulus of the embankment and the foundation material were fixed to be the same for simplicity, and lack of further information. The elastic modulus for the

foundation calculated using the Winkler model was used as a starting value for the elastic modulus for the foundation materials in the FE modelling.

5.2.3 Young's Modulus for the Foundation Material

To obtain an estimate of the Young's modulus (E_F) for the foundation material for various depths, the depth of the foundation was set and the E_F value was varied to fit the deflections from the analytical model. The E_F was ascertained for modelled depths of 2.5 m, 5 m, 10 m and 15 m, for both the cross section model and the length-wise model and the results are plotted in Figure 5.23.

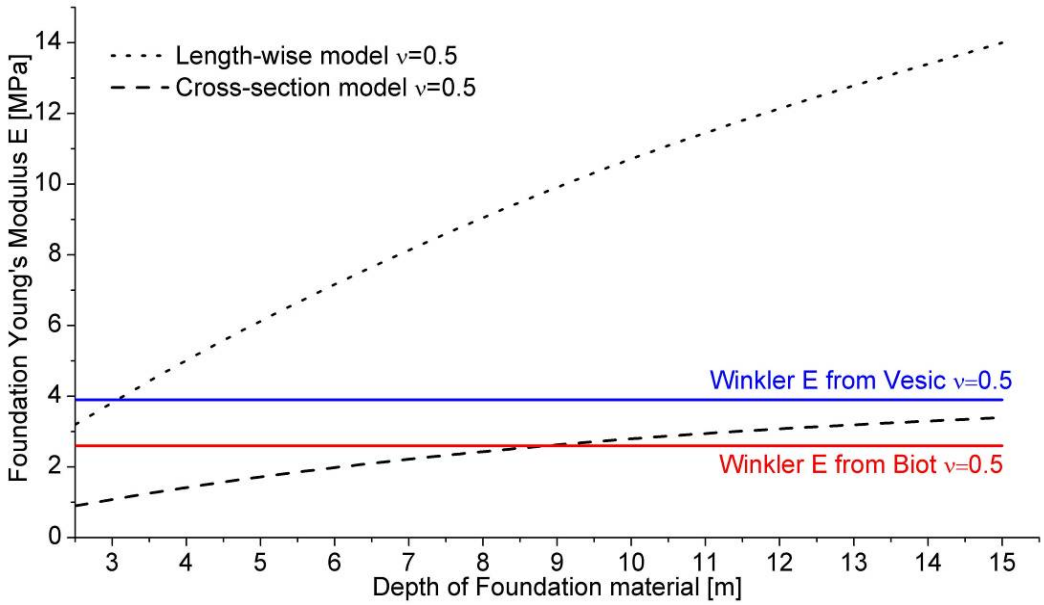

Figure 5.23: Plotted values of E_F determined with FE modelling, from both the cross-section model and the length-wise model.

The differences in the E_F from the two models are a result of the application of the plane strain condition. For the length-wise model the plane strain condition overestimates the confining stresses, leading to the upwards deflection between the bogies to be greatly overestimated. The plane-strain condition also overestimates the applied loads as infinite line loads; this causes the embankment fill material and foundation material to be modelled as overly stiff to resist this loading. From the graph in Figure 5.23 it is apparent that as the modelled depth of foundation material increases, the E_F approaches the modulus of the foundation determined from Vesic (1963) in the analytical modelling. Vesic (1963) calculates the material modulus with

the assumption of an infinite depth of foundation material. This convergence of E_F on the Vesic (1963) E_S value lends further credence to the plane strain condition being applicable to the cross-sectional analysis, and that the E_F values from the cross-section model provide a good representation of the average strength of the embankment fill material and the foundation material.

The Young's modulus of the foundation is modelled to range from approximately 3.9 MPa for a very deep foundation to less than 1 MPa for a shallow (less than 2.5 m) foundation. Unconsolidated peat with less than 10% inorganic can have a range of Young's modulus of 0.1 MPa to 0.6 MPa (Davidson 2000), to match the modelled properties this would require the depth of the soft foundation material to be less than 2.5 m. From Hobbs (1986), peat and peaty organic soils have a large variation in properties; decomposition, non-organic content and consolidation due to loading can significantly increase stiffness of the soil. The construction of the embankment and subsequent loading will have consolidated the embankment fill and foundation materials. The depth of the foundation material cannot be estimated from this modelling and a ground investigation is required to determine the depth and stiffness of these materials.

5.2.4 Stiffening Mechanisms

There are two stiffening mechanisms by which the embankment and/or foundation material can be modified to decrease the deflection due to the train loading. These mechanisms are to further spread the loading over the embankment through an increase in the stiffness of the ballast layer and reducing the strains within the foundation and embankment by stiffening the embankment fill and foundation material.

Ballast stiffening

As the ballast is a relatively stiff component of the embankment and therefore undergoes very little strain, the effect of the stiffening of the ballast is to spread the load over the surface of the soft material. The method used to stiffen the ballast material would be the use of a geogrid within the ballast layer, similar to the installation used in the case study using the Tensar geogrid presented in Fenwick (1992).

For this analysis the Young's modulus for the ballast was increased by factors of 5, 10, 25, 50, and 100, for two foundation depths (2.5 m and 10 m) the results of this modelling are plotted in Figure 5.24. The results show a large discrepancy between the reductions in deflection modelled from the cross-section model and those modelled from the length-wise model. This discrepancy between the results from the two models is due to the differences in the application of the load to the ballast layer, and the differing limitations imposed on the ballast, because of geometry, in its ability to distribute the loading. The deflections from the length-wise model show that large reductions are possible with large increases in ballast stiffness. Further modelling was attempted to directly model the use of a geogrid at the base of the ballast layer using structural elements. This preliminary modelling was stopped as it quickly became too involved and exceeded the scope of this thesis. The preliminary results from the modelling showed very little reduction in deflections were possible (maximum of 1.8 mm corresponding to a 3 fold increase in ballast stiffness) by simply adding a geogrid to the ballast layer, as the horizontal strains within the embankment are too small to mobilize the strength of the geogrid. The limited amount of reduction in the displacement is theorized to be due to the fact that the deflection bowls under the bogies are very shallow relative to their diameter (13 mm compared to 14 m or 1:1000). This indicates that the loading is already largely spread out over the embankments.

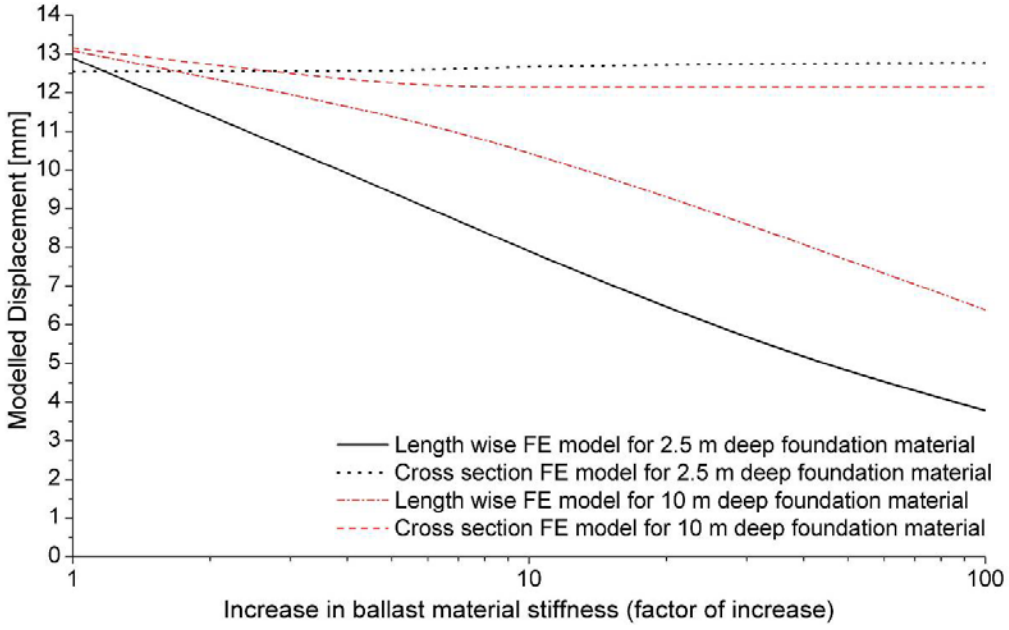

Figure 5.24: The results from the modelling the increasing of the ballast layer stiffness.

Embankment fill and foundation stiffening

The strains which produce the large deflection observed on the surface occur within the embankment fill and foundation material. The stiffening of these materials would directly reduce this strain.

For this FE analysis the Young's modulus for the embankment fill and foundation material (E_F) was increased by factors of 5, 10, 25, 50, and 100, for two foundation depths (2.5 m and 10 m), the results of this modelling are plotted in Figure 5.25. The results from both the cross-section model and the length-wise model are in very close agreement, and show large reductions of deflections are possible from relatively small increases in the E_F (86% reduction with a 10x increase in E_F).

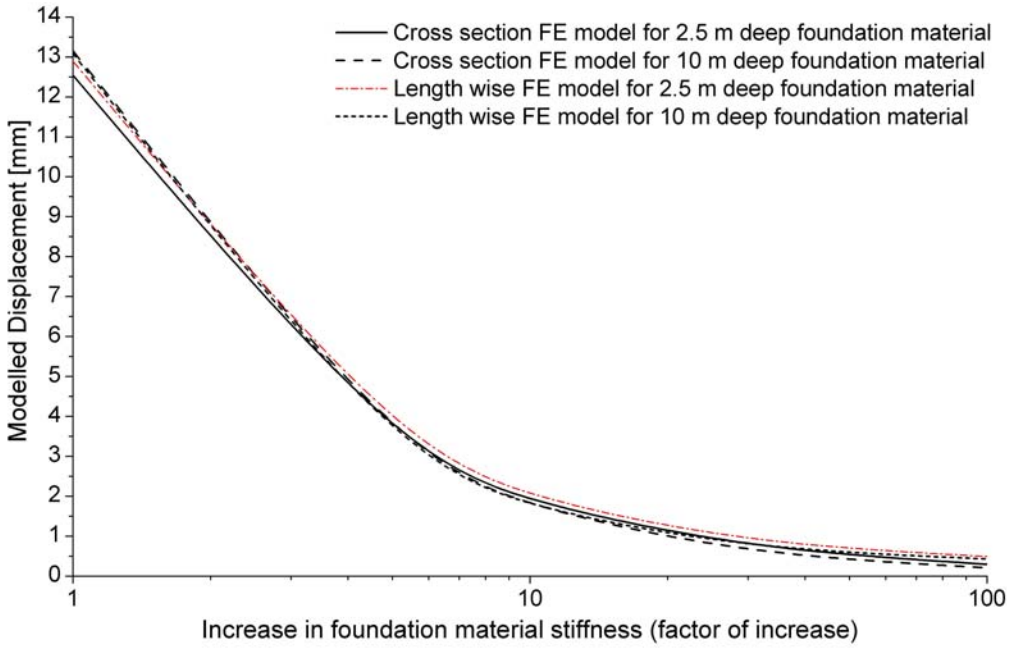

Figure 5.25: The results from the modelling the increasing stiffness of the embankment fill and foundation materials.

Due to the low stiffness of the materials, increases in modulus by factors of 10 to 20 should be possible (Hebib and Farrell 2003; Hebib and Farrell 2004). However, without any knowledge of the material properties or composition of the foundation material it is impossible to say to what extent the foundation material can be strengthened.

As stated in the analytical modelling analysis of the mass stabilization; the grouting of the foundation soil in the mass stabilization process is usually done before the construction of the embankments. It is difficult to use the mass stabilization technique used in Ireland in the case of these embankments (Hernandez-Martinez and Al-Tabbaa 2002; Hebib and Farrell 2003; Hebib and Farrell 2004). There are two methods of stiffening that have been proposed in the course of this project, the first is to grout, or use vibration techniques to introduce granular material to the embankment fill and upper foundation material in order to stiffen these materials. The other method suggested is that the foundation material on either side of the embankment could be stiffened to horizontally confine the foundation material directly below the embankment, thereby indirectly causing the foundation to react as if it had been made stiffer.

To model the impact of stiffening the embankment fill material the length-wise and cross-section FE models were used with increasing stiffness applied to the embankment fill material. From the resulting stress distributions from the FE model this method reduces the strain within the embankment fill material and further spreads the loading over the foundation material. The resulting maximum deflections from this modelling are presented in Figure 5.26.

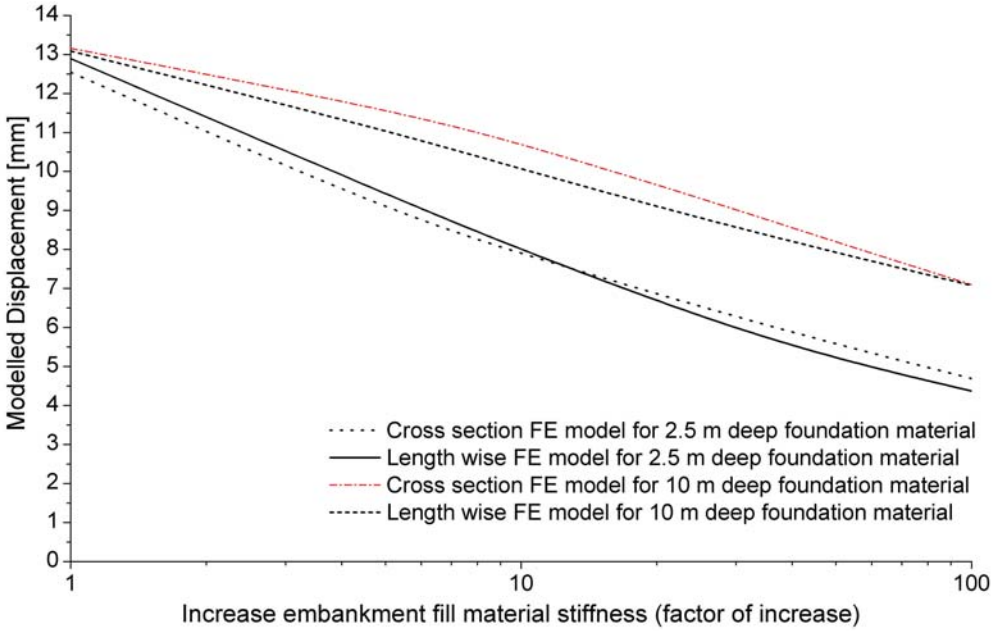

Figure 5.26: The results from the modelling the increasing stiffness of the embankment fill material.

The strong agreement between the length-wise and cross-sectional models is apparent. Models of differing foundation depths show differences in the reduction in the deflections; this is due to the difference in the estimates of the amount of deflection occurring within the embankment fill material. This method shows that large decreases in deflection are possible, but the suitability of these methods for the materials in or below this embankment is uncertain. Grouting of peaty materials has, in other studies, yielded 10-20 fold increases in stiffness (Hernandez-Martinez and Al-Tabbaa 2002). Further reductions in embankment deflections are possible if the material stiffening is extended down into the foundation material.

The FE modelling was further employed to illustrate the possible impact of horizontal confinement of the foundation material (Figure 5.27). Due to the geometry of the models this technique could only be applied to the cross-sectional FE model. A boundary condition of no vertical or horizontal movement was applied on the nodes corresponding to the inside of the stabilized sections (Figure 5.27). This boundary condition was added to model the maximum achievable stiffening of the foundation through this method for an idealized case. The results from this modelling are presented in Figure 5.28.

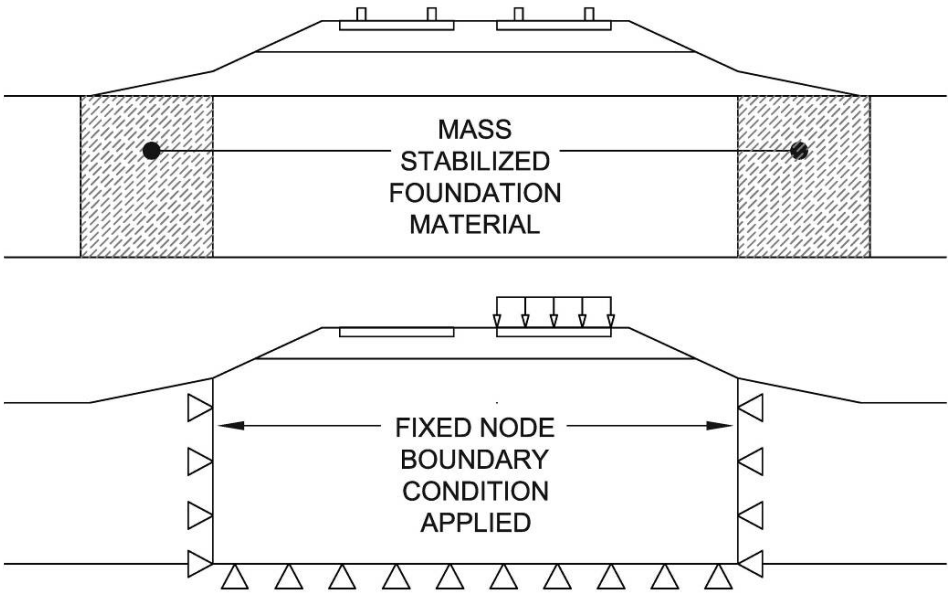

Figure 5.27: Mass stabilization method of grouting on either side of the embankment to confine the foundation material, and the corresponding boundary conditions applied to the FE model.

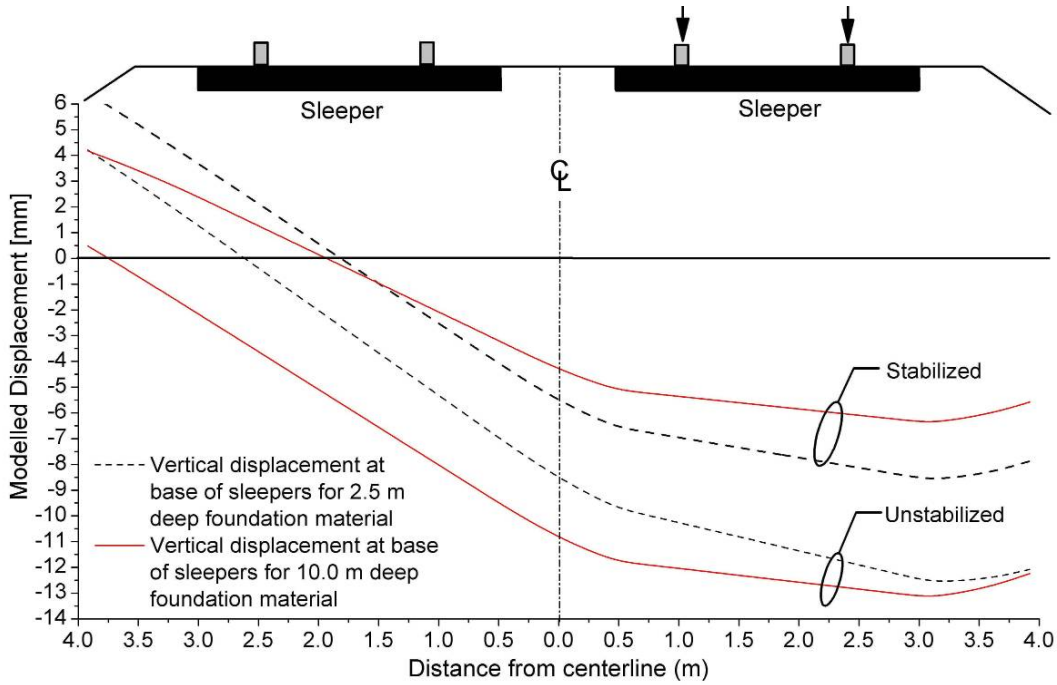

Figure 5.28: The results from the modelling the mass stabilization technique of confining foundation material.

The modelling results presented in Figure 5.28 indicate that there is a possibility of reducing displacement through the horizontal confinement of the embankment foundation material. The results from the modelling of the reductions in displacement in the 2.5 m deep foundation model and the 10 m deep foundation model are analogous to increasing the strength of the embankment foundation material (Figure 5.25) by a factor of 2 and 3 respectively.

5.2.5 Summary of Finite Element Modelling Results

A summary of the strengthening techniques is provided in Figure 5.29, this graph shows the percent reductions of the maximum deflection modelled in the finite element models.

From the comparison of the modelled results for the embankment fill stiffening it becomes apparent that the increase in the modulus of the embankment fill, is more effective if the foundation is 2.5 m deep as opposed to if the foundation is 10 m deep. This is due to the assumption that the embankment and fill material have the same modulus, and that in the 2.5 m depth model a larger component of the strain is

occurring within the embankment. Although this result is derived from this assumption it does hold true that this method is more effective for the case of a shallower foundation as either the foundation and/or embankment material must be very soft. This means that very large factors of increasing stiffness are possible and that the materials which need to be stiffened are easily accessible as they are close to the surface.

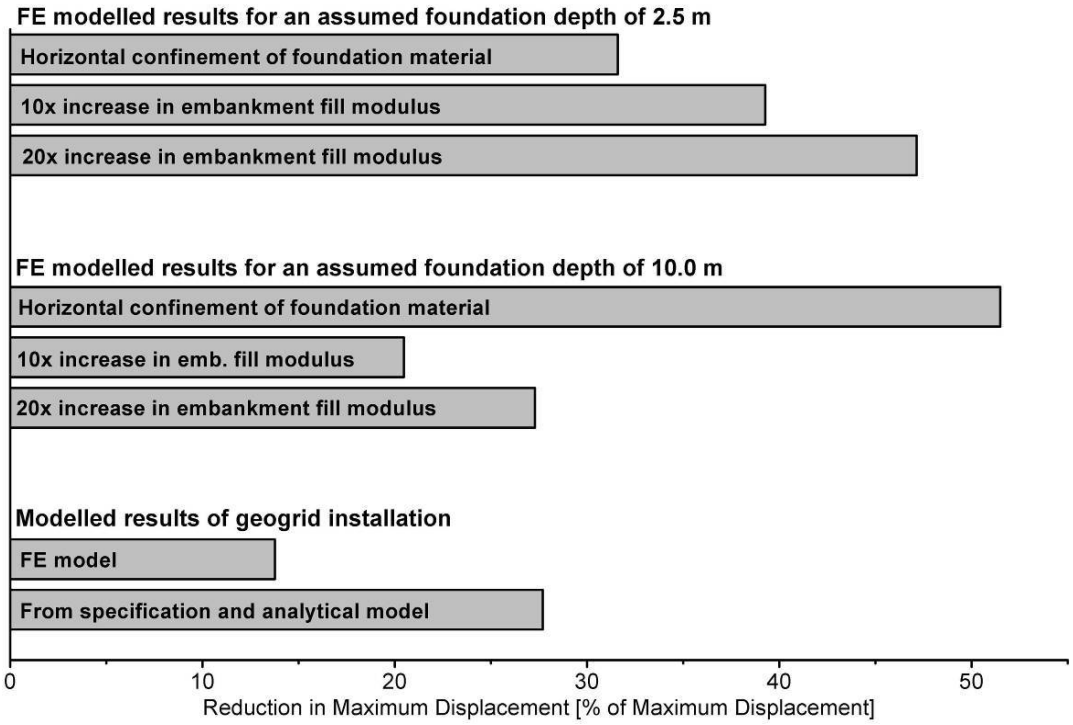

Figure 5.29: Summary of the reductions in the maximum train-induced displacements modelled using the finite element models.

From the comparison of the modelled results for the horizontal confinement of the foundation material it becomes evident that the confinement of the foundation material is more effective in the case of a 10 m deep foundation as opposed to a shallow 2.5 m deep foundation. This is also due to the assumption that the embankment and fill material have the same modulus and that in the 2.5 m depth model a larger component of the strain is occurring within the embankment which is not being confined. This may or may not be the case. The models have still provided useful results, that significant reductions in the embankment deflections (possibly upwards of 50%) can be attained through this method providing that a large fraction of the strains are occurring within the confined foundation material. Further exploration of this method will be possible upon the completion of a ground investigation, which can provide a depth of the soft

foundation and a ratio of the strength of the embankment fill and the strength of the foundation material.

A comparison of the results from the stiffening of the embankment fill and the confinement of the foundation material as presented in Figure 5.29 are not necessarily accurate. The modelled results from the confinement of the foundation material show the maximum achievable reduction in embankment displacements from a confined foundation, due to the confinement provided by the lateral boundary conditions. This is not directly comparable to the embankment fill stiffening which is presented for a possible range of increased stiffness, and can be substantially increased extending these methods into the foundation material. What can be determine from the results is for a shallow foundation (2 m) the stiffening of the embankment fill material solution appears to be more effective, as the results from the lateral confinement of the foundation will fall short of the modelled results, and the results from the embankment stiffening should fall within the range presented. For a deeper foundation (10 m) the results are much less clear; the results from lateral confinement of the foundation will fall short of the modelled results, possibly falling short of the range presented for the increased embankment fill stiffness. A ground investigation will provide much more information as to the actual depth of the foundation and reduce the uncertainty in these models.

The modelled results due to the installation or the geogrid are also presented in Figure 5.29. The results are not as dependant on the foundation conditions. This option does not present as large a reduction in embankment deflection as the other options do. It must be kept in mind that the modelled maximum un-remediated deflection under a locomotive bogie is 13.1 mm, thus a 20 % reduction represents a 2.6 mm reduction. NIR has yet to provide a stated required reduction in embankment deflection. The use of a geogrid may still be useful in any future remediation design to increase the integrity of the ballast layer and reduction of sleeper movement.

Chapter Six: Conclusions and Recommendations

This chapter summarizes the conclusions drawn in the course of the analysis of the collected data and presents recommendations for the continuation of this project to find a solution for NIR.

6.1 Conclusions

The measurements of the displacements and the analysis through numerical and Finite Element Modelling have provided insight into the mechanism and sources of weakness in the embankment and foundation. This has allowed for modelling to determine the potential effectiveness of several methods of embankment/foundation stiffening.

6.1.1 Characterization of Dynamic Displacement

The data interpretation using the Winkler model suggested that the critical velocity at both sites is greater than the operating speeds of NIR. This difference between NIR operating speeds and the modelled critical train speed means that large increases in train-induced displacements are unlikely to occur on these sections of the line under current loading conditions. An analyses of the change in engine power required to maintain a constant speed when the train traverses these sections of track, highlights the sense the train engineers may have of 'bogging down'. This would obviously lead to concerns regarding the safety of this section of track and would subsequently require a reduced speed.

This Winkler modelling also suggests that the dynamic component of displacement is small compared to the displacement from a static train load. Following this interpretation, the solution can be evaluated with a static model of the problem and

potential stabilization techniques as the significant portion of the displacement is not dynamically induced.

6.1.2 Analytical and Finite Element Modelling of Material Strengths

Estimates of the material stiffness of the embankment fill and foundation material were developed from both the analytical and finite element modelling of the response of the embankments to train loading.

The analytical modelling, specifically the Winkler modelling, was unable to differentiate between the embankment fill material and the foundation material. The correlations provide an E_S for the visco- elastic foundation material based on an infinite depth of the material; which is unlikely to be the case for these sites. Hence the E_S calculated here is not the elastic modulus of the material but the modulus for the embankment/foundation structure. A range of moduli were estimated for the combined stiffness of the structure and foundation, and ranged from approximately 2.9 MPa (as per Biot (1937)) and 4.3 MPa (as per Vesic (1963)) for the Brackagh bog site, and 4.3 MPa (as per Biot (1937)) and 5.9 MPa (as per Vesic (1963)) for the Adavoyle bog site.

The finite element modelling using a linear soil model was used to provide an estimate of the Young's modulus for the foundation material for various depths of foundation. The Young's modulus of foundation material and the embankment fill material were assumed to be the same due to a lack of further information. The estimate of the material stiffness of 0.9 MPa for a foundation depth of 2.5 m, 1.8 MPa for a foundation depth of 5 m, 2.9 MPa for a foundation depth of 10 m, and 3.4 MPa for a foundation depth of 15 m. These values are from the cross-sectional two-dimensional model, which was shown to converge on a value similar to the modulus of 4.3 MPa estimated as per Vesic (1963), for an infinity deep foundation with a Poisson's ratio of 0.5.

Both models predict very high compressibility in the materials supporting the train loading. This suggests that the cause of the magnitude of the train-induced displacements is the embankment fill and/or the foundation material is too weak to support the loading.

6.1.3 Modelling of Stabilization Methods

Several methods of stabilization the embankment or the foundation were modelled in this thesis. However, few methods provided significant and achievable reductions in the train-induced displacements.

Removal of Ballast

This solution entails the reduction of the thickness of the ballast layer. The goal of this is to reduce the mass and therefore the inertia of the beam element. A reduction in the inertial forces significantly reduces the dynamic component of the displacement, but also increases the static component. As the dynamic component is very small compared to the static component, there is a net increase in deflection within NIR operating speeds, thus this solution is counter-productive.

Addition of Ballast

This solution entails decreasing the train-induced displacements of the embankments by adding ballast to the top of the embankment. The ballast would serve to further spread out the load on the soft fill and foundation materials.

The analytical model was used to estimate possible reductions in displacement. Significant reductions are possible through the increased ability of the ballast layer to spread out loading. These reductions were modelled as 13% for a 0.5 m increase in ballast and 20% for a 1.0 m increase in ballast at the Brackagh bog site; and a 11% for a 0.5 m increase in ballast and 17% for a 1.0 m increase in ballast at the Adavoyle bog site.

There are a couple of concerns to be addressed before the implementation of this method. The first is the increase in ballast height will require the embankment to be widened as it is currently very narrow from past increases in ballast height without widening. The second and more pressing concern is the effect of the large increase in surcharge of the poor fill and foundation material. Large settlements and further unforeseen changes in the response and condition of the material could occur.

Increasing the stiffness of the ballast layer

The geogrid is installed in the base of the ballast layer; it acts in tension to increase the activation of the strength within the ballast layer, to spread the loading over more fill and foundation material.

The literature from the manufacturer Tensar listed significant reductions in deflections up to 40% in the reinforcement of ballast railway embankments. Also from the Tensar case studies, reductions in required ballast thickness were given for the construction of embankments due to the installation of a geogrid. This was calculated to be comparable to an approximate reduction in displacements of 26 to 28% at the Brackagh bog site and a 13 to 15% reduction at the Adavoyle bog site. However, this analysis is made without a full understanding of the site conditions of the case study or the current site.

The finite element modelling of the Brackagh bog embankment shows that as the ballast is a relatively stiff component of the embankment and therefore undergoes very little strain. The purpose of the stiffening of the ballast is to spread the load over the surface of the soft material. This is analogous to the use of a geogrid to stiffen the ballast material. The results of the modelling showed that using a geogrid produced little reduction in deflections (maximum of 1.8 mm or 13.1% corresponding to a 3 fold increase in ballast stiffness). The limited amount of reduction in the displacement modelled is theorized to be due to the deflection bowls under the bogies being very shallow relative to their diameter (13 mm to 14 m); therefore it can be concluded that the loading is probably already largely spread out over the embankments.

Stiffening of the foundation material

The large deflection observed on the surface are due to strains which occur within the embankment fill and foundation material, the stiffening of these materials would directly reduce this strain. A finite element analysis was conducted increasing the Young's modulus for the embankment fill and foundation material, the results of this modelling from both the cross-section model and the length-wise model show large reductions of deflections are possible from relatively small increase in the Young's modulus.

Two alternative methods of stiffening were modelled; increasing the modulus of the embankment fill and upper foundation material; and stiffening the foundation material on either side of the embankment thereby constraining the foundation material directly below the embankment.

Stiffening of the embankment fill material reduces the strain within the embankment fill material but also further spreads the loading over the foundation material. This method shows that substantial decreases in deflection are possible, and in the case of soft embankment fill, a shallow foundation material appears to the preferred option.

The finite element modelling was employed to model the effectiveness constraining the later strains in the foundation material directly bellow the embankment by mass stabilization of the material on either side of the embankment. The results indicate that there is a possibility of reductions in displacement analogous to increasing the stiffness of the embankment/ foundation material by a factor of 2 and 3 for the foundations depths of 2.5 m and 10 m respectively (Figure 5.25). This method shows the most promise in cases of deeper foundation material with the largest component of deflection due to strain within the foundation material.

It is important to note that the finite element analyses presented in this thesis are quite limited; primarily due to the lack of specific subsurface geometry and soil properties and by the assumption of plane strain conditions. However, these models do illustrate that confinement of the foundation material below the embankment will cause to foundation to act as a stiffer support and limit vertical displacements.

6.2 Recommendations

A final solution for the stabilization of the embankment sites and the determination of the cause of the long-term deformations, and of the site and the sleeper/track structure still remains to be determined. The work in this thesis has been a first step in accomplishing this task and further work remains. The following sections contain recommendations for the further study and analysis of the embankment sites.

6.2.1 Necessity of a Ground Investigation

A ground investigation is an important part of any geotechnical review or modelling of any earth structure. Its purpose is to provide information as to the construction of the earth structure and the properties of the foundation and the material used in the construction of the embankment. A ground investigation would also allow for the determination of the suitability of the materials for the proposed strengthening techniques.

Instrumentation should be installed during the course of a ground investigation. The purpose of this instrumentation should be to measure the pore-water pressure and to measure both the vertical and horizontal deformation within the embankment. These measurements will allow for the determination of amount and location of the stress and strain within the embankment.

Within this thesis a large amount of analysis has been undertaken on relatively few dynamic displacement measurements. This is sufficient to begin the analysis of the embankment and start in the direction of possible solutions to this problem. However, the modelling undertaken has been based on assumptions. Although these assumptions are well-founded in the information provided; they are assumptions nonetheless. Thus, a site investigation is required to confirm and provide a stronger basis for the analysis conducted.

6.2.2 Long-term Deformation Monitoring

This thesis has been restricted to analysing the dynamic deflections as the recoverable elastic straining of the rail/embankment structures. Questions remain to the extent of the long-term deformation of the embankments, and the root causes of the increased maintenance requirements. The long-term deformation may be due to a plastic component of train-induced displacements or some other mechanism yet to be determined. As well, the mechanism causing the sleepers to skew and to become unevenly spaced has yet to be investigated.

To begin this investigation into the long-term deformations in the embankment, instrumentation this would need to be installed. In-place inclinometers and piezometer

measurements would be a logical first step. The inclinometers would ideally be installed vertically in the side slopes of the embankments to monitor lateral plastic deformation; and, the piezometers would be installed within the embankment to monitor the increase in pore water pressure within the embankment during the passage of a train. Along with this instrumentation there is a need to determine the frequency of loading (train passages), and to determine if a correlation to the long-term deformation can be made.

6.2.3 Proceeding with Stiffening of Embankment

The potential effectiveness of the possible stiffening techniques have been illustrated using analytical and FE modelling. Further study must be undertaken with the results of the ground investigation and the long-term deformation monitoring (discussed above in sections 6.2.1 and 6.2.2) before the implications and effectiveness of any of the remediation methods discussed in this thesis can be fully determined. The project should continue to examine these remedial methods for NIR; and expand the most promising into implementation on a test section of railway.

References

Athanasopoulos, G.A., Pelekisa, P.C., and Anagnostopoulos, G.A. 2000. Effect of soil stiffness in the attenuation of Rayleigh-wave motions from field measurements. Soil Dynamics and Earthquake Engineering, **19**(4): 277-288.

Biot, M.A. 1937. Bending of an Infinite Beam on an Elastic Foundation. Journal of Applied Mechanics, **12**(2): 155-164.

Boulanger, R.W., Arulnathan, R., Harder, L.F.J., Torres, R.A., and Driller, M.W. 1998. Dynamic Properties of Sherman Island Peat. Journal of Geotechnical and Geoenviromental Engineering, **124**(1): 12-20.

Brandl, H. 2001. Geotechnics of railtrack structures. *In* Geotechnics for Roads, Rail Tracks and Earth Structures: Outcome of ETC (European Technical Committee No.11). *Edited by* A.G. Correia and H. Brandl. January, 2001. Taylor & Francis, pp. 271-287.

Cooley, J.W., and Tukey, J.W. 1965. An algorithm for the machine calculation of complex Fourier series. Math. Comput., **19**: 297-301.

Criner, H.E., and McCann, G.D. 1954. Rails on Elastic Foundations Under the Influence of High-Speed Traveling Loads. Journal of Applied Mechanics, **76**: 13-22.

Davidson, L. 2000. Basic mechanics of soils. University of the West of England, Bristol, http://environment.uwe.ac.uk/geocal/SoilMech/basic/stiffness.htm

De Deitrich 1994. Intercity Passenger Coaches Standard Class 71 Seats: Schematic of Passenger Coaches. De Deitrich Ferroviaire

De Deitrich 1995. Intercity Passenger Coaches Driving Control Car: Schematic of Control Car. De Deitrich Ferroviaire

DRDNI 2005. Regional Strategic Transport Network Transport Plan 2015, Department for Regional Development.

Durham 2006. EL In-place inclinometer (Manual). Durham Geo slope Indicator

Fenwick, T.H. 1992. Electrification of British Railways' East Coast Main Line Civil Engineering Works, Doncaster to Berwick. Proceedings of the Institution of Civil Engineers: Transportation, **95**: 227-238.

Ferguson McIlveen 2002. Northern Ireland Railways: Embankment Stability Portadown to Border: Preliminary Report, Belfast, Northern Ireland.

Frýba, L. 1972. Vibrations of Solids and Structures under Moving Loads. Noordhof International Publications.

GEO-SLOPE 2004. SIGMA/W. *In* Geostudio 2004. GEO-SLOPE International Ltd., Calgary, Alberta, www.geo-slope.com

GM 1993. Locomotive Outline. General Motors Locomotive Group, London, Ontario, Canada

Hall, L. 2000. Simulations and Analyses of Train-Induced Ground Vibrations. Doctoral Thesis, Royal Institute of Technology, Stockholm, Sweden.

Hall, L. 2003. Simulations and analyses of train-induced ground vibrations in finite element models. Soil Dynamics and Earthquake Engineering, **23**: 403-413.

Hanrahan, E.T. 1954. An Investigation of Some Physical Properties of Peat. Geotechnique, **4**(3): 108-123.

Hanrahan, E.T. 1964. A Road Failure on Peat. Geotechnique, **14**(3): 185-202.

Hanrahan, E.T. 1986. Mire Morphology and the Properties and Behaviour of some British and Foreign Peats. Quarterly Journal of Engineering Geology, **19**: 7-80.

Hanrahan, E.T., and Rogers, M.G. 1981. Road on Peat: Observations and Design. Journal of Geotechnical Engineering Division, Proceedings of the American Society of Civil Engineers, **107**(GT10): 1403-1415.

Hebib, S., and Farrell, E.R. 2003. Some experiences on the stabilization of Irish peats. Canadian Geotechnical Journal, **40**(1): 107-120.

Hebib, S., and Farrell, E.R. 2004. Stabilisation of Irish Soils. Presented to the Institution of Engineers of Ireland, pp. 1-15

Heelis, M.E., Dawson, A.R., Collop, A.C., Chapman, D.N., and Krylov, V. 1999. Resilient Modulus of Soft soil Beneath High-speed Rail Lines. Transportation Research Record, **1687**: 39-46.

Heelis, M.E., Collop, A.C., Dawson, A.R., Chapman, D.N., and Krylov, V. 2000. The 'Bow-Wave' Effect in Soft Subgrade Beneath High Speed Rail Lines. "Performance Verification of Constructed Geotechnical Facilities", Geotechnical Engineering Special Publication(94): 338-349.

Hendry, M., Hughes, D., Barbour, L., and Atkinson, M. 2006a. Train Induced Dynamic Response of Railway Track and Embankments Constructed Over Soft Peat Foundations. *In* 59th Canadian Geotechnical Conference: Sea to Sky Geotechnique 2006. Vancouver, Canada, pp. 947-954.

Hendry, M., Hughes, D., Barbour, L., and Atkinson, M. 2006b. Measuring and Modelling the Train Induced Dynamic Response of a Railway Track and Embankment Constructed over a Soft Peat Foundation. *In* Railway Foundations: RailFound 06 International Conference on Railway Track Foundations. *Edited by* G.S. Ghataora and M.P.N. Burrow. Birmingham, U.K. University of Birmingham Press., pp. 274-282.

Hernandez-Martinez, T.G., and Al-Tabbaa, A. 2002. Strength Properties of Stabilised Peat.

Hobbs, N.B. 1986. Mire Morphology and the Properties and Behaviour of some British and Foreign Peats. Quarterly Journal of Engineering Geology, **19**: 7-80.

Inman, D.J. 2000. Engineering Vibration. Prentice-Hall, Inc., Upper Saddle River, NJ.

Kaynia, A.M., Madshus, C., and Zackrisson, P. 2000. Ground Vibrations from High-Speed Trains: Prediction and Countermeasure. Journal of Geotechnical and Geoenviromental Engineering, **126**(6): 531-537.

Kenny, J.T. 1954. Steaty-State Vibrations of Beam on Elastic Foundation for Moving Load. Journal of Applied Mechanics, **76**: 359-364.

Kerr, A.D. 2000. On the determination of the rail support modulus k. International Journal of Solids and Structures, **37**(32): 4335-4351.

Krahn, J. 2004. Stress and Deformation Modeling with SIGMA/W. GEO-SLOPE International Ltd.

Kramer, S.L. 2000. Dynamic Response of Mercer Slough Peat. Journal of Geotechnical and Geoenviromental Engineering, **126**(6): 504-510.

Krylov, V. 1995. Generation of Ground Vibrations by Superfast Trains. Applied Acoustics, **44**: 149-164.

Krylov, V., Dawson, A.R., Heelis, M.E., and Collop, A.C. 2000. Rail Movement and Ground Waves caused by High-speed Trains Approaching Track-Soil Critical Velocities. Proceedings of the Institution of Mechanical Engineers, Part F: Journal of Rail and Rapid Transit, **214**(2): 107-116.

MacMillan, R. 1998. Identification of Whole-Body Vibrations: Accelerometers. The Safetyline Institute, Worksafe Western Austrailia, http://www.safetyline.wa.gov.au/institute/level2/course19/lecture60/l60_05.asp

Madshus, C. 2001. Modelling, Monitoring and controlling the behaviour of Embankments Under High Speed Train Loads. *In* Geotechnics for Roads, Rail Tracks and Earth Structures: Outcome of ETC (European Technical Committee No.11). *Edited by* A.G. Correia and H. Brandl. January, 2001. Taylor & Francis, pp. 225-238.

Madshus, C., and Kaynia, A.M. 2000. High-Speed Railway Lines on soft Ground: Dynamic Behaviour at Critical Train Speeds. Journal of Sound and Vibration, **231**(3): 689-701.

Michaels, P. 1996. In situ Determination of Soil Stiffness and Damping. Journal of Geotechnical and Geoenviromental Engineering, **124**(8): 709-719.

OLC 2002. Origin 7 SR1. Origin Lab Corporation, Northampton, MA

Paolucci, R., and Spinelli, D. 2006. Ground Motion Induced by Train Passage. Journal of Engineering Mechanics, **132**(2): 201-210.

Pigon, P.T., Hanrahan, E.T., and Somers, N. 1992. Major canal reconstruction in peat areas. *In* Proceedings of the Institution of Civil Engineers: Water Maritime and Energy. September, 1992., Vol.96, pp. 141-152.

Popp, K., Kruse, H., and Kaiser, I. 1999. Vehicle-track dynamics in the mid-frequency range. Vehicle System Dynamics, **31**(5-6): 423-464.

Porbaha, A., Hanzawa, H., and Kishida, T. 2000. Analysis of a Failed Embankment on Peaty Ground. Geotechnical Special Publication, **101**.

Radampola, S.S. 2006. Evaluation and Modelling Performance of Capping Layer in Rail Track Substructure. PhD Doctorate, Central Queensland University.

Ridley, A.M. 2003. Field measurement of pore water pressures. Quality Services, Civil engineering division, Highways Agency: 1 thru 37

Ridley, A.M., Vaughan, P.R., McGinnity, B., and Brady, K. 2004. Pore pressure measurements in infrastructure embankments. *In* Advances in Geotechnical Engineering: The Skempton Conference. Thomas Telford.

Slope Indicator 2004. Rod Extensometer. Slope Indicator Company, pp. 1-27, www.slopeindicator.com

Tensar 2000. Track Bed Stabilisation - Brno-Ceska Trebova Line, European Corridor No. 4, Czech Republic 1996-1998. Tensar International Case Study, pp. 1-2

Tensar 2001. Ballast Reinforcement - NS2 Rail, The Netherlands 2000. Tensar International Case Study

Tensar 2006a. Railway: Reinforcing ballast and sub-base layers under railway track. Tensar International, p. 8

Tensar 2006b. Tensar SSLA30-G Geocomposite Model Specification. Tensar International Limited, Blackburn, U.K., p. 2

Timoshenko, S.P. 1926. Method of Analysis of Statical and Dynamical Stresses in Rail. *In* 2nd International Conference of Applied Mechanics. Zurick, Switzerland, pp. 407-418.

Vesic, A.B. 1963. Beams on elastic Subgrade and the Winkler's Hypothesis. *In* 5th International Conference on Soil Mechanics and Foundation Engineering, Vol.1, pp. 845-850.

Vostroukhov, A.V., and Metrikine, A.V. 2003. Periodically supported beam on a visco-elastic layer as a model for dynamic analysis of a high-speed railway track. International Journal of Solids and Structures, **40**: 5723-5752.

Wehling, T.H., Boulanger, R.W., Arulnathan, R., Harder, L.F.J., and Driller, M.W. 2003. Nonlinear Dynamic Properties of a Fibrous Organic Soil. Journal of Geotechnical and Geoenviromental Engineering, **129**(10): 929-939.

Winkler, E., and Dominicus, H. 1867. Die Lehre der Elasticitat und Festigkeit, Prague

Woods, R.D. 1978. Measurement of Dynamic Soil Properties. *In* ASCE Geotechnical Specialty Conference, Vol.1, pp. 91-178.

Appendix A: All Data Sets from Dynamic Measurements

Brackagh Bog Data Sets

Data Set	Date	Time	Destination	Measure Method	Speed	Max Displ.		Mean Displ.	
						Loco	PC	Loco	PC
BB001	2005 09 22	1103	-	Video	-	-	-	-	-
BB002	2005 09 22	1107	-	Video	-	-	-	-	-
BB003	2005 09 22	1230	Dublin	Video	57.5	15.0	7.0	15.0	8.0
BB004	2005 09 22	1301	Belfast	Video	63.4	19.0	7.0	17.5	8.0
BB005	2005 09 22	1445	Belfast	Video	63.3	10.0	6.0	18.5	8.0
BB006	2005 09 22	1449	Dublin	Video	64.3	16.0	5.0	15.0	6.5
BB007	2005 09 23	1109	-	Video	-	-	-	-	-
BB008	2005 09 23	1227	Dublin	Video	46.5	14.0	6.0	14.0	7.0
BB009	2005 09 23	1302	-	Video	-	-	-	-	-
BB010	2005 09 23	1442	-	Video	-	-	-	-	-
BB011	2005 09 23	1454	Dublin	Video	53.3	15.0	5.0	14.5	7.0
BB012	2005 12 20	1411	Belfast	Photosensor	55.2	13.2	5.4	13.3	5.6
BB013	2005 12 20	1550	Belfast	Photosensor	56.2	14.3	5.3	13.7	6.3
BB014	2005 12 20	1604	Dublin	Photosensor	49.9	14.4	5.0	14.3	5.0
BB015	2006 03 12	1100	-	Photosensor	-	-	-	-	-
BB016	2006 03 12	1131	-	Photosensor	-	-	-	-	-
BB017	2006 03 12	1144	Belfast	Photosensor	38.7	-	5.1	-	5.0
BB018	2006 03 12	1201	Belfast	Photosensor	66.5	-	6.7	-	7.0
BB019	2006 03 12	1208	-	Photosensor	-	-	-	-	-
BB020	2006 03 12	1230	Belfast	Photosensor	65.6	14.9	4.8	14.2	5.8
BB021	2006 03 12	1242	-	Photosensor	-	-	-	-	-
BB022	2006 03 12	1311	Belfast	Photosensor	2.49	13.0	4.8	12.8	4.9

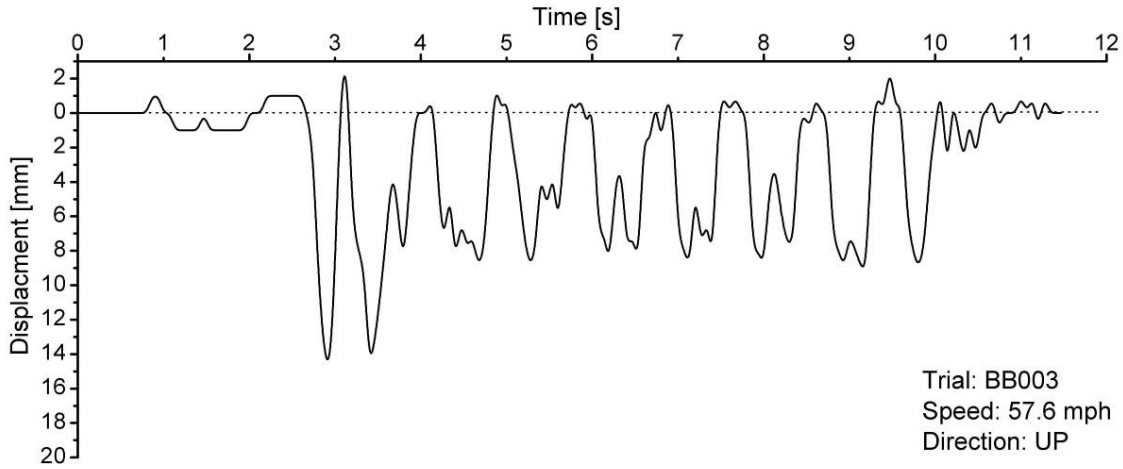
Time [s]
Displacment [mm]
Trial: BB003
Speed: 57.6 mph
Direction: UP

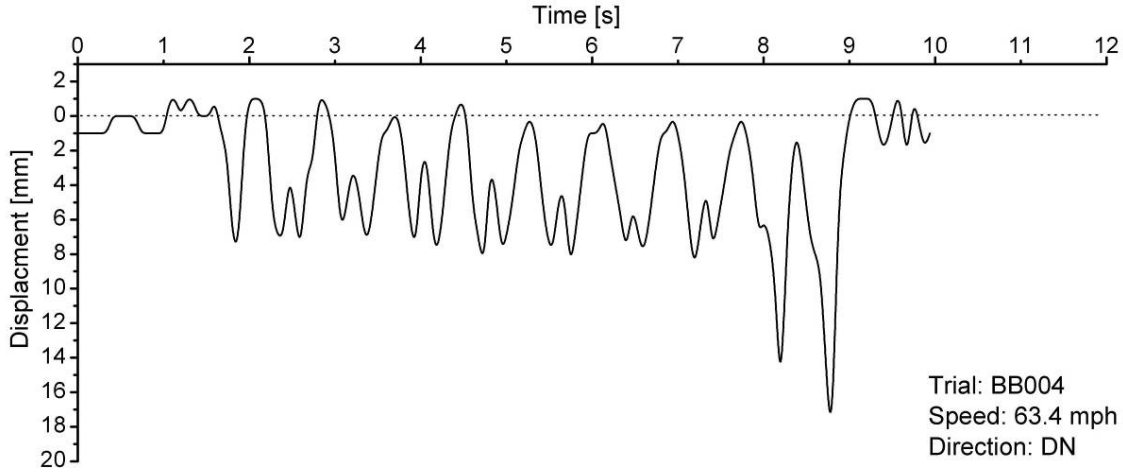
Time [s]
Displacment [mm]
Trial: BB004
Speed: 63.4 mph
Direction: DN

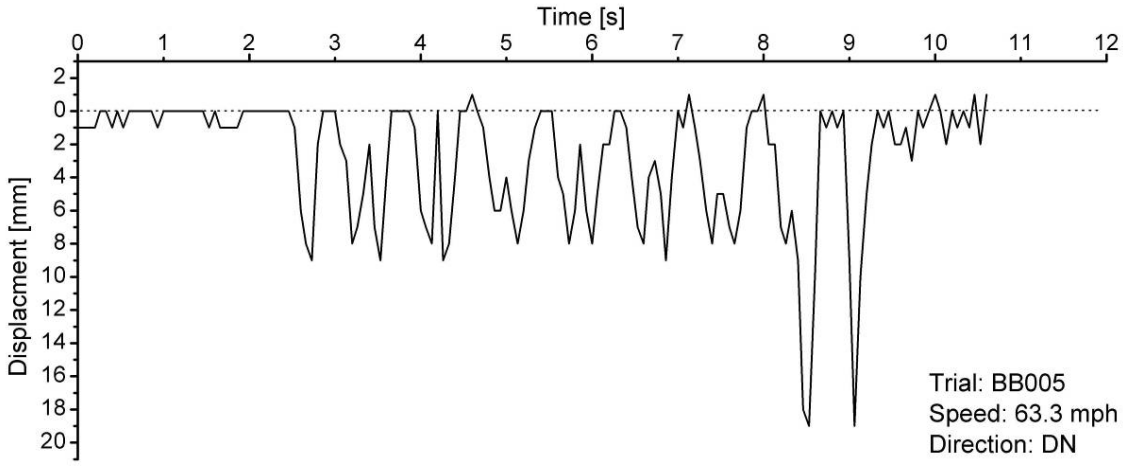
Time [s]
Displacment [mm]
Trial: BB005
Speed: 63.3 mph
Direction: DN

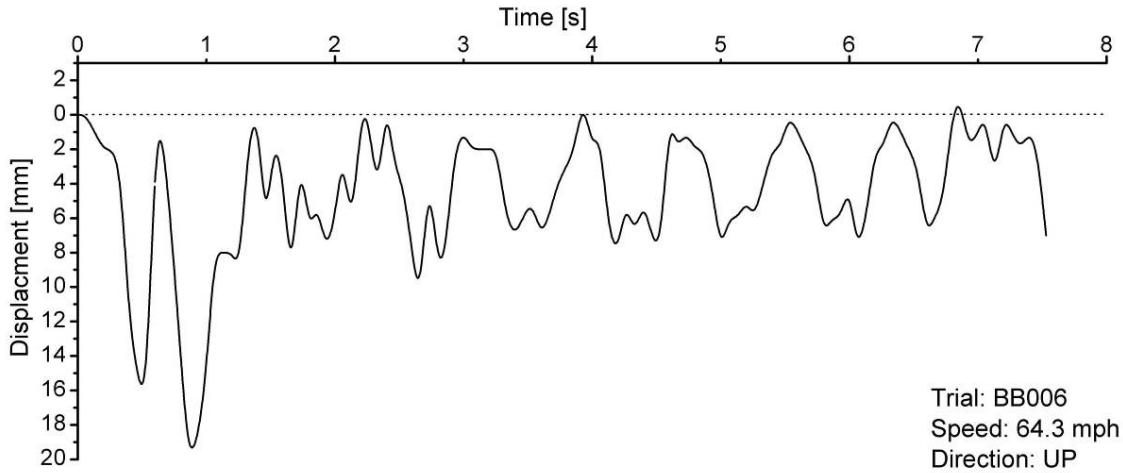
Time [s]
Displacment [mm]
Trial: BB006
Speed: 64.3 mph
Direction: UP

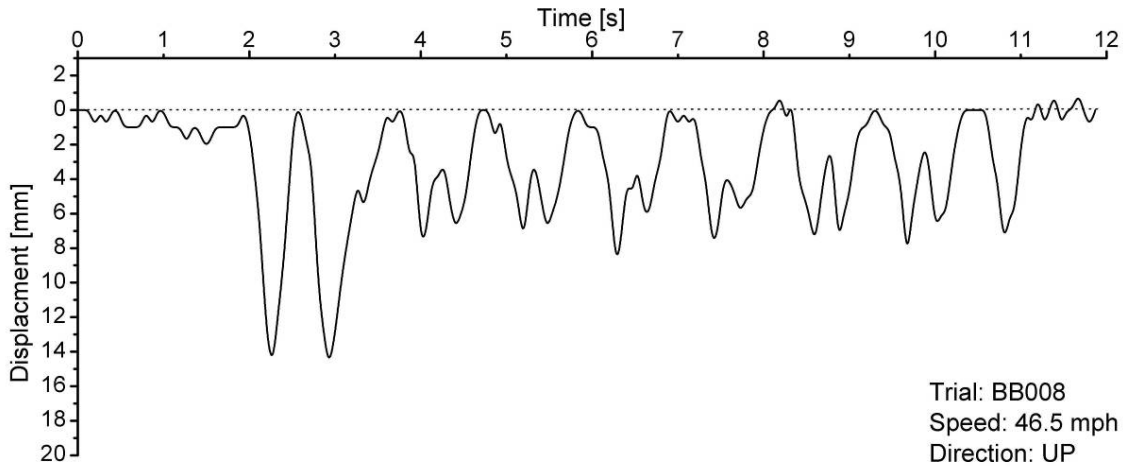
Time [s]
Displacment [mm]
Trial: BB008
Speed: 46.5 mph
Direction: UP

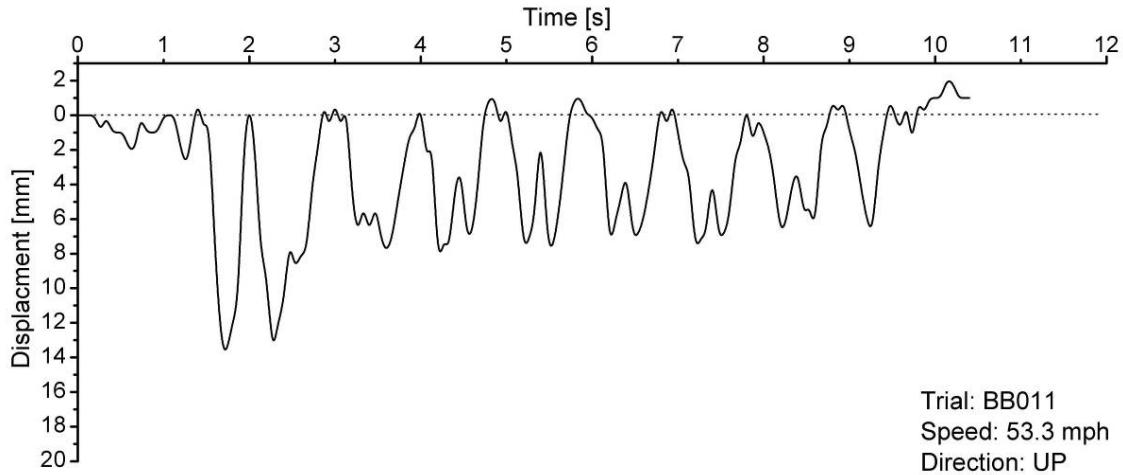
Time [s]
Displacment [mm]
Trial: BB011
Speed: 53.3 mph
Direction: UP

Appendix A: All Data Sets from Dynamic Measurements

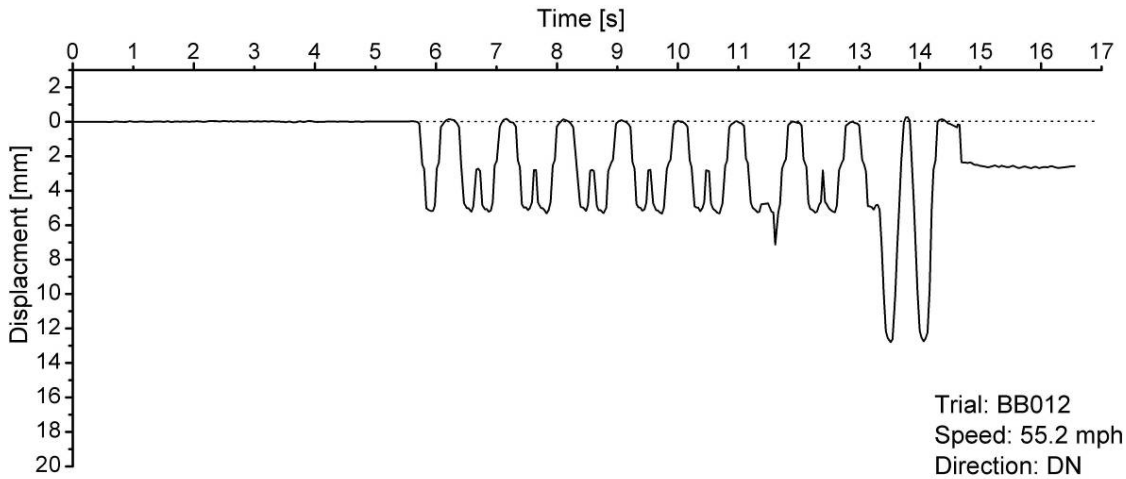

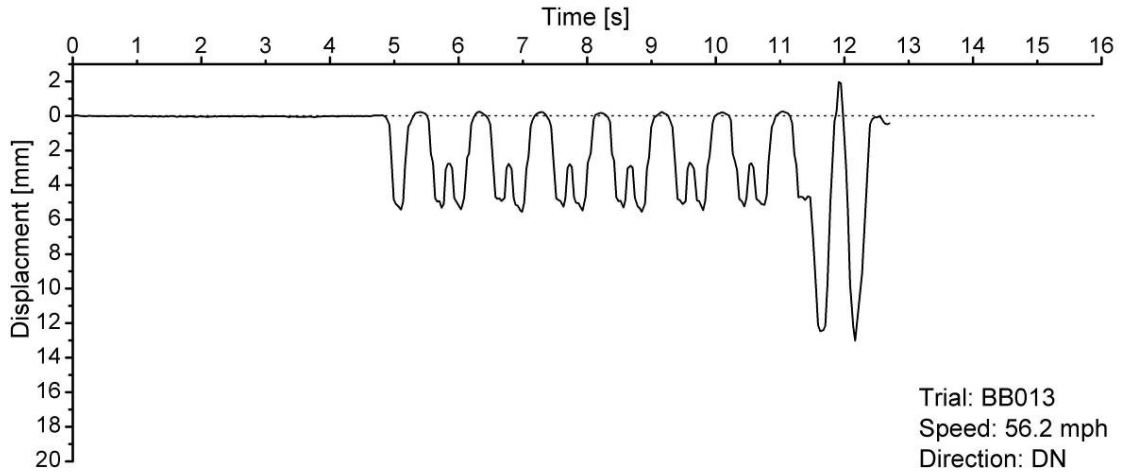

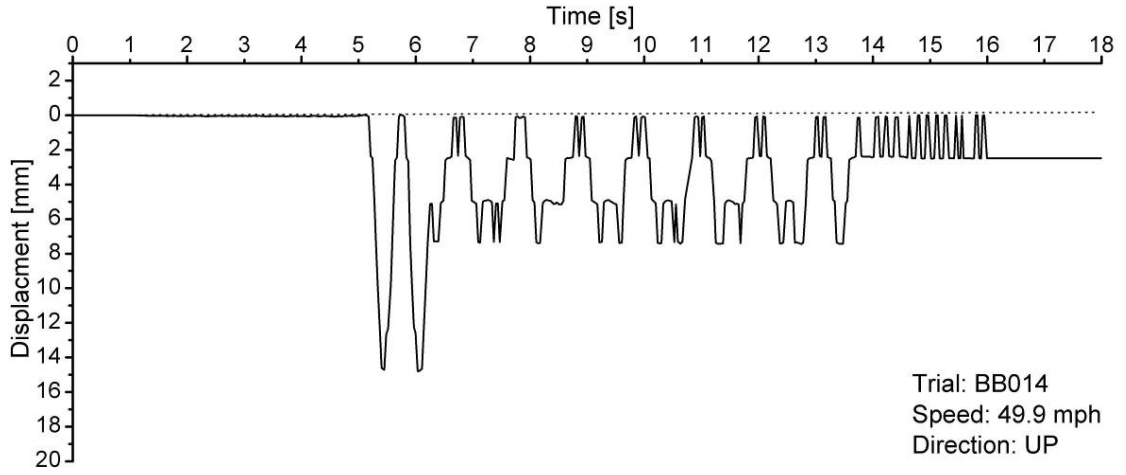

Appendix A: All Data Sets from Dynamic Measurements

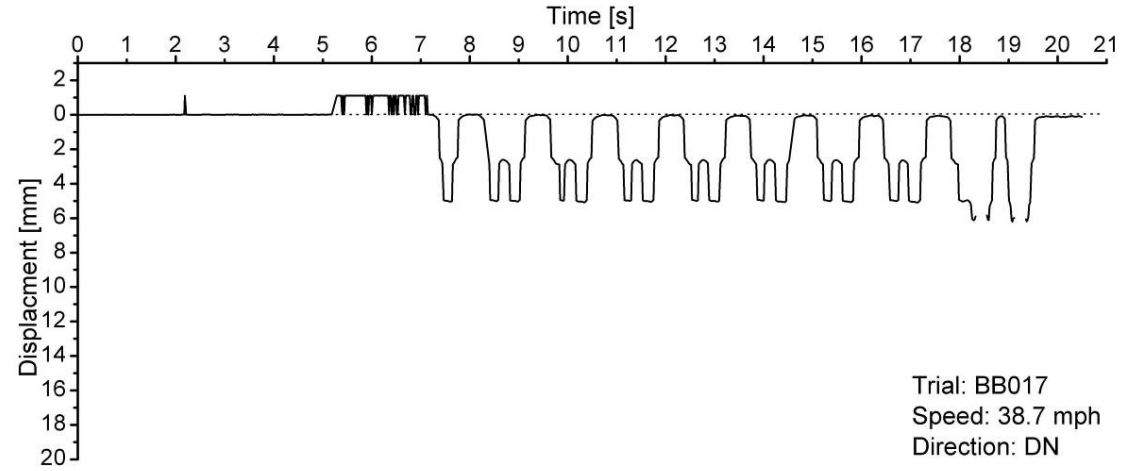

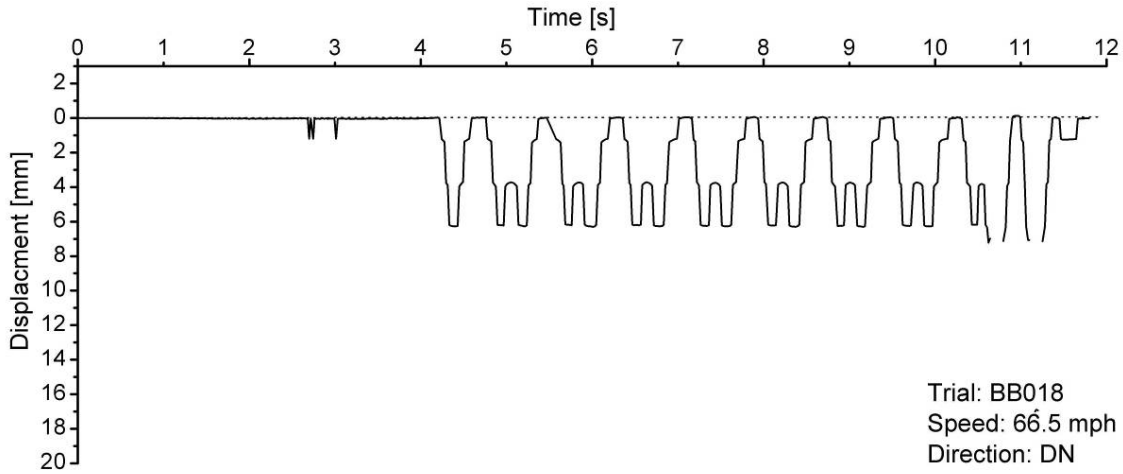

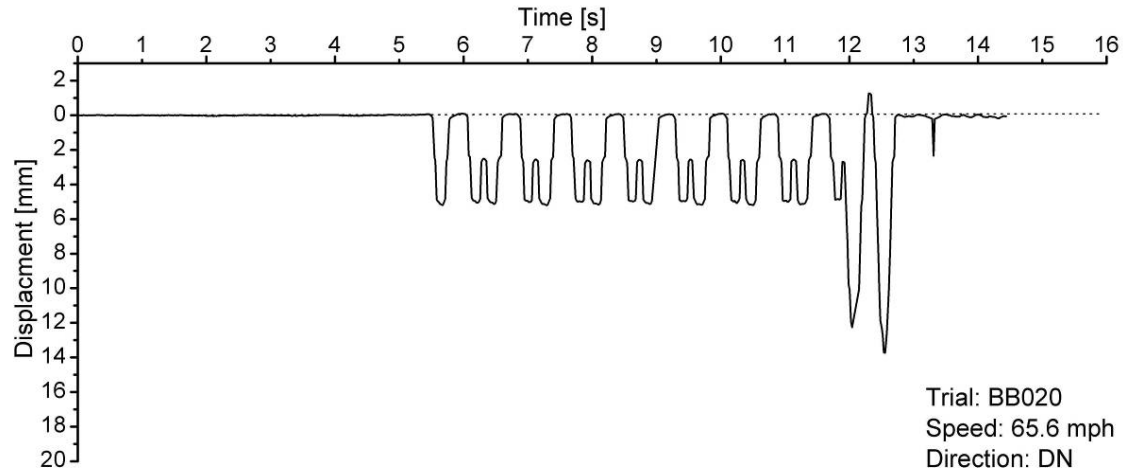

Appendix A: All Data Sets from Dynamic Measurements

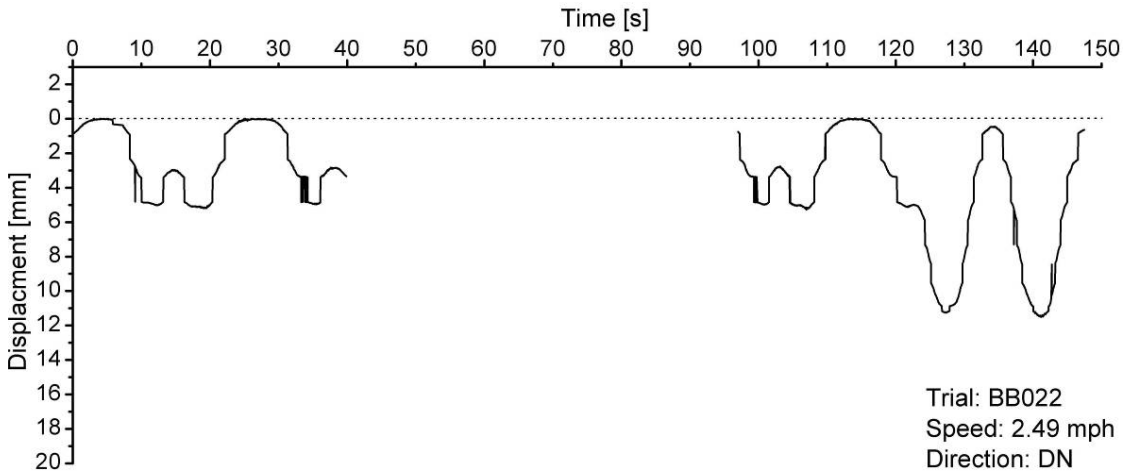

Adavoyle Bog Site Data Sets

Data Set	Date	Time	Destination	Measure Method	Speed	Max Displ.		Mean Displ.	
					[mph]	Loco	PC	Loco	PC
AB001	2005 09 22	1103	Belfast	Photosensor	72.8	-	5.0	-	5.0
AB002	2005 09 22	1107	Belfast	Photosensor	74.4	-	5.4	-	5.3
AB003	2005 09 22	1230	Dublin	Photosensor	56.2	9.3	5.0	8.5	4.8
AB004	2005 09 22	1301	-	Photosensor	-	-	-	-	-
AB005	2005 09 22	1445	Dublin	Photosensor	70.1	9.8	5.0	8.7	4.6
AB006	2005 09 22	1449	Belfast	Photosensor	68.2	-	5.1	-	5.0
AB007	2005 09 23	1109	-	Photosensor	-	-	-	-	-

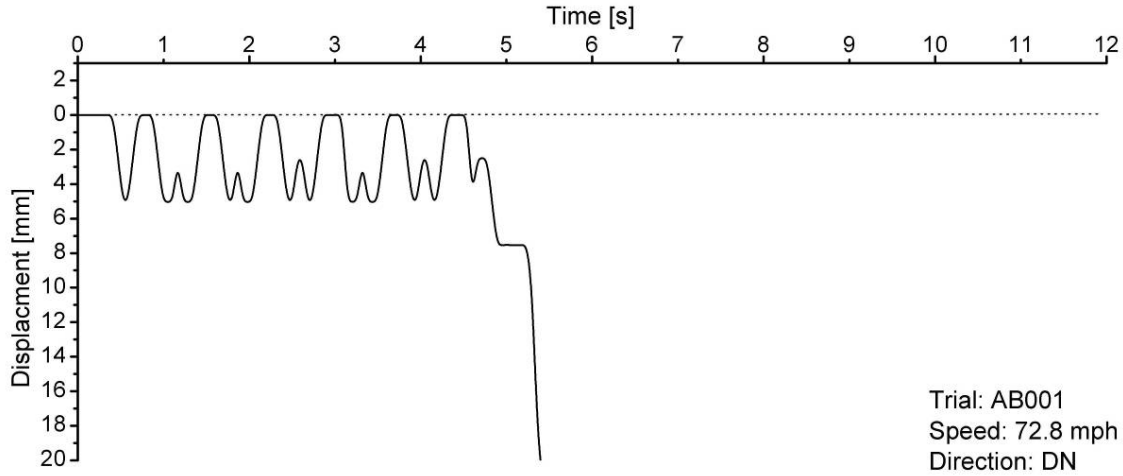
Time [s]
Displacment [mm]
Trial: AB001
Speed: 72.8 mph
Direction: DN

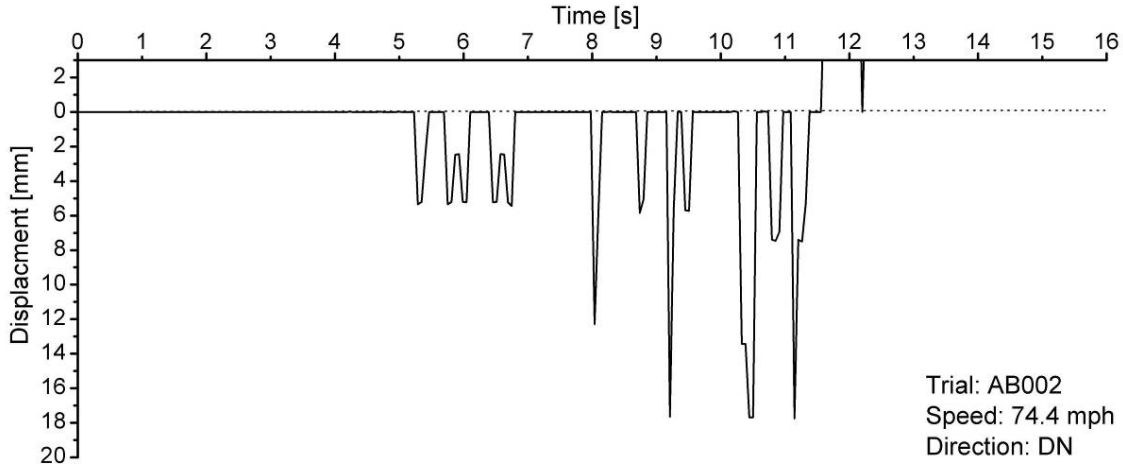
Time [s]
Displacment [mm]
Trial: AB002
Speed: 74.4 mph
Direction: DN

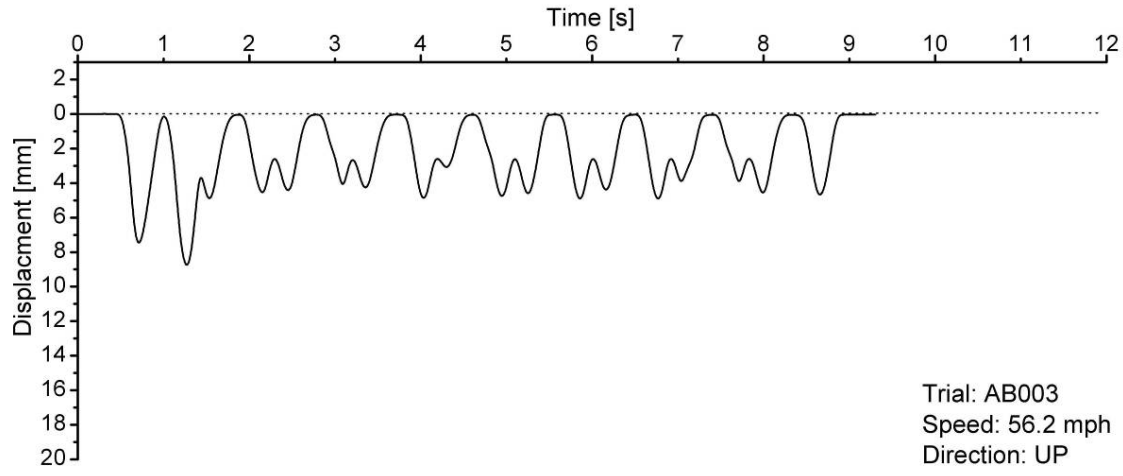
Time [s]
Displacment [mm]
Trial: AB003
Speed: 56.2 mph
Direction: UP

Appendix A: All Data Sets from Dynamic Measurements

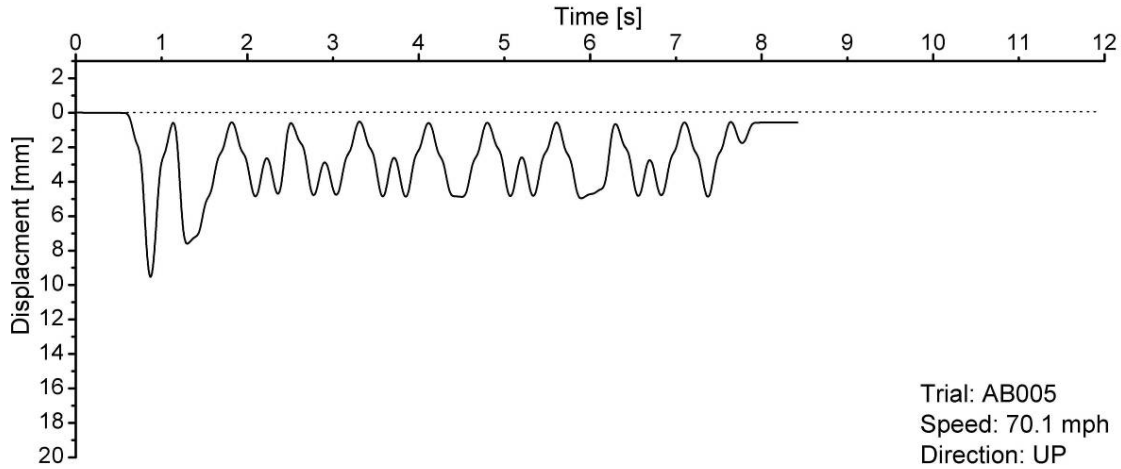

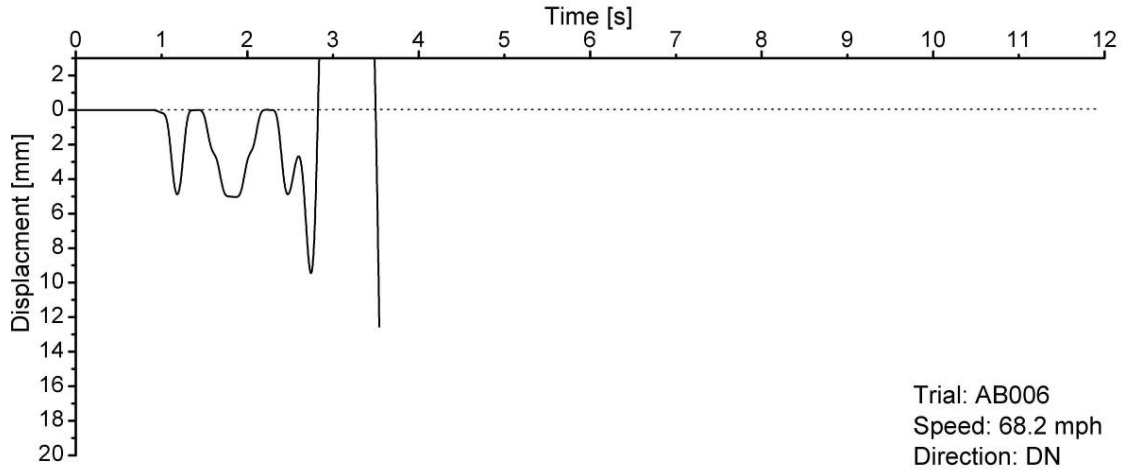

Appendix B: Derivation of Power Lost to Damping

Appendix B: Derivation of Power Lost to Damping

This Appendix provides the derivation of Equation 5.1 from Section 5.1.6. This equation is used to calculate the power lost to damping by the foundation.

From the Winkler model's constitutive equation (Equation 2.7) the only irreversibility present in this system is due to the foundation damping. It is from this irreversibility that the power lost is calculated.

$$EI\frac{\partial^4 y}{\partial x^4}+\rho A\frac{\partial^2 y}{\partial t^2}+c\frac{\partial y}{\partial t}+ky=P\delta(x,t) \tag{2.7}$$

Equation B.1 is from the definition of work, where W is the work done to overcome damping, F is the force exerted to do this work and Δy is the distance over which the work was done. From this definition of work we can determine the rate work done to overcome damping or the power lost to damping (L); this is presented in Equation B.2, where Δt is the interval of time over which the work from Equation B.1 is done.

$$W=F\cdot\Delta y \tag{B.1}$$

$$L=\frac{F\cdot\Delta y}{\Delta t} \tag{B.2}$$

As the constitutive equation (Equation 2.7) is a force balance for an elemental section of the beam, we can attain the force exerted by the damping as the damping coefficient (c) multiplied by the velocity at which the displacement occurs (Equation B.3).

$$F=c\cdot\frac{\partial y}{\partial t}\approx c\cdot\frac{\Delta y}{\Delta t} \tag{B.3}$$

From definition of the critical damping (c) and the damping coefficient (β) in Equations 2.22 and 2.23 we can present the damping coefficient as a function of the damping coefficient, the stiffness coefficient for the foundation (k) and the mass per unit length of the beam (ρA) (Equation B.4).

Appendix B: Derivation of Power Lost to Damping

$$c = 2\beta\sqrt{k\rho A} \tag{B.4}$$

Substituting in Equation B.4 into Equation B.2 we obtain Equation B.5, which can be used to calculate the power lost to damping from Winkler model.

$$L = 2\beta\sqrt{k\rho A}\frac{\Delta y^2}{\Delta t^2} \tag{B.5) or (5.1}$$